

Search For a Counterpart to the Subsolar Mass Gravitational Wave Candidate S251112cm

NICHOLAS VIEIRA ¹, NOAH FRANZ ², BHAGYA SUBRAYAN ², CHARLES D. KILPATRICK ¹, DAVID J. SAND ²,
WEN-FAI FONG ^{1,3}, GRIFFIN HOSSEINZADEH ⁴, KATE D. ALEXANDER ², K. AZALEE BOSTROEM ²,
JILLIAN RASTINEJAD ^{5,*}, KERRY PATERSON ⁶, MANISHA SHRESTHA ^{7,8}, PHILLIP NOEL ^{9,1},
JENIVEVE PEARSON ², AYSHA AAMER ², A. SOUZA SANTOS ⁹, LUIDHY SANTANA-SILVA ^{10,9}, CLECIO R. BOM ⁹,
REGIS CARTIER ¹¹, HEMANTH BOMMIREDDY ^{12,13}, ÓSMAR RODRÍGUEZ ^{14,15}, JENNIFER E. ANDREWS ¹⁶,
CONOR RANSOME ², VASILEIOS PASCHALIDIS ^{2,17}, JAY STRADER ¹⁸, ALDANA GRICHENER ²,
J. QUIROLA-VÁSQUEZ ¹⁹, SERGIY VASYLYEV ⁴, MARCELLE SOARES-SANTOS ²⁰, COLLIN T. CHRISTY ²,
BRIAN HSU ², D. CARSON FULS ²¹, YIZE DONG ²², DANIEL E. REICHART ²³, JONATHAN PINEDA-GARCÍA ²⁴,
KATHRYNE J. DANIEL ², DARYL JANZEN ²⁵, C. E. FIELDS ², ANN ZABLUDOFF ², NICOLAS MEZA ²⁶,
FELIPE OLIVARES E. ²⁷, KRISTINE SPEKKENS ²⁸, BENJAMIN WEINER ²⁹, MAIA WILLIAMS ^{1,3}, ALEX R. GIBBS ^{17,21},
FRANK SHELLY, ^{17,21} ARAVIND P. RAVI ²⁶, SAURABH W. JHA ³⁰, STEFANO VALENTI ²⁶, JOSHUA HAISLIP ³¹ AND
DAVID E. TRILLING ³²

¹Center for Interdisciplinary Exploration and Research in Astrophysics, Northwestern University, 1800 Sherman Ave., 8th Floor, Evanston, IL 60201, USA

²Department of Astronomy and Steward Observatory, University of Arizona, 933 North Cherry Avenue, Tucson, AZ 85721-0065, USA

³Department of Physics and Astronomy, Northwestern University, 2145 Sheridan Road, Evanston, IL 60208, USA

⁴Department of Astronomy & Astrophysics, University of California, San Diego, 9500 Gilman Drive, MC 0424, La Jolla, CA 92093-0424, USA

⁵Department of Astronomy, University of Maryland, College Park, MD 20742-2421, USA

⁶Max-Planck-Institut für Astronomie, Königstuhl 17, 69117 Heidelberg, Germany

⁷School of Physics and Astronomy, Monash University, Clayton, Victoria 3800, Australia

⁸OzGrav: The ARC Centre of Excellence for Gravitational Wave Discovery, Clayton, Victoria 3800, Australia

⁹Laboratório de Inteligência Artificial, Centro Brasileiro de Pesquisas Físicas, 138 Rua Dr. Xavier Sigaud 150, CEP 22290-180, 139 Rio de Janeiro, RJ, Brazil

¹⁰Observatório do Valongo, UFRJ, Ladeira do Pedro Antônio, 43 - Centro, Rio de Janeiro - RJ, 20080-090, Brazil

¹¹Centro de Astronomía (CITEVA), Universidad de Antofagasta, Avenida Angamos 601, Antofagasta, Chile

¹²Department of Astronomy, Universidad de Chile, Camino el Observatorio 1515, Las Condes, Santiago, Chile

¹³Data and Artificial Intelligence Initiative (IDIA), Faculty of Physical and Mathematical Sciences, Universidad de Chile, Santiago, Chile

¹⁴Pontificia Universidad Católica de Chile, Vicuña Mackenna 4860, Macul, Santiago, Chile

¹⁵Instituto Milenio de Astrofísica (MAS), Nuncio Monseñor Sótero Sanz 100, Of. 104, Santiago, Chile

¹⁶Gemini Observatory/NSF's NOIRLab, 670 N. A'ohoku Place, Hilo, HI 96720, USA

¹⁷Department of Physics, University of Arizona, Tucson, AZ 85721, US

¹⁸Center for Data Intensive and Time Domain Astronomy, Department of Physics and Astronomy, Michigan State University, East Lansing, MI 48824, USA

¹⁹Department of Astrophysics/IMAPP, Radboud University, P.O. Box 9010, 6500 GL, Nijmegen, The Netherlands

²⁰Department of Physics, University of Zurich, Winterthurerstrasse 190, Zurich, 8057, Switzerland

²¹Lunar and Planetary Laboratory, University of Arizona, 1629 E. University Blvd., Tucson, AZ 85721-0092, USA

²²Center for Astrophysics | Harvard & Smithsonian, 60 Garden Street, Cambridge, MA 02138-1516, USA

²³Department of Physics and Astronomy, University of North Carolina at Chapel Hill, Campus Box 3255, Chapel Hill, NC 27599-3255

²⁴Universidad Andrés Bello, Facultad de Ciencias Exactas, Departamento de Ciencias Físicas, Instituto de Astrofísica, Av. Fernández Concha 700, Santiago, Chile

²⁵Department of Physics and Engineering Physics, University of Saskatchewan, 116 Science Place, Saskatoon, SK S7N 5E2, Canada

²⁶Department of Physics, University of California, 1 Shields Avenue, Davis, CA 95616-5270, USA

²⁷UKIRT Observatory, Institute for Astronomy, 640 N. A'ohoku Place, University Park, Hilo, Hawai'i 96720, USA

²⁸Department of Physics, Engineering Physics and Astronomy, Queen's University, 64 Bader Lane, Kingston, ON K7L 2E1, Canada

²⁹MMT and Steward Observatory, University of Arizona, 933 North Cherry Avenue, Tucson, AZ 85721-0065, USA

³⁰Department of Physics and Astronomy, Rutgers, The State University of New Jersey, Piscataway, NJ 08854, USA

³¹Department of Physics and Astronomy, University of North Carolina, 120 East Cameron Avenue, Chapel Hill, NC 27599, USA

³²Department of Astronomy and Planetary Science, Northern Arizona University, PO Box 6010, Flagstaff, AZ 86011 USA

ABSTRACT

The recent gravitational-wave (GW) alert from a compact object merger involving at least one subsolar mass (SSM) object has prompted questions about their origins. S251112cm is reported by LIGO/Virgo with a false alarm rate of 1 per 6.2 years, nearby luminosity distance 93 ± 27 Mpc, probability of containing a SSM object of 100%, and probability of containing a $1 - 3 M_{\odot}$ object of just 8%. Such a system likely did not involve the supersolar neutron stars or black holes invoked to explain kilonovae. One must then also invoke hitherto unobserved and speculative models to produce SSM mergers and the resultant electromagnetic (EM) counterparts. We introduce a framework which vets and scores candidate counterparts to SSM GW events to inform follow-up in search of any among the zoo of potential EM transients: kilonovae, kilonovae-within-supernovae, super-kilonovae, or AGN flares from binary black hole mergers. We use a suite of telescopes to perform tiling, galaxy-targeted observations, and photometric/spectroscopic follow-up of promising candidates. In near-real time, we ingest candidates reported by the community, including some of the first observations reported by the Vera C. Rubin Observatory. We vet and score a total of 248 candidates, including 67 from Rubin, but find no likely counterpart. We nonetheless highlight candidates which demonstrate the ability of our framework to distinguish between different transient types and describe strategies to maximize the chances of detecting a counterpart to the next SSM event. Our framework will be implemented in the forthcoming Multimessenger Tool for Rapid Object Vetting and Examination (TROVE).

Keywords: Time domain astronomy (2109), Gravitational wave astronomy (675), Gravitational wave sources (677), Neutron stars (1108), Supernovae (1668)

1. INTRODUCTION

The landmark detection of both gravitational waves (GWs) (LIGO Scientific Collaboration & Virgo Collaboration 2017) and electromagnetic (EM) emission (LIGO Scientific Collaboration et al. 2017; see R. Margutti & R. Chornock 2021; M. Nicholl & I. Andreoni 2025 for reviews) from the binary neutron star (BNS) merger GW170817 ushered in the era of GW + EM multimessenger astronomy. Yet, no new unambiguous GW + EM detections have been made since. This period of quiet has endured despite the LIGO-Virgo-KAGRA (LVK) GW detector network operating during two observing runs (Observing Run 3 (O3), April 2019 - March 2020; Observing Run 4 (O4), April 2023 - November 2025; R. Abbott et al. 2023; The LIGO Scientific Collaboration et al. 2025a). Each run has seen substantial increases in detector sensitivity (A. Buikema et al. 2020; F. Acernese et al. 2023; A. G. Abac et al. 2025), increasing the number of GW events which merit EM follow-up. Multimessenger endeavors have been supported by the advent of tools such as the GW Treasure Map (S. D. Wyatt et al. 2020), *teglon* (D. A. Coulter et al. 2025), Target and Observation Managers (TOMs; R. A. Street et al. 2018a), and increased adoption of existing tools such as General Coordinates Network (GCN) alerts and the Transient Name Server (TNS). One such tool in ac-

tive development is the Tool for Rapid Object Vetting and Examination (TROVE; N. Franz et al. 2025a). TROVE will assist in efficiently allocating finite photometric and spectroscopic resources when searching for counterparts associated with poorly localized events, such as GWs.

These tools, and maximum coordination among the community, will be crucial with the advent of regular operations from the Vera C. Rubin Observatory and its ten-year optical Legacy Survey of Space and Time (LSST) (Ž. Ivezić et al. 2019; I. Andreoni et al. 2022; F. B. Bianco et al. 2022). Moreover, the LVK is planning for a 6-month observing run (IR1) in late 2026, and additional observing runs in the coming years (B. P. Abbott et al. 2018). Tools such as TROVE are timely as we are currently witnessing the possible emergence of a new class of GW events for which our expectations for EM counterparts are not developed: events involving the merger of one or more objects which are subsolar in mass.

The LVK began applying two pipelines (GstLAL; L. Tsukada et al. 2023 and MBTA; C. Alléné et al. 2025) to search for GWs from subsolar mass (SSM) compact object mergers in their data stream, and began reporting the probability that a system contains at least one subsolar mass object (HasSSM), in February 2025.³³ These

³³ <https://emfollow.docs.ligo.org/userguide/changes.html#version-26-2025-02-20>

* NHFP Einstein Fellow

pipelines rely on a new bank of template GW waveforms (C. Hanna et al. 2025) for mergers which include at least one object in the mass range $[0.2, 1.0] M_\odot$, spanning mass ratios $q = m_2/m_1 = 0.1$ to 1.0 , where $m_2 \leq m_1$ (and thus $q \leq 1.0$) by convention.

The GW event S251112cm was observed on 12 November 2025 at 15:18:45.363443 UTC with contributions to detections from all three operational GW detectors (LIGO Scientific Collaboration et al. 2025a,b), with a False Alarm Rate (FAR) of 1 per 6.2 years³⁴ and a GW luminosity distance of 93 ± 27 Mpc. The signal is reported with a high log-Bayes coherence factor $\ln B = +6.1$ across the three contributing GW detectors, indicating a likely coherent signal. It is also reported with a probability that the system contains at least one subsolar mass object $\text{HasSSM} = 1.0$ and probability that the system contains a neutron star $\text{HasNS} = 0.08$. For the purposes of SSM events, the LVK defines neutron stars as objects of mass $1 - 3 M_\odot$. Parameter inference yields a source frame chirp mass \mathcal{M} in the bin $[0.10, 0.87] M_\odot$. These facts make S251112cm the first significant (FAR $< 0.5 \text{ year}^{-1}$, for SSM events) and relatively nearby GW event reported by LVK to involve at least one subsolar mass object.

Whether subsolar mass GW mergers exist in nature is unknown. But, the LVK reports that S251112cm is a significant GW signal with a high coherence factor across the three GW detectors, warranting further exploration of potential EM counterparts and optimal search strategies. We therefore take the prospect of SSM GW events seriously in this work.

The progenitor of this novel GW signal, if astrophysical in origin, is unknown. Figure 1 shows primary and secondary masses m_1 and m_2 for varying chirp mass in the reported $[0.10, 0.87] M_\odot$ range. As $m_1 \geq m_2$ and $\text{HasSSM} = 1.0$, m_2 must be subsolar. We truncate this plot for m_1 or $m_2 \leq 0.2 M_\odot$ and mark the region in which $q \leq 0.1$ given the limits of the template banks, and highlight in gray the aforementioned range $m_1 = 1 - 3 M_\odot$. To explore which m_1 are allowed, we write:

$$m_1 = \mathcal{M} \left(\frac{1+q}{q^3} \right)^{1/5}. \quad (1)$$

For near-symmetric $q \sim 1.0$ and sufficiently small \mathcal{M} , m_1 may also be subsolar. Considering the limitations of the template banks and low HasNS probability, it is

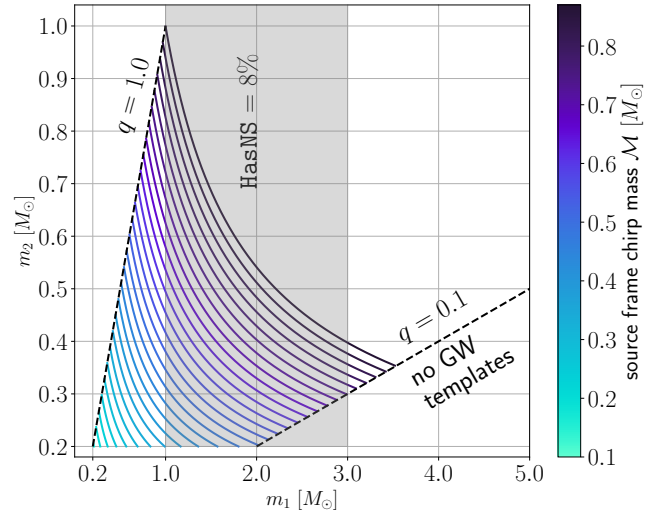


Figure 1. Primary and secondary masses m_1 and m_2 for varying source frame chirp mass \mathcal{M} in the range $[0.10, 0.87] M_\odot$. The progenitor system (m_1, m_2) for S251112cm may lie along any of the plotted curves. We adopt the LVK convention that $m_1 \geq m_2$ such that the mass ratio $q = m_2/m_1 \leq 1.0$. Depending on the chirp mass, m_1 may also be sub or supersolar in mass. We truncate for both m_1 and $m_2 \leq 0.2 M_\odot$ and $q \leq 0.1$, given the limits of waveform template banks (C. Hanna et al. 2025). We highlight the range $1 - 3 M_\odot$. S251112cm was reported by the LVK with a probability of containing a $1 - 3 M_\odot$ object (HasNS) of just 0.08.

most likely that S251112cm was produced by the merger of two subsolar mass objects with a fairly symmetric mass ratio. But, $m_1 \sim 1.0 - 3.5 M_\odot$ and mass ratios approaching 0.1 are not completely ruled out.

The merging system could consist of two black holes (BBH), two neutron stars (BNS), or a neutron star-black hole binary (NSBH), but, at least one of the objects must be subsolar in mass. Mergers involving white dwarfs (WDs) or the nondegenerate cores of stars are disfavored as these produce GWs with frequencies of mHz to dHz, outside of LIGO/Virgo bands (A. Maselli et al. 2020; A. Grichener 2025). Such a subsolar mass neutron star (ssNS) or black hole (ssBH) would be the lightest neutron star or black hole known to date. How such subsolar mass compact objects could be formed remains an open question, as ssNS/ssBHs have not been definitively observed. V. Doroshenko et al. (2022) propose that the compact object at the center of supernova remnant HESS J1731-347 may have a mass of $0.77^{+0.20}_{-0.17} M_\odot$, but J. A. J. Alford & J. P. Halpern (2023) highlight that this measurement is highly distance-dependent and did not analyze all available XMM-Newton data, arguing instead for a supersolar object. The next-lightest known NSs are supersolar: a NICER

³⁴ The latter GCN reports a FAR of 1 in 4 years, while the number on GraceDB and in the most recently published localization regions remains at 1 in 6.2 years: <https://gracedb.ligo.org/superevents/S251112cm/view/>

analysis infers a mass of $1.04_{-0.03}^{+0.05} M_{\odot}$ for pulsar PSR J1231-1411 (T. Salmi et al. 2024), and there is evidence for a $1.174 \pm 0.004 M_{\odot}$ NS in the binary pulsar system J0453+1559 (J. G. Martinez et al. 2015, but see T. M. Tauris & H.-T. Janka 2019 for an argument that the object is instead a WD). Moreover, it is challenging to explain how standard binary evolution could yield a system of ssNSs/ssBHs. Modern 3D simulations of neutrino-driven core collapse supernovae do not yield remnant NSs lighter than $\sim 1.17 - 1.19 M_{\odot}$ (Y. Suwa et al. 2018; B. Müller et al. 2025). Accretion-induced collapse of WDs similarly yields NSs of $\gtrsim 1.1 - 1.2 M_{\odot}$ (K. Nomoto & Y. Kondo 1991). We therefore explore alternative formation channels for ssNSs or ssBHs, how they might merge, and the resultant EM counterparts.

Mergers of these objects may produce EM counterparts under specific conditions. In the case of BNS/NSBH mergers in isolation, we expect a kilonova (KN; see B. D. Metzger 2019 for a review) powered by the radioactive decay of elements freshly synthesized by rapid neutron capture onto heavy seed nuclei (the r -process; J. J. Cowan et al. 2021). Other models propose hitherto unobserved and somewhat speculative transients. B. D. Metzger et al. (2024) and Y.-X. Chen & B. D. Metzger (2025) explore scenarios where ssNSs form and merge with each other in the BH accretion disks around collapsars, yielding a “kilonova-within-a-supernova”. D. M. Siegel et al. (2022) explore more massive collapsar disks, yielding “super-kilonovae”. Finally, a BBH merger which occurs in a baryon-rich environment could be EM-bright, with the disks of active galactic nuclei (AGN) being a promising environment (e.g., B. McKernan et al. 2019; S. S. Kimura et al. 2021; H. Tagawa et al. 2024; J. C. Rodríguez-Ramírez et al. 2025).

Associating a SSM GW event with any EM counterpart would have far-ranging physical implications: on the viability of these GW+EM multimessenger signals, formation channels for subsolar mass compact objects, and the search for primordial black holes and their mergers (Y. Ali-Haïmoud et al. 2017; B. Carr et al. 2021), but also the origins of the heavy elements, the neutron star equation of state, constraining the Hubble constant using combined GW + EM detections, and tests of general relativity. Unsurprisingly, several teams searched for an EM counterpart to S251112cm, yielding a total of 248 candidate counterparts reported in GCN alerts and/or to the TNS in the localization region of S251112cm up to 10 days immediately following the GW signal (see Section 4.4 for a justification of this timescale). However, none have been confidently associated with S251112cm.

Considering this zoo of potential progenitors and EM counterparts, searches for counterparts to SSM events may need to adopt additional strategies beyond those used in searching for counterparts to BNS or NSBH events. We therefore introduce a framework for scoring and ranking candidate EM counterparts to GW events with substantial probability of containing a subsolar mass object. This framework builds on that introduced in N. Franz et al. (2025a) (hereafter F25) for scoring candidates as kilonova counterparts to BNS/NSBH mergers. We introduce new scores for kilonovae-within-supernovae (KNe-in-SNe), super-kilonovae (super-KNe), and BBH merger-induced AGN flaring. The scores introduced in our framework here will be a part of the forthcoming multimessenger TROVE.

2. POSSIBLE PROGENITOR SYSTEMS OF SUBSOLAR-MASS MERGERS

The potential progenitor systems for SSM events fall into two categories: (1) those hosting one or more NSs and (2) BBH systems. Considering the viability of detection for both EM and GW signals, we explore systems which might produce KNe, KNe-in-SNe, and super-KNe in Section 2.1. We consider BBH mergers which induce AGN flaring in Section 2.2. Here, we focus on introducing the potential progenitors; in Section 4, we quantify the corresponding transient EM signatures and introduce a framework for scoring candidate counterparts based on comparison to these different transients.

2.1. Neutron Star-Bearing Systems

The S251112cm GW alert is inconsistent with a BNS/NSBH merger involving two supersolar objects, which can generate a KN. However, W. E. East et al. (2015) propose a scenario in which a highly eccentric NSBH system results in the BH stripping the NS on a first grazing orbit, rendering it subsolar, before later merging. Such a system could, in theory, produce two EM signatures and just one SSM GW signal. More modeling is required to determine the time separation between the EM signatures, so we include these events under the broader umbrella of KNe, which we search for among candidates following F25.

B. D. Metzger et al. (2024) and Y.-X. Chen & B. D. Metzger (2025) propose a channel for ssNS formation in the accretion disk of a BH left behind by the collapse of a rapidly-rotating massive star, *i.e.*, a collapsar. In this scenario, gravitational instabilities in the disk lead to fragmentation into clumps which condense to form ssNSs. The requisite conditions may arise if the original star has a mass $\gtrsim 20 M_{\odot}$ and is rotating with enough angular momentum at collapse to leave behind a

$\sim 1-10 M_{\odot}$ disk around a $\sim 3-30 M_{\odot}$ BH. The recently-formed ssNSs in the disk may merge with each other, producing a GW inspiral signal. Multiple such mergers can occur if more than two ssNSs are formed. These mergers ultimately yield some hierarchically-formed object with mass $\lesssim 2 M_{\odot}$, which finally merges with the central remnant BH, producing one final GW inspiral signal.

This proposed sequence of collapse and mergers has unique EM signatures. Before any mergers, one expects a long gamma-ray burst (IGRB) which could be detected if beamed towards the observer, and the beginning of a core-collapse supernova (CCSN) (A. I. MacFadyen & S. E. Woosley 1999; S. E. Woosley & J. S. Bloom 2006; M. G. Dainotti et al. 2022). Among CC-SNe, stripped-envelope supernovae (SESNe) and especially SNe Ic-BL are more favored, as they are the only SNe associated with GRBs. The mergers of ssNSs then produce a KN-in-SN (B. D. Metzger et al. 2024). These KNe are unlikely to resemble AT2017gfo due to their embedding in the bright SN and the dense accretion disk, but the lightcurves and spectra of the SN may nonetheless be marked by the presence of r -process elements (D. M. Siegel et al. 2019; J. Barnes & B. D. Metzger 2022; A. Patel et al. 2024) or energy injection from a hierarchically-formed millisecond magnetar (N. Bucciantini et al. 2012; B. D. Metzger & A. L. Piro 2014).

We also explore the potential for ssNS mergers in disks left behind by more massive (zero-age main sequence mass $\gtrsim 260 M_{\odot}$; helium core $\gtrsim 130 M_{\odot}$) stars. D. M. Siegel et al. (2022) show that for sufficiently high accretion rates, disk winds in such systems unbind as much as $\gtrsim 50 M_{\odot}$, hosting $\gtrsim 5-10 M_{\odot}$ of r -process material and $\sim 0.1-1.0 M_{\odot}$ of nickel-56 (^{56}Ni). The predicted transient might then resemble a lanthanide-rich KN in color, but evolve on much longer timescales $\gtrsim 1$ month. D. M. Siegel et al. (2022) thus term these events super-KNe. If the collapsar disk in this scenario also experiences fragmentation, this fragmentation might yield ssNS mergers and produce GW inspiral signals. Y.-X. Chen & B. D. Metzger (2025) point out that fragmentation might be even easier to achieve for these more massive collapsar disks given higher mass-infall rates. A detailed study of fragmentation in these more massive disks could clarify any differences between expected GW signals.

We include two important caveats to the KN-in-SN and super-KN schemes. First, we note the absence of other GW signals spatially or temporally associated with S251112cm. If more than two subsolar mass objects were formed in a collapsar disk, one would expect multiple S251112cm-like GW signals within \sim hours to $\lesssim 1$

day of each other, though potentially weaker if the objects were less massive. The inspiral and merger of the hierarchically formed product of these merger(s) with the central BH should also be detectable. If such a $\sim 2 M_{\odot}$ object finally merged with a central remnant BH of $\sim 20 M_{\odot}$, this final merger might resemble the $\sim 23+2.6 M_{\odot}$ merger GW190814 (R. Abbott et al. 2020), detected by LIGO and Virgo at ~ 260 Mpc at O3 sensitivities. If a $\sim 2 M_{\odot}$ object finally merged with the more massive ($\gtrsim 60 M_{\odot}$) BH expected to be present in super-KNe, such a merger would also lie within existing GW template banks (The LIGO Scientific Collaboration et al. 2025b), though no such $\gtrsim 60 + \sim 2 M_{\odot}$ merger has been published by LIGO/Virgo to date (R. Abbott et al. 2023; The LIGO Scientific Collaboration et al. 2025a). Second, neither KNe-in-SNe nor super-KNe have been unambiguously observed. M. M. Kasliwal et al. (2025) argue that the candidate counterpart SN 2025ulz to GW event S250818k may have been a KN in a SN IIb,³⁵ but see several other arguments against this (N. Franz et al. 2025a; J. H. Gillanders et al. 2025; X. J. Hall et al. 2025b,c; B. O’Connor et al. 2025; Y.-H. Yang et al. 2026). We agree that SN 2025ulz is a normal SN IIb.

Nonetheless, the advent of a potential SSM GW detection requires that we consider a multitude of potential pathways for production of SSM compact objects, their mergers, and predicted EM counterparts. Although the absence of coincident GW signals challenges the KN-in-SN and super-KN models, the S251112cm GW alert is also inconsistent with a canonical supersolar BNS or NSBH merger. We thus search for KNe among candidate counterparts, but also, introduce metrics within TROVE to search for KNe-in-SNe and super-KNe.

2.2. Binary Black Hole Systems

An exciting potential progenitor pathway for an SSM GW event is if one or both compact objects are primordial black hole (PBHs) with masses $< 1 M_{\odot}$. There are few predictions for the EM counterparts to PBH mergers (C.-M. Deng et al. 2018; L. Liu et al. 2020), but we assume that the EM signal hypothesized to originate from massive BBH mergers is mass-scale invariant and may still apply in this low-mass regime. Such BBH mergers may be EM-bright if they occur in an environment rich in baryons and among the most promising environments for this scenario is within the disk of an AGN. In this

³⁵ M. M. Kasliwal et al. (2025) suggest broadening the definition of super-KNe to refer to any CCSNe hosting some KN-like r -process nucleosynthesis, including KNe-in-SNe as explored in B. D. Metzger et al. (2024). We retain the distinction here, for precision.

scenario, a BBH merger yields a kicked remnant which accretes material, producing a hotspot of emission off-center from the AGN before exiting the AGN disk (B. McKernan et al. 2019). Based on predicted temperatures, such a merger could manifest as a UV/optical flare (B. McKernan et al. 2019; S. S. Kimura et al. 2021; J. C. Rodríguez-Ramírez et al. 2023; H. Tagawa et al. 2024; P. Darc et al. 2025; J. C. Rodríguez-Ramírez et al. 2025; E. McPike et al. 2026). We can also gain some insight into the pre- and post-merger behavior of BBH systems embedded in disks from GRMHD studies of supermassive black hole (SMBH) binary systems (R. Gold et al. 2014; A. Khan et al. 2018; J. C. Bright & V. Paschalidis 2023; M. J. Avara et al. 2024; L. Ennoggi et al. 2025; V. Manikantan et al. 2025; V. Manikantan & V. Paschalidis 2025). Systems of ssBH binaries in AGN disks would benefit from similar explorations.

Such a flare may have been seen in AGN J124942.3+344929, tentatively associated with the BBH merger GW190521 (M. J. Graham et al. 2020, but see G. Ashton et al. 2021). However, GW190521 involved a far more massive binary system ($\sim 85 + 66 M_{\odot}$), and the works referenced above also consider more massive systems. This difference matters, as models invoke Bondi-Hoyle-Lyttleton accretion onto the remnant BH and thus generically predict that flare luminosities scale as $L \propto M_{\text{BBH}}^2 = (m_1 + m_2)^2$. A merger with S251112cm-like masses (*e.g.*, $0.5 + 0.5 M_{\odot}$) could therefore be a factor of $\sim 10^4$ less luminous than the flare potentially associated with GW190521, based on mass alone.

However, the luminosity and timescale of the flare also depend on the kick velocity of the remnant, the angle between the kick and the AGN disk midplane, the density of the ambient AGN disk, and the mass of the SMBH at the center of the AGN. Though likely challenging for a BBH merger with S251112cm-like masses to yield a sufficiently luminous flare, there may be select regions of the parameter space allowed by S251112cm, kick configurations, and AGN disks with favorable conditions which combine to produce an observable flare. Associating such a flare with S251112cm would thus place tight constraints on the progenitor and the host AGN itself. We thus also introduce metrics to search for AGN flares as EM counterparts to SSM GW events in TROVE.

3. SEARCH FOR AN ELECTROMAGNETIC COUNTERPART TO S251112cm

SSM GW events have unclear origins, progenitors, and EM counterparts. Furthermore, we see only one GW signal in S251112cm, while some of the speculative models discussed here predict multiple GW signals. Despite these important caveats, we begin from the po-

sition that S251112cm may be an astrophysical GW signal produced by a merger involving one or more subsolar mass compact objects. We vet and score candidate EM counterparts to S251112cm found during the intensive follow-up campaign for the event.

Several teams searched for an EM counterpart in the localization region of S251112cm in the optical/IR, X-rays, and gamma-rays. Other teams serendipitously contributed to the wealth of candidates by conducting their regularly-scheduled wide-field transient surveys and reporting transients to the TNS. In all, we find 248 candidate counterparts in the 10 days following the event, including 218 in the optical and 30 in X-rays. We impose this cutoff at 10 days, as extending to much later times would yield an infeasible number of serendipitously detected candidates, and the slowest-rising transients we consider (super-KNe) reach at minimum $\sim 50\%$ of their peak brightness by this time (Section 4.4).

Our own search for a counterpart involved (1) tiling as much of the localization region as possible with larger field-of-view (FOV) instruments, (2) galaxy-targeted observations with smaller-FOV instruments, (3) vetting candidate counterparts with TROVE, and (4) targeted optical and spectroscopic follow-up of promising candidates. The majority of this work was conducted within the Searches After Gravitational waves Using ARizona Observatories (SAGUARO) collaboration (M. J. Lundquist et al. 2019), which used the SAGUARO TOM (G. Hosseinzadeh et al. 2024)³⁶ and a suite of telescopes to search for and characterize candidate EM counterparts to GW events. All photometry used in this work will be made publicly available on the Open mulTiwavelength Transient Event Repository (OTTER; N. Franz et al. 2026a,b)³⁷.

3.1. Search for an Optical Counterpart

We searched for an optical counterpart to S251112cm using (1) the 1.5 m Mt. Lemmon telescope operated by the Catalina Sky Survey (CSS) in Arizona, (2) the 0.82 m T80-South (T80-S) Telescope at the Cerro Tololo Inter-American Observatory (CTIO) in Chile, and (3) the 0.4 m Panchromatic Robotic Optical Monitoring and Polarimetry Telescopes (PROMPT) (D. Reichart et al. 2005) at CTIO and the Meckering Observatory in Australia, as part of the Distance Less Than 40 Mpc (DLT40) Survey. We show all pointings with these tele-

³⁶ For other examples of TOMs, see R. A. Street et al. (2018b); S. J. van der Walt et al. (2019); M. W. Coughlin et al. (2023); D. A. Coulter et al. (2023), and P. J. Mikolajczyk et al. (2025).

³⁷ <https://otter.idies.jhu.edu>

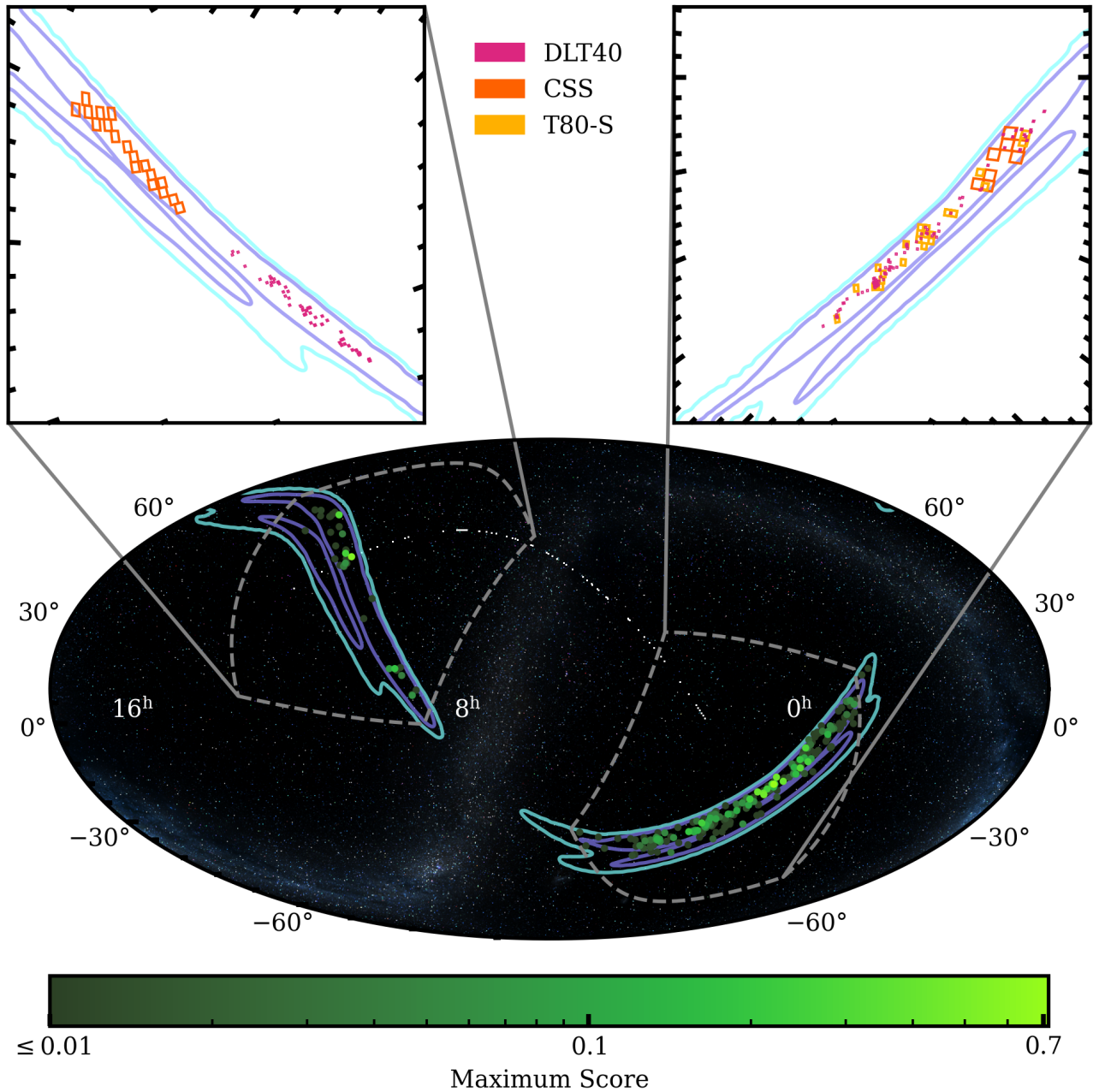


Figure 2. GW localization region of S251112cm, with our telescope pointings in search of an optical counterpart, and candidates identified by all teams. Purple and blue contours denote the 50% and 90% confidence localization regions, which span 371 and 1,681 deg², respectively. *Top left and right:* Zoomed-in insets show our telescope pointings in search of a counterpart with DLT40 (magenta), CSS (orange), and T80-S (yellow), in the two lobes of the localization region. *Bottom:* Points denote the 248 candidate counterparts reported to the TNS and/or in GCNs within 10 days of the GW signal, color-coded by score, where we select the maximum score among KN, KN-in-SN, and super-KN scores (Section 4).

scopes in Figure 2. All pointings have been uploaded to the GW Treasure Map (S. D. Wyatt et al. 2020).

During normal operations, the 1.5 m Mt. Lemmon telescope is used by the CSS to discover and characterize solar system objects. It is equipped with a 5

deg² prime focus imager and observations are taken with no filter, then calibrated to the Gaia *G*-band. When a GW alert of interest is reported, SAGUARO is able to rapidly request observations using the SAGUARO TOM (G. Hosseinzadeh et al. 2024) to survey the localiza-

tion region (see M. J. Lundquist et al. 2019; K. Paterson et al. 2021, for a further description of SAGUARO operations). Candidate transients are found by running a difference imaging pipeline (K. Paterson et al. 2023) based on the algorithm of B. Zackay et al. (2016) and a standard machine learning classifier. Our first epoch of observations tiled $\sim 55 \text{ deg}^2$ of the southern lobe of the S251112cm localization region in this mode, at $\sim 12.8 - 12.9$ hours post-merger. In addition to triggered observations, the CSS serendipitously observed a further $\sim 90 \text{ deg}^2$ of the northern lobe during normal solar system search operations at $\sim 43.6 - 44.4$ hours post-merger, in which we searched for counterparts as well. In all, SAGUARO searched a total area of 145 deg^2 , reaching a mean 5σ limiting magnitude of ~ 20.7 (AB) mag at 0.5 and 1.8 days post-merger.

At the same time as our first CSS observations, we used the $1.4 \times 1.4 \text{ deg}^2$ T80S-Cam on T80-S to observe 23 unique fields in the 90% localization region, covering approximately 45 deg^2 , in the i -band. We reduced all imaging using `photpipe` (A. Rest et al. 2005), following standard reduction procedures as described in A. Santos et al. (2024). We ran difference imaging on all imaging using Dark Energy Camera (DECam) i -band templates to search for transient emission. We achieved an average 3σ limiting magnitude for sources in the difference images of $i > 21.2$ mag at 0.5 days post-merger.

Finally, we performed galaxy-targeted observations with DLT40 (L. Tartaglia et al. 2018). DLT40 is designed as a high cadence SN search, with 0.4 m telescopes in Chile, Australia, and Canada³⁸, each equipped with identical $10 \times 10 \text{ arcmin}^2$ imagers. When a GW event of interest is announced, DLT40 performs a prompt galaxy-targeted search with real-time difference imaging and candidate identification, down to a limiting magnitude of $r \lesssim 19$ mag. Details of DLT40’s GW counterpart search program are provided in S. Valenti et al. (2017) and S. Yang et al. (2019). The DLT40 galaxy catalog is drawn from the Gravitational Wave Galaxy Catalog (GWGC; D. J. White et al. 2011) with further cuts on recession velocity ($< 7000 \text{ km s}^{-1}$), declination ($< +20^\circ$), absolute magnitude ($M_B < -18$ mag), and Milky Way extinction ($A_V < 0.5$ mag). Since LIGO/Virgo’s Observing Run 2 (O2), DLT40 has built imaging templates for galaxies matching the above criteria out to ~ 100 Mpc, beyond the original ~ 40 Mpc, specifically for GW follow-up. For S251112cm, DLT40

³⁸ The Canadian telescope was offline during S251112cm and thus did not play a role in our search.

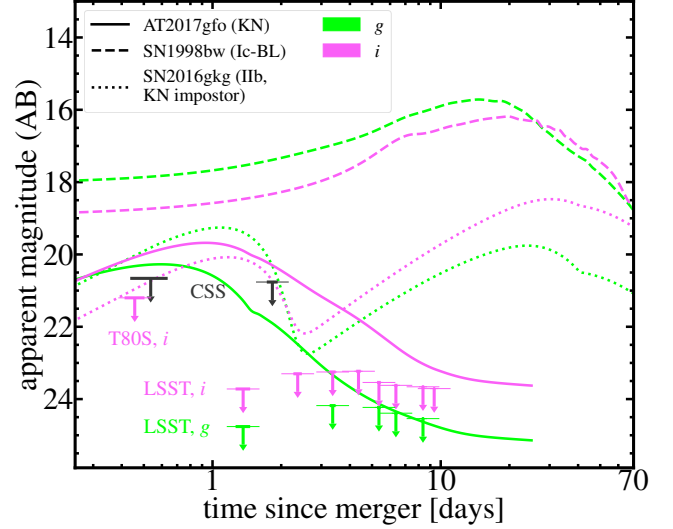


Figure 3. Depths achieved by our CSS and T80-S observations, compared to a prototypical KN, SN Ic-BL, and SN I Ib. Models are generated from `redback` following an AT2017gfo-like kilonova, SN1998bw (Ic-BL), and SN2016gkg (I Ib; a class of SESNe but also noted KN impostors), scaled to the GW luminosity distance 93 ± 27 Mpc to S251112cm (Section 3.1). Translucent bands reflect the uncertainty on this distance. The KN model is truncated at 25 days, beyond which it loses reliability. Our CSS and T80-S observations would have likely found any KNe, SNe Ic-BL, or SNe I Ib, in our observed fields. We also include median g - and i -band depths achieved by Rubin-LSST, as the greatest depths achieved by any search (S. MacBride et al. 2025; S. Anand et al. 2025a).

observed 184 unique galaxies within the localization region. Several galaxies were visited multiple times.

With CSS, we detect one new transient, AT2025adjd (D. Sand 2025). With T80-S and DLT40, we do not recover any new transients. To further assess our ability to have detected transients of interest, we compare the depths achieved by our search to relevant models. Figure 3 shows the limiting magnitudes obtained with our CSS and T80-S wide-field search, compared to models for an AT2017gfo-like KN, a SN Ic-BL, and a SN I Ib. We also include the median depths achieved by Rubin-LSST, as the greatest depths achieved by any search (S. MacBride et al. 2025; S. Anand et al. 2025a). We use `redback` (N. Sarin et al. 2024) to generate these models, scaling all to the GW luminosity distance 93 ± 27 Mpc of S251112cm. To produce AT2017gfo-like lightcurves, we use the `three_component_kilonova` model, with parameters from the homogeneous, three-component model in V. A. Villar et al. (2017). To compare to a SN Ic-BL, we show the prototypical SN1998bw, using the `sn1998bw_template` model (M. Vincenzi et al. 2019). For a double-peaked SN I Ib,

we adopt a `shock_cooling_and_arnett` model with SN 2016gkg-like envelope mass $0.03 M_{\odot}$, envelope radius $43 R_{\odot}$, explosion energy 10^{51} erg, total ejecta mass $2 M_{\odot}$, ejecta velocity 8100 km s^{-1} (I. Arcavi et al. 2017), and set all other parameters to defaults. The depth of our CSS observations suggests that we could have detected KNe, SNeIc-BL, and SNeIIB in our observed fields at early times. Rubin-LSST could have likewise detected any of these transients.

These models provide a useful benchmark because SNeIc-BL and IIB are classes of SESNe, which may be the SNe in which KNe are embedded in KNe-in-SNe (B. D. Metzger et al. 2024; Y.-X. Chen & B. D. Metzger 2025). Super-KNe may also resemble SNeIc-BL or IIB (D. M. Siegel et al. 2022). The SNIIB also demonstrates their ability to act as KN impostors at early times. Indeed, we emphasize that SNeIc-BL or IIB, or other SESNe, are not viable counterparts to SSM GW events on their own. Clear deviations from these models which indicate the presence of r -process material, *e.g.*, deviations in color, would be required to establish a candidate as more than a standard CCSN/SESN (Section 4.4). Association with a GRB would also provide evidence for the presence of a collapsar.

3.2. Public Optical and High-Energy Observations

The broader community used a suite of optical telescopes to search for a counterpart. Observations were largely reported through GCN alerts and to the TNS. Over the first \sim day, the Gravitational-wave Optical Transient Observer (GOTO; K. Ackley et al. 2025), BlackGEM/MeerLICHT (P. J. Groot et al. 2025), and the Asteroid Terrestrial-impact Last Alert System (ATLAS) (J. H. Gillanders et al. 2025a) reported five transients within the localization region. Within the next 10 days, additional candidates and observations were reported with FTW, the Zwicky Transient Facility (ZTF), DECam, GRANDMA, Rubin-LSST, the Wide Field Survey Telescope (WFST), J-GEM, SVOM/VT, the Lulin Observatory Telescope (LOT), GECKO/KMTNet, and ATLAS (J. Gassert et al. 2025; S. Anand et al. 2025b; A. Smith et al. 2025; X. J. Hall et al. 2025a; O. Burkhonov et al. 2025; P. Hello et al. 2025; S. MacBride et al. 2025; Z. Y. Liu et al. 2025; K. Taguchi et al. 2025; Y. N. Ma et al. 2025; J. H. Gillanders et al. 2025b; M. Jeong et al. 2025). The largest influx of candidates came from observations with Rubin-LSST, conducted from 1.4 to 9.4 days post merger, and posted to the TNS and announced via GCN at 45 days post-merger (S. Anand et al. 2025a). This Rubin-LSST search increased the number of optical candidates in our sample from 151 to 218.

Higher-energy (X-ray and gamma-ray) observatories were also employed in the search for a counterpart. In gamma-rays, the Fermi-GBM and all-sky Glowbug observed the localization region at the time of the initial LVK alert, but identified no candidates (S. Bala et al. 2025; M. Kerr et al. 2025). In X-rays, the all-sky MAXI/GSC (2 – 20 keV) found no potential counterparts within hours of the initial alert (H. Hiramatsu et al. 2025). The Swift X-Ray Telescope (Swift-XRT; 0.2 – 10 keV) searched the GW localization region over 0.1 to 1.4 days, identifying 7 previously-uncataloged and 13 previously-cataloged candidates (K. L. Page et al. 2025). Concurrently, the Einstein Probe’s Follow-up X-ray Telescope (EP-FXT; 0.5 – 4 keV) searched from 0.01 to 1.8 days, identifying 10 new X-ray candidates (Q. Y. Wu et al. 2025). These X-ray candidates are of interest given the recent increase in the number of fast X-ray transients (FXTs), detected mostly by EP since 2024. A selection of FXTs have been associated with GRBs (*e.g.*, A. J. Levan et al. 2024) and optical counterparts (*e.g.*, J. H. Gillanders et al. 2024), including CCSNe and potentially compact object mergers (R. A. J. Eyles-Ferris et al. 2025; P. G. Jonker et al. 2026). AGN flares induced by BBH mergers may also have X-ray counterparts (S. S. Kimura et al. 2021).

3.3. Vetting of Candidates with TROVE & Optical Follow-up

Following the GW detection of S251112cm, we continuously ingested and vetted candidate counterparts from our searches and the community using the TROVE KN-vetting algorithm described in F25. Optical candidates were automatically ingested in near real-time directly from the TNS. For the small subset of optical candidates or photometry which were shared in GCNs but not to the TNS ($< 1\%$ of all candidates/photometry), we ingested these manually. We also manually ingested the 30 Swift-XRT and EP-FXT X-ray sources, reported in GCNs. We regularly queried the ATLAS forced photometry server (J. L. Tonry et al. 2018; K. W. Smith et al. 2020; L. Shingles et al. 2021) to supplement candidates’ lightcurves.

On 13 November 2025, at 31 hours post-merger, we released a GCN (N. Franz et al. 2025b) identifying four candidates which received a high score with TROVE: AT 2025adgp, AT 2025adhf, AT 2025adhs, and AT 2025adht. We included the caveats that some showed pre-GW detections with ATLAS and all putative host galaxies’ redshifts were only marginally consistent with the localization of S251112cm. Three of the four galaxies had photometric redshifts, with large uncertainties. Nonetheless, this list of candidates was then used

Table 1. Spectra of Candidates and Host Galaxies

Name	Observation Date [UTC]	Source	Type	z	Ref.
SN 2025adgp	2025-11-15	SOAR/Goodman	Ia	0.046 ± 0.003	2
SN 2025adhf	2025-11-17	SOAR/Goodman	Ia	0.098 ± 0.003	1
SN 2025adhsh	2025-11-15	SOAR/Goodman	II	0.044 ± 0.003	2
AT 2025adht	2025-11-26	Bok/B&C	–	0.1848 ± 0.0001	This paper
SN 2025adim	2025-11-17	SOAR/Goodman	Ia	0.091 ± 0.003	1
SN 2025adiw	2025-11-17	SOAR/Goodman	Ia	0.165 ± 0.002	1
SN 2025adiz	2025-11-14	MMT/Binospec	Ia	0.132 ± 0.002	This paper
AT 2025adjf	2025-11-17	SOAR/Goodman	–	0.124 ± 0.002	1
AT 2025adra	2025-11-26	Bok/B&C	–	0.0784 ± 0.0001	This paper

NOTE—Spectroscopic observations with Bok/B&C, MMT/Binospec, and SOAR/Goodman, as described in Section 3.3. Spectral types for transient spectra are noted along with spectroscopic redshifts. Where we measured the host-galaxy redshift, we omit spectral type. References for discovery and classification of each candidate are (1) A. Santos et al. (2025) and (2) H. Bommireddy et al. (2025).

by members of the community and ourselves in planning follow-up observations.

3.3.1. Spectroscopic Follow-up

We spectroscopically followed up on a total of six candidates using the Goodman High-Throughput Spectrograph (J. C. Clemens et al. 2004) on the 4.1 m Southern Astrophysical Research (SOAR) Telescope to classify these transients or their host galaxies (program PIs: (1) Bom and (2) Bommireddy). We show all follow-up spectra in Figure 4 with the target, source classification, and measured redshift for each source. Our observations are compiled in Table 1. We processed all SOAR spectra following standard procedures with `pypeit` (J. X. Prochaska et al. 2020a,b,c) using dome flat and arc lamp observations taken on the same night and instrumental configuration. Each spectrum was calibrated using a sensitivity function derived from a standard star spectrum obtained on the same night and corrected for telluric absorption. We systematically classified each spectrum using `SNID-SAGE` (F. Stoppa in prep., 2025) to derive their spectroscopic type and redshift.

We obtained optical spectra of two of the four TROVE-identified candidates (AT 2025adgp, AT 2025adhsh), and find them consistent with a SN Ia at $z = 0.046 \pm 0.003$ and SN II at $z = 0.044 \pm 0.003$, respectively; we released these redshifts and classifications by GCN shortly thereafter (H. Bommireddy et al. 2025) and reported all to TNS. We later obtained a spectrum of a third candidate (AT 2025adhf), finding it consistent with a SN Ia at $z = 0.098 \pm 0.003$, also released in a GCN (A. Santos et al. 2025). On the same night, we pursued three other candidates (AT 2025adim, AT 2025adiw, AT 2025adjf) with notable scores and host galaxies consistent with

the GW localization volume (A. Santos et al. 2025). We classify both AT 2025adim and AT 2025adiw as SNe Ia, at $z = 0.091 \pm 0.003$ and $z = 0.165 \pm 0.002$, respectively. We were unable to obtain a spectrum of AT 2025adjf itself, so we obtained a spectrum of its host galaxy, measuring $z = 0.124 \pm 0.002$. Based on these classifications and distances well outside the GW localization volume, we disqualify all six candidates as viable counterparts.

We also acquired a spectrum of one candidate (AT 2025adiz) with Binospec on the 6.5 m MMT (D. Fabricant et al. 2019). Observation of this spectrum was triggered by the SAGUARO team using the PyMMT package (M. Shrestha et al. 2024). As with other candidates, AT 2025adiz had a noteworthy score and potential host with an uncertain photometric z . We find AT 2025adiz consistent with a SN Ia at $z = 0.132 \pm 0.002$, outside the localization volume for S251112cm, disqualifying it.

Lastly, we obtained spectra for the putative host galaxies of one candidate mentioned in our initial GCN (AT 2025adht) and another notable candidate (AT 2025adra) with the Boller & Chivens (B&C) Spectrograph on the 2.3 m Bok telescope. We find that the hosts of AT 2025adht and AT 2025adra both have emission line spectra and lie at $z = 0.1848 \pm 0.0001$ and $z = 0.0784 \pm 0.0001$, respectively, both well outside the localization volume of S251112cm. We thus disqualify AT 2025adht and AT 2025adra as well.

3.3.2. Photometric Follow-up

We also performed photometric follow-up on one X-ray source, S251112cm.X78, initially reported by Swift-XRT (K. L. Page et al. 2025), with SOAR-Goodman. Our follow-up was motivated by its association with a putative host galaxy with a photometric redshift $z =$

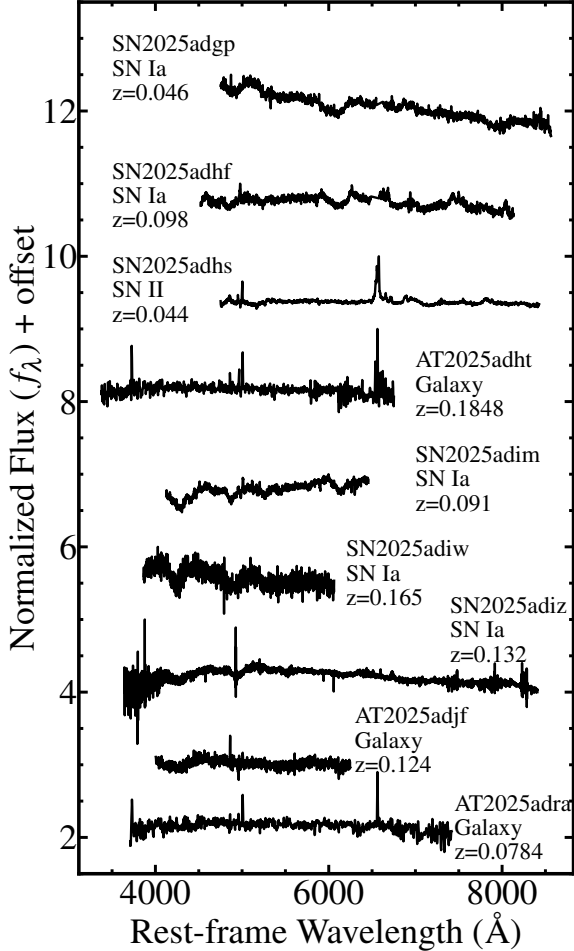


Figure 4. Spectra of candidate counterparts or the putative hosts of candidate counterparts, with source classification and measured redshift. Observations are compiled in Table 1. We obtained SOAR/Goodman spectra of five candidates (AT 2025adgp, AT 2025adhf, AT 2025adhs, AT 2025adim, and AT 2025adiw) and the host of AT 2025adjf, MMT/Binospec spectra of AT 2025adiz, and Bok/B&C spectra of the host galaxies of AT 2025adht and AT 2025adra. All candidates resemble SNeIa or II at redshifts z too distant to correspond to S251112cm. All host galaxies similarly lie outside of the localization volume.

0.02 ± 0.01 (Pan-STARRS1, R. Beck et al. 2021), within the localization volume of S251112cm. S251112cm_X78 was previously uncataloged, though X-ray detections from $\sim 0.1 - 1.4$ days were not brighter than previous upper limits (K. L. Page et al. 2025). We observed this field at 15.4 days post-merger for 6×200 s in the g - and r -bands, in relatively poor conditions. Processing these data using `photpipe`, we searched for point-like sources in the 90% containment localization of S251112cm_X78.

We detected no optical counterpart, down to limiting magnitudes of $g > 22.0$ and $r > 21.87$.

AT 2025adht, one of the candidates identified in our initial GCN, was followed up with the Maidanak Observatory on behalf of GRANDMA at 2.4 days (O. Burkhonov et al. 2025) and with the LOT at 9.2 and 10.2 days (J. H. Gillanders et al. 2025b). After its initial detection with ZTF (S. Anand et al. 2025b), this follow-up demonstrated that AT 2025adht faded from 0.8 to 10.2 days at a rate slower than expected of a transient KN. J. H. Gillanders et al. (2025b) interpret this evolution as consistent with an unrelated background SN near peak. Given our Bok/B&C measurement of a redshift $z = 0.1848 \pm 0.0001$ for the putative host galaxy, regardless of the nature of the transient, AT 2025adht lies outside the GW localization volume.

4. SCORING CANDIDATE COUNTERPARTS TO SUBSOLAR MASS GRAVITATIONAL-WAVE EVENTS

Our search for a counterpart to S251112cm outlined in the previous section leveraged our existing algorithm for vetting candidates in search of KN counterparts to GW events (F25). Here, we extend this algorithm and introduce metrics for vetting candidate counterparts to SSM events which scores candidates in comparison to multiple classes of transient. We develop a framework which searches for KNe, KNe-in-SNe, super-KNe, and BBH-induced AGN flaring. This framework can and should evolve as our knowledge of SSM mergers advances.

The score (between zero and one) for a candidate to potentially be transient T that is also associated with a GW event is the product of five subscores:

$$S_T = S_{2D} \times S_{\text{dist},T} \times S_{\text{PSMPC},T} \times S_{\text{AGN},T} \times S_{\text{phot},T}, \quad (2)$$

where we use the subscript T to indicate that the subscore is dependent on the transient type being vetted. We assign a subscore S_{2D} based on the candidate's 2D position in the GW localization region. $S_{\text{dist},T}$ quantifies the overlap between the distance to the candidate (via direct spectroscopy or host galaxy) and the GW localization. We use $S_{\text{PSMPC},T}$ to discard candidates associated with point sources or minor planets, and the newly-implemented $S_{\text{AGN},T}$ favors or disfavors candidates associated with AGN. Finally, $S_{\text{phot},T}$ is computed by comparing photometry to expectations for a given transient. Our overall framework is presented in Figure 5.

In this framework, the score described in F25 would be S_{KN} , with the caveat that F25 did not incorporate 2D

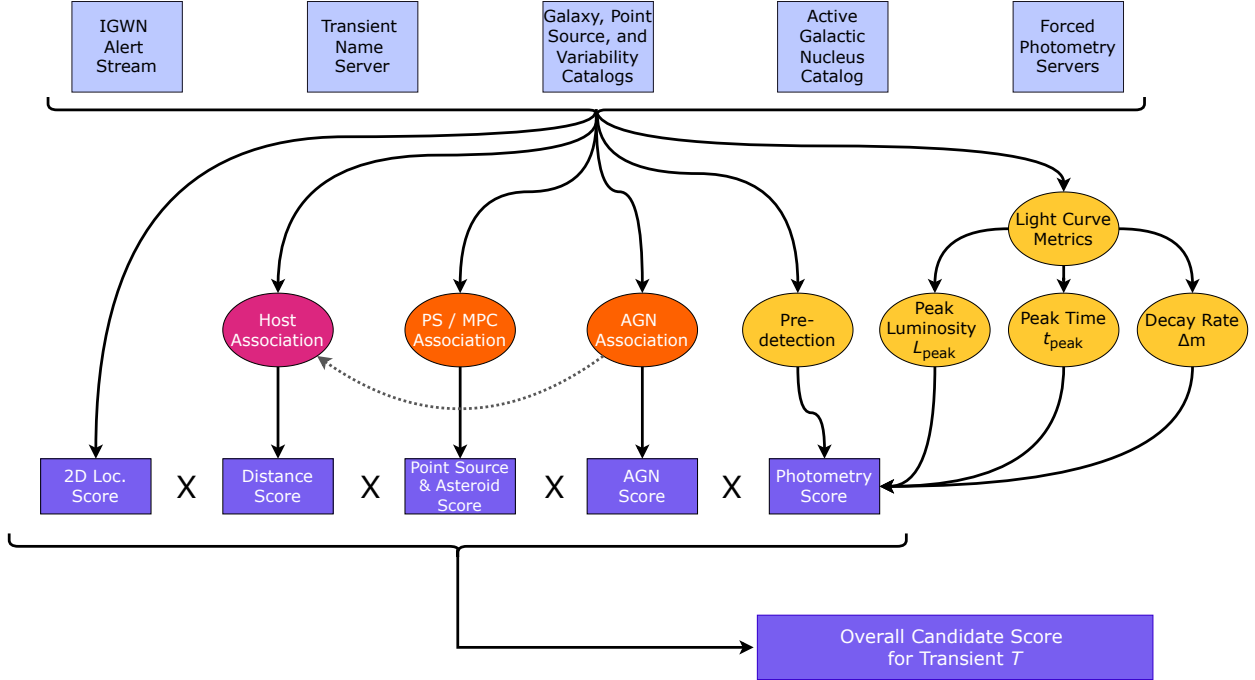


Figure 5. Overall framework for scoring and ranking candidate counterparts to a SSM GW event. We ingest GW alerts from the International Gravitational-Wave Observatory Network (IGWN) alert stream, transients and their photometry/classifications from the TNS, galaxies, point sources, variable objects, minor planets, and AGN from relevant catalogs, and forced photometry. For each candidate, GW alerts are used to compute the 2D localization subscore S_{2D} and in combination with galaxy catalogs to compute distance subscores S_{dist} . Candidates’ positions are compared to those of point sources, minor planets, and variable objects to compute S_{PSMPC} . Association of candidates with AGN using an AGN catalog yields the AGN association subscore S_{AGN} . If vetting for AGN flaring, the distance to any associated AGN is used in distance scoring, as represented with a dotted line. Photometry scores S_{phot} are computed by checking for predetections and comparing candidates’ photometry to predictions for peak luminosity L_{peak} , peak time t_{peak} , and decay rate Δm , dependent on transient type T . Our framework introduces a dependence on the EM transient class T in question (KNe, KNe-in-SNe, super-KNe, or AGN flares) for distance, point source/minor planet association, AGN association, and photometry scoring. Taking the product of the five subscores, we produce unique overall scores S_T for each candidate for each class of EM transient T (Equation 2).

AGN association into scoring.³⁹ For known counterpart AT 2017gfo to GW170817, we compute an overall score of $S_{\text{KN}} = 0.54$ ($S_{\text{KN}} = 0.56$) if using the photometric (spectroscopic) z of the host galaxy NGC 4993. Here, we introduce the following new overall scores: $S_{\text{KN-in-SN}}$, $S_{\text{super-KN}}$, and $S_{\text{AGN-flare}}$. Our 2D localization subscore S_{2D} is identical to that presented in F25. We describe the new S_{AGN} , updates to S_{PSMPC} and S_{dist} , and differences in S_{phot} across transients.

4.1. AGN Association Score

We introduce a new subscore for 2D association with AGN. For most of the relevant transients (KNe, KNe-in-

SNe, and super-KNe), association with an AGN should disqualify the candidate as being the EM counterpart to the GW event. When vetting for BBH-induced AGN flaring, association with an AGN should instead favor the candidate. We thus define $S_{\text{AGN},T}$, which takes on a value of zero or one dependent on the transient in question and association with an AGN or lack thereof. When vetting for KNe, KNe-in-SNe, or super-KNe (*i.e.*, when $T = \text{KN}$, KN-in-SN , or super-KN), a candidate is assigned $S_{\text{AGN},T} = 0$ when associated with an AGN, disfavoring the candidate, and 1 when unassociated. When vetting for AGN flares ($T = \text{AGN-flare}$), a candidate is assigned $S_{\text{AGN},T} = 1$ when associated with an AGN, favoring the candidate, and 0 when unassociated.

We crossmatch candidates with AGN using version 8 of the Million Quasars (Milliquas) catalog (E. W. Flesch 2023). We consider a candidate associated with an AGN if it lies within $2''$ (~ 1 kpc at ~ 93 Mpc) of said AGN, consistent with our criterion for point source association.

³⁹ However, both Gaia Data Release 3 (DR3; Gaia Collaboration et al. 2023) and the Pan-STARRS 1 Source Types and Redshifts with Machine Learning catalog (PS1-STRM; R. Beck et al. 2021), used in F25 for point source association, contain AGN.

4.2. Point Source/Minor Planet Association Score

We define this subscore as the product of two score factors, $S_{\text{PSMPC}} = S_{\text{PS}} \times S_{\text{MPC}}$, for point source (PS) and Minor Planet Center⁴⁰ (MPC) object association. We set the score factor to zero for candidates that are confidently identified with known point sources or asteroids, and to one otherwise.

As in F25, we employ several catalogs for point source association.⁴¹ Here, we also include the ZTF Variable Stars catalog (X. Chen et al. 2020). To exclude galaxies in PS1-STRM from our catalog of point sources, we ignore objects with a probability of being a galaxy (as computed in R. Beck et al. 2021) of >0.7 . When vetting for BBH-induced AGN flaring, since AGN association should favor a candidate, association with a PS1-STRM object with probability of being a quasar >0.7 also does not disfavor the candidate.

Our minor planet association largely follows that of F25, where we query the MPC and perform a two-body evolution around the Sun to identify asteroids within 10° of a candidate at the time of its detection. For any matches, we then perform a full n -body simulation to find the precise location of the asteroid, and we consider candidates within $25''$ of an asteroid to be associated with said asteroid. In this work, we impose an additional constraint: we consider any candidate with more than one $\geq 5\sigma$ detection not to be an asteroid. This procedure aligns with our expectations for contamination from asteroids: the moving asteroid should be detected once at some position associated with a candidate, and then move on from that position.

4.3. Distance Score

We also update how we calculate the distance subscore. If the candidate has a known distance (*e.g.*, a SN with some measured spectroscopic z) we select that distance. If no distance is known, we instead search for galaxies within $5'$ (~ 150 kpc at ~ 93 Mpc) and with probability of chance coincidence (J. S. Bloom et al. 2002) $P_{\text{cc}} \leq 0.15$, following J. C. Rastinejad et al. (2022). For galaxies which pass this filtering, we then assign a potential host based on the provenance of their distance measurement, prioritizing (in descending order): redshift-independent measurements, spectroscopic z , and photometric z . If any galaxies possess a redshift-

independent distance measurement, we compute the distance score S_{dist} as the maximum among all galaxies with redshift-independent measurements. If no such galaxy exists, we move on to spectroscopic z , and so on to photometric z . Finally, if no galaxies with $P_{\text{cc}} \leq 0.15$ reside within $5'$, distance scoring is not factored in to the candidate's score, and $S_{\text{dist}} = 1.0$.

As in F25, we use a number of galaxy catalogs.⁴² In this work, we replace the DESI EDR with Data Release 1 (DR1; DESI Collaboration et al. 2025) and incorporate the NASA/IPAC Extragalactic Database Local Volume Sample (NED-LVS; D. O. Cook et al. 2023). The completeness of galaxy catalogs at these nearby distances merits further exploration. This galaxy catalog completeness will be enhanced by upcoming surveys, and especially future data releases from DESI.

When vetting for BBH-induced AGN flaring, if a candidate is associated with an AGN, that AGN is taken to be the host and the distance to the AGN is used. To obtain uncertainties on the distance to the AGN, we follow Milliquas (E. W. Flesch 2023) guidelines: for AGN with only a known photometric z , we assign an uncertainty $\Delta z = 0.1z$ ($0.01z$) when z is known to one (two) decimal places. When a spectroscopic z is available, we set the uncertainty to a constant $\Delta z = 10^{-3}$.

4.4. Photometry Score

Our photometric vetting scores candidate counterparts based on (1) the presence of any pre-GW detections, (2) the peak luminosity, (3) the epoch at which lightcurve peaks (*i.e.*, rise time), and (4) the rate of evolution in their lightcurve (*i.e.*, decay rate), for some class of transient T . We define the subscore for photometry:

$$S_{\text{phot},T} = S_{\text{PD},T} \times S_{L,T} \times S_{\text{RT},T} \times S_{\text{DR},T}, \quad (3)$$

where the four score factors each take values of 1.0 if a condition is met and 0.1 if not. For example, for KNe, we require no predetections, a peak luminosity $L_{\text{peak}} < 10^{43}$ erg s^{-1} , a rise time $t_{\text{peak}} < 4$ days, and decay rate $\Delta m > 0.1$ mag day^{-1} . A candidate which meets all of these criteria will have $S_{\text{phot,KN}} = 1$; a candidate which meets none will have $S_{\text{phot,KN}} = 10^{-4}$.

Our calculation of the maximum luminosity L_{peak} differs from that of F25. In F25, the maximum lumi-

⁴⁰ <https://www.minorplanetcenter.net>

⁴¹ The All-Sky Automated Survey for Supernovae Variable Star Catalog X (ASAS-SN X; B. J. Shappee et al. 2014; C. T. Christy et al. 2023), Gaia Data Release 3 (DR3; Gaia Collaboration et al. 2023), and Pan-STARRS 1 Source Types and Redshifts with Machine learning catalog (PS1-STRM; R. Beck et al. 2021).

⁴² Galaxy List for the Advanced Detector Era + (GLADE+; G. Dálya et al. 2022), Gravitational Wave Galaxy Catalog (GWGC; D. J. White et al. 2011), Heraklion Extragalactic Catalogue (HECATE; K. Kowlakas et al. 2021), Legacy Survey Data Release 10 (LS DR10; R. Zhou et al. 2023), PS1-STRM (R. Beck et al. 2021), and Sloan Digital Sky Survey Data Release 12 (SDSS DR12) photo- z catalog (S. Alam et al. 2015).

Table 2. Metrics for Computing Photometry Subscore

GW progenitor	EM signature	pre-detections allowed?	L_{peak} [erg s $^{-1}$]	t_{peak} [days]	Δm [mag day $^{-1}$]
BNS / NS+BH merger	KN	no	$< 10^{43}$	< 4	> 0.1
ssNS merger in $\sim 1 - 10 M_{\odot}$ collapsar disk	KN-in-SN ^a \approx SESN	< 1 day	$[5 \times 10^{41}, 10^{44}]$	< 35	$[-2.0, +0.1]$
ssNS merger in $\sim 10 - 50 M_{\odot}$ collapsar disk	super-KN ^b	< 1 day	$[10^{41}, 10^{43}]$	$[10, 70]$	-
BBH merger in AGN disk	AGN flare	yes	-	-	-

NOTE—Photometry constraints (whether pre-GW detection is allowed, and allowed peak luminosities, rise times, and decay rates), for different classes of EM transient which could accompany a particular GW progenitor. Where left empty with ‘-’, the metric is not usefully constrained by available observations or models.

^aB. D. Metzger et al. (2024) and Y.-X. Chen & B. D. Metzger (2025)

^bD. M. Siegel et al. (2022)

nosity νL_{ν} is computed by converting the flux density F_{ν} at the brightest observed point in the candidate’s lightcurve into the luminosity at the GW luminosity distance. Here, we instead use the same distance prioritization scheme as used in computing the distance score. The GW luminosity distance is used if and only if no host is identified.

Most substantially, the metrics for computing score factors which multiply to generate the $S_{\text{phot},T}$ different classes of transient. We summarize the different photometry metrics in Table 2. These metrics also inform the time up to which we ingest new candidates. Based on predictions for super-KNe, the slowest-rising transient among those considered, we ingest no new candidates with initial detections later than 10 days post-merger. Super-KNe attain at least $\sim 50\%$ of their peak luminosity by this time, though they may continue to rise in brightness. Finally, metrics inform the time window over which we extract photometric quantities. For KNe, we extract rise times and decay rates considering photometry from only the first 25 days post-merger, following J. C. Rastinejad et al. (2022). For KNe-in-SNe and super-KNe, we consider photometry up until 100 days, given the longer timescales of the transients. In all cases, we only use photometry detected at $\geq 5\sigma$.

In the KN-in-SN model (B. D. Metzger et al. 2024; Y.-X. Chen & B. D. Metzger 2025), accretion of the collapsar disk onto the central remnant BH occurs on timescales of seconds to minutes, while merger(s) of ssNSs occur over hours to $\lesssim 1$ day. To account for this possible delay between the beginning of a transient SN and a GW signal, we conservatively allow for predetection of a transient, but no earlier than 1 day pre-merger. We impose the same constraint for super-KNe.

We elaborate on luminosity, rise time, and decay rate metrics for KNe-in-SNe and super-KNe below. For BBH-induced AGN flares, we are unable to set useful

constraints on luminosities, rise times, or decay rates; we discuss the challenges in doing so in Appendix A.

4.4.1. Kilonovae-within-Supernovae

We first identify the classes of SNe to which we will compare. While SNe Ic-BL are frequently coincident with IGRBs and thought to arise at least in part from collapsars (S. E. Woosley & J. S. Bloom 2006), these are not the only SESNe which might be associated with collapsars (S. E. Woosley 1993; A. I. MacFadyen & S. E. Woosley 1999; M. G. Dainotti et al. 2022), so we broaden our horizons and consider SNe Ib, Ic, Ic-BL, and Iib. These SESNe may then be modified by the presence of the high-opacity r -process material from ssNS mergers in the collapsar disk or energy injection from a hierarchically formed millisecond magnetar. However, searches for r -process signatures in SNe Ic-BL (S. Anand et al. 2024) and GRB-SNe (J. C. Rastinejad et al. 2024) have thus far not confirmed the presence of r -process elements, and modeling work is ongoing (*e.g.*, J. Barnes & B. D. Metzger 2022; G. Ricigliano et al. 2025). We therefore simplify our expectations for an EM signature and simply vet for SESNe, but add some buffer to our expected peak luminosities, rise times, and decay rates to account for deviations from standard SESNe. Indeed, we expect KNe-in-SNe to deviate from standard SESNe, and only clear deviations may establish a candidate as more than a normal SESN.

We explore a sample of SESNe to identify broad photometric behavior. Ó. Rodríguez et al. (2023) examine a sample of 191 SESNe, expanding on the samples in J. D. Lyman et al. (2016) and S. J. Prentice et al. (2019). F. Taddia et al. (2019) and G. P. Srinivasaragavan et al. (2024) focus specifically on SNe Ic-BL. Broadly, we find that SESNe peak at bolometric luminosities in the range $L_{\text{bol,peak}} \sim 7 \times 10^{41}$ to 5×10^{43} erg s $^{-1}$, between ~ 3 and ~ 33 days from explosion. SESNe display post-peak decay rates of approximately 0.01 to at steepest

0.1 mag day⁻¹. Finally, they brighten by at most approximately -0.3 mag day⁻¹ before peak.

We use these samples to constrain the luminosity, rise time, and decay rate that we expect of KNe-in-SNe. We note that we have compiled here samples of $L_{\text{bol,peak}}$, the peak bolometric luminosity, but we estimate the peak luminosity with TROVE as $L_{\text{peak}} = \nu L_{\nu}$, where ν is the effective frequency of the filter at the brightest observed point, and $L_{\text{bol}} > \nu L_{\nu}$ by definition. Allowing some buffer on the lower bound due to differences between L_{bol} and νL_{ν} , and on both lower and upper bounds to account for deviations from SESNe, we impose that L_{peak} must lie between 5×10^{41} and 10^{44} erg s⁻¹. Allowing for a slightly earlier or later peak than in typical SESNe, we adopt that the rise time $t_{\text{peak}} < 35$ days. Finally, we apply that the decay rate $\Delta m < 0.1$ mag day⁻¹. We limit how rapidly a candidate may fade (*i.e.*, apply an upper limit on Δm) in vetting for KNe-in-SNe to contrast with vetting for KNe, which requires that the candidate fade sufficiently rapidly. The relevant SESNe (with the exception of the shock-cooling phase in some SNe IIb, which may mimic the rapid decline in KNe) evolve more slowly than isolated KNe, and the KN embedded in the SN might further slow the decline by extending the photospheric phase (J. Barnes & B. D. Metzger 2022). However, to ensure that not all brightening is allowed, we also impose a lower limit on Δm . The compiled samples generally brighten by at most ~ -0.3 mag day⁻¹ in the 10 days pre-peak. We invoke for the sake of example the exceptionally fast-rising SN (II-P) 2018lab, which rises by ~ -1 to -2 mag day⁻¹ in the first day post-explosion (J. Pearson et al. 2023). SNe II-P are not included in our list of SNe in which a KN might be embedded. We therefore finally impose -2 mag day⁻¹ $< \Delta m < +0.1$ mag day⁻¹. This lower limit is conservative and satisfied by all but the most rapidly brightening transients.

These metrics allow us to pick out SESNe spatially and temporally associated with a SSM GW event based on $S_{\text{KN-in-SN}}$ scores. However, a high score alone is not sufficient to establish the presence of a KN embedded in a SESN; high scores motivate follow-up. As modeled in J. Barnes & B. D. Metzger (2022), a clear signature of r -process material from a KN-in-SN would be a near-infrared (NIR) excess at late times, manifesting with colors $r - J$, $r - H$, and $r - K$ in excess of $\approx 1 - 2$, especially after ~ 75 days. r -process material might also shift rise times and extend the photospheric phase of the SN. Comparisons to such models, as conducted in J. C. Rastinejad et al. (2024) and S. Anand et al. (2024), are a promising avenue for assessing whether r -process material is present. These comparisons would benefit

from sustained, multi-band optical/IR monitoring up to late times $\sim 75 - 100$ days, as will be supported by LSST.

4.4.2. Super-Kilonovae

As D. M. Siegel et al. (2022) present the only detailed exploration of optical/IR signatures of collapsars with r -process material enrichment in the relevant mass regime, we rely on their predictions. D. M. Siegel et al. (2022) explore models spanning total ejecta masses of $8.6 - 60.0 M_{\odot}$, with differing proportions of r -process and non- r -process (including ⁵⁶Ni) material. Their bolometric lightcurves peak at $\sim 15 - 60$ days and luminosities $\sim 5 \times 10^{41} - 5 \times 10^{42}$ erg s⁻¹. We thus conservatively impose constraints of 10^{41} erg s⁻¹ $< L_{\text{peak}} < 10^{43}$ erg s⁻¹ and 10 days $< t_{\text{peak}} < 70$ days.

Because the different presented models brighten or fade by factors of $\sim 10 - 100\times$ over several weeks depending on the model, we cannot impose any useful constraints on Δm . These large variations in photometric behavior across models arise from differences in total ejecta mass and the relative proportions of r -process and ⁵⁶Ni ejecta, which yield different radioactive heating rates driving the time evolution of the transient. D. M. Siegel et al. (2022) note that detailed nucleosynthesis calculations could better constrain the composition of the ejecta, and thus this photometric evolution.

These imposed metrics are broad, but select slow-rising candidates at predicted luminosities. Nonetheless, as with KNe-in-SNe, a high score is not sufficient to argue that a candidate is a super-KN, and follow-up is required. D. M. Siegel et al. (2022) compare their predicted bolometric luminosities to a selection of SNe Ia (SN 2011fe), Ic-BL (SN 2002ap), II-P (SN 2013ab), and electron-capture SNe (ECSNe; SN 2018zd). They find that super-KNe do not attain the peak luminosities of SN 2011fe (Ia) nor SN 2018zd (ECSNe), but may masquerade as SNe Ic-BL or II-P at early times $\lesssim 50$ days. Such SNe might thus receive a high super-KN score. Spectra could be a key differentiator, as the spectra of super-KNe are predicted to be redder and display broader absorption features than in SNe due to the presence of faster ($v \sim 0.1c$) outflows and higher-opacity material. Though SNe Ic-BL show similar broad absorption features (M. Modjaz et al. 2016; G. Finneran et al. 2025), these features in super-KNe should emerge at redder wavelengths $\gtrsim 10,000$ Å. We concur that observations of these red spectra and broad absorption features, near peak luminosity ($\sim 10 - 70$ days), are a minimum for identifying a candidate as a potential super-KN.

5. SCORING ALL CANDIDATE COUNTERPARTS TO S251112cm

With our vetting framework, we assign scores to all 248 transients in the localization region of S251112cm with initial detections up to 10 days following the GW alert. We compute final scores using all available information at 100 days. Tables 4 and 5 (Appendix B) contain detailed scores, whether the candidate is detected pre-GW signal, and estimates for luminosities, rise times and decay rates which inform photometry scores, for all candidates. We examine broad trends in scores and our ability to distinguish KNe, KNe-in-SNe, and super-KNe in Section 5.1, and the time evolution of scores in Section 5.2. We highlight candidates of particular interest in Section 5.3. Because only two candidates are associated with AGN, we primarily focus on KNe, KNe-in-SNe, and super-KNe. Throughout, we emphasize that our framework assigning high scores to candidates with limited information is by design, as these are some of the candidates which might have benefited most from follow-up. Indeed, the aim of TROVE is to motivate the follow-up which is necessary to identify a true counterpart.

5.1. Scoring All Candidate Counterparts

In all, 118 of 248 candidates receive an overall score for at least one transient class of ≥ 0.01 . These include 77 candidates for KNe, 96 for KNe-in-SNe, 66 for super-KNe, and 1 for AGN flaring. For some candidates, the overall score is the same across transient classes, especially when photometry is minimal or a distance is not known. Indeed, distance and photometry are the most discriminating factors. By construction, most candidates have 2D localization scores $S_{2D} \geq 0.01$, with a few exceptions for candidates identified with Rubin-LSST. We find that seven candidates are associated with point sources, none are associated with minor planets, and only two (AT 2025adnc and S251112cm_X3) are associated with AGN. These small numbers reflect that many teams already discard minor planets or candidates associated with point sources before reporting them in GCNs or to the TNS.

Many candidates are disqualified due to a potential host galaxy or direct distance measurement that lies outside the GW localization volume. In total, over half (163) of all candidates receive distance scores $S_{\text{dist}} \leq 0.10$, and 57 further below with $S_{\text{dist}} \leq 0.01$. Only 10 candidates have neither a measured redshift nor a known potential host galaxy in our galaxy catalogs, such that distance does not factor into their overall score. The fact that a large number of candidates are disfavored based on existing information is consistent with other

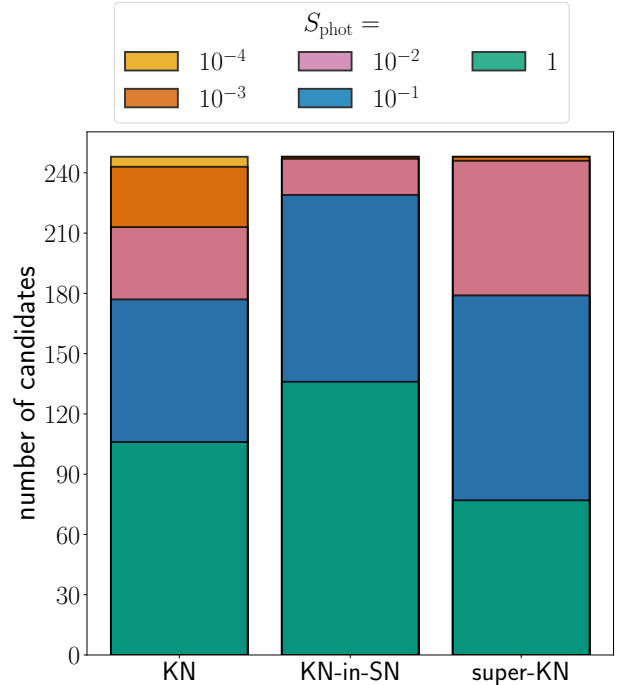


Figure 6. Distributions of KN, KN-in-SN, and super-KN photometry subscores. Relative distributions of photometry subscores reflect the constraining power of the photometry metrics imposed on candidates (Table 2).

works (C. D. Kilpatrick et al. 2021; J. C. Rastinejad et al. 2022). Spectroscopic follow-up provides refined distance estimates (and classifications) for several candidates: nine are directly classified as SNe confidently outside the localization volume, and three candidates’ host galaxies are also found to lie outside the localization volume.

In photometry scoring, we impose the constraints defined in Table 2 to further vet candidates and differentiate between potential transient types. Figure 6 shows the distribution of photometry scores ($S_{\text{phot}} = 1.0, 0.1, 0.01, 0.001, \text{ or } 0.0001$) for each transient type. Overall, 142 candidates receive $S_{\text{phot,KN}} \leq 0.10$, while 112 receive $S_{\text{phot,KN-in-SN}} \leq 0.10$, and 171 receive $S_{\text{phot,super-KN}} \leq 0.10$. These tallies are not mutually exclusive: 70 candidates have photometry scores of 1.0 for all transient types (*i.e.*, are not constrained by photometry), while 20 have photometry scores of 0.1 (weakly constrained by photometry) for all transient types. The relative numbers of candidates in each tier of S_{phot} demonstrate the constraining power of each transient class’ photometry metrics. We observe the following behavior from differing constraints:

- **Pre-detections:** 20 candidates are considered pre-detected by our KN metrics. Since we allow that KNe-in-SNe and super-KNe may be pre-

tected up to 1 day pre-merger, only 14 are pre-detected by KN-in-SN or super-KN metrics.

- **Luminosities:** 112 candidates with $L_{\text{peak}} > 10^{43} \text{ erg s}^{-1}$ are disfavored as KNe or super-KNe. In comparison, only 43 candidates are disfavored as KNe-in-SNe due to the more permissive bounds on their luminosities.
- **Rise times:** 107 candidates have an inferred rise time shorter than 10 days, disfavoring them as super-KNe. Only 53 are disfavored as KNe due to a rise time longer than 4 days, and just 16 are disfavored as KNe-in-SNe due to a rise time longer than 35 days.
- **Decay rates:** 65 candidates are disfavored as KNe due to an inferred $\Delta m < 0.1 \text{ mag day}^{-1}$ (fading too slowly or brightening). 71 candidates are disfavored as KNe-in-SNe due to an inferred $\Delta m > 0.1 \text{ mag day}^{-1}$ (fading too rapidly), and just four have $\Delta m < -2.0 \text{ mag day}^{-1}$.

Summarizing these trends, we find that $S_{\text{phot,KN}}$ scores are largely shaped by luminosities, followed by decay rates, and then rise times. $S_{\text{phot,KN-in-SN}}$ scores are shaped by decay rate estimates, some candidates disfavored due to their luminosities, and a comparatively negligible number due to their rise times. $S_{\text{phot,super-KN}}$ scores are most strongly impacted by rise time estimates, with some contribution from luminosity estimates. Our imposed metrics result in super-KN scores consistently being the same or smaller than KN or KN-in-SN scores for a given candidate. We ascribe these small scores to the significant number of candidates with rise times < 10 days, which reflects observational strategies and the concentration of publicly available photometry at early times, as addressed in the next section.

Despite the different constraining powers of our metrics, overall ranges in scores are comparable for KNe, KNe-in-SNe, and super-KNe. However, we reiterate that a high score alone is not sufficient to establish a candidate as a KN, KN-in-SN, or super-KN, and selecting the highest score among the three is not a tested form of classification. Examining candidates' scores as a function of time can provide further insight.

5.2. Time Evolution of Candidate Scores

Figure 7 shows the time evolution of overall KN, KN-in-SN, and super-KN scores for all 218 optical candidates. We omit Swift-XRT and EP-FXT X-ray sources as these are not reliably detected in optical photome-

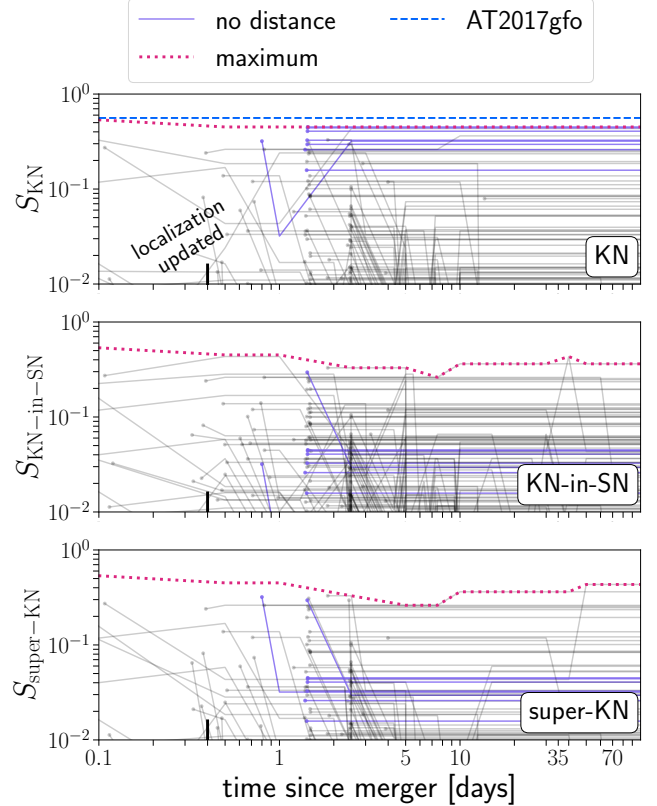


Figure 7. Overall scores as a function of time for all candidate optical counterparts to S251112cm. Each trace tracks the score for one of 218 candidates. Traces begin (as marked with a dot) at the time of first $\geq 5\sigma$ optical detection. Candidates with no distance score due to a lack of direct distance measurement or viable host galaxy are highlighted in purple. The localization region of S251112cm is updated at 0.4 days, but most candidates are discovered after this time. Several candidates are discovered at ~ 1.4 days with DECam (X. J. Hall et al. 2025a) and at ~ 2.4 days with Rubin-LSST (S. Anand et al. 2025a). Candidates for which scores quickly drop are those targeted by spectroscopic follow-up, driving their distance score to ~ 0 when the distance to the candidate or its host is found to lie outside the localization volume. We highlight the final score $S_{\text{KN}} = 0.56$ of AT2017gfo, known KN counterpart to the BNS merger GW170817. The highest score across all candidates at any given time, for a given transient type, is highlighted with a dotted magenta line. This maximum need not correspond to the same candidate at all times (Section 5.2).

try.⁴³ We highlight candidates which have no distance score (purple, solid lines). As a benchmark, we highlight the final score $S_{\text{KN}} = 0.56$ of AT2017gfo, known KN

⁴³ Seven Swift-XRT sources are marginally ($\sim 5\sigma$) detected with ATLAS, but not significantly brighter than limiting magnitudes at adjacent epochs, so these detections may be noise. We claim no optical counterparts to any X-ray sources.

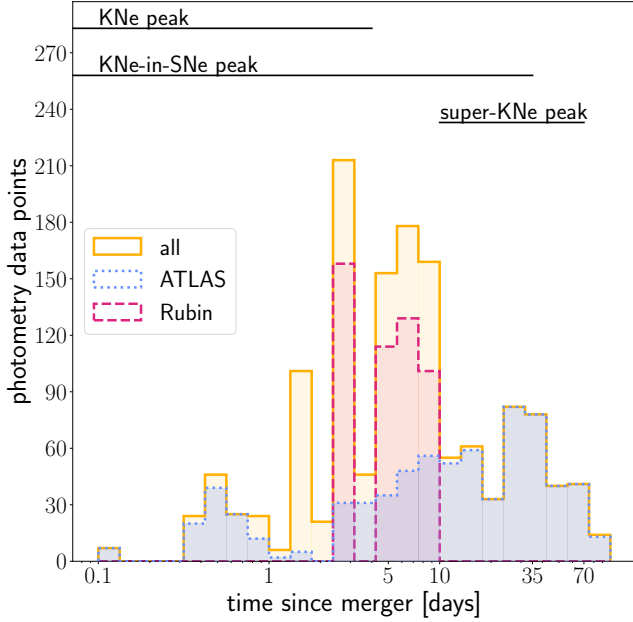


Figure 8. Time distribution of photometry data points acquired for all candidates. We distinguish ATLAS forced photometry (blue), Rubin-LSST photometry (magenta), and the sum of all photometry (yellow). Horizontal lines show the time range over which we expect KNe (up to 4 days), KNe-in-SNe (up to 35 days), and super-KNe (10–70 days) to peak. DECam photometry (X. J. Hall et al. 2025a) dominates at 1.4 days. Rubin-LSST photometry (S. Anand et al. 2025a) dominates at 2.4, 4.4, 6.4, 7.4, and 9.4 days. Beyond 10 days, when super-KNe are predicted to peak, most teams stopped acquiring photometry.

counterpart to BNS merger GW170817 (blue, dashed). Finally, we highlight the highest score (magenta, dotted line), which need not correspond to the same candidate at all times.

Improved GW localization between the LVK’s initial low-latency analysis and refined offline analysis, generally released within just a few days of the initial, can change 2D localization and distance scores for all candidates. For S251112cm, the refined offline analysis was released at 0.4 days. The updated skymap introduces changes in S_{2D} on average ± 0.2 (at most $+0.5$ or -0.4), which propagate to largely negligible differences $\sim \pm 0.01$ in overall scores. Moreover, most candidates are discovered after the release of this refined localization. Spectroscopic follow-up and classification leads twelve candidates’ scores to drop to ~ 0 once these establish the candidates as residing outside the GW localization volume or yield a classification (in most cases, SNIa) inconsistent with predictions. All remaining evolution in scores is then a consequence of acquiring more photometry such that luminosity, rise time, and decay rate estimates evolve. Given the different timescales for the

transients of interest, there is a natural point at which scores stop evolving. S_{KN} is frozen after 25 days as we do not include photometry beyond this time when estimating photometric quantities, following J. C. Rastinejad et al. (2022), while $S_{KN-in-SN}$ and $S_{super-KN}$ may continue to evolve as we fit photometry up to 100 days.

Several candidates with no distance measurement (highlighted in purple in Figure 7) or limited photometry retain high scores at all times. The highest KN score ($S_{KN} = 0.45$) is that of AT2025adoi, a candidate with $S_{2D} = 0.45$ and no distance measurement. In contrast, the $S_{KN-in-SN}$ and $S_{super-KN}$ of AT2025adoi both drop to ≈ 0.05 when a single point of g -band photometry from DECam at 1.4 days (X. J. Hall et al. 2025a) yields an estimated $L_{peak} \approx 3.3 \times 10^{40}$ erg s^{-1} , too faint for either KNe-in-SNe or super-KNe at the GW luminosity distance. Several other candidates (AT2025adnk, AT2025adnm, AT2025adoe, AT2025adoh, AT2025adov, and AT2025adpd) behave similarly, retaining high $S_{KN} \sim 0.20 - 0.50$ but low $S_{KN-in-SN}$ and $S_{super-KN} \sim 0.02 - 0.05$ due to a low peak luminosity estimate based on a single data point. More photometry for these candidates might have revealed brightening or fading.

Candidates with distance measures broadly have lower scores, but many (AT2025adib, AT2025admn, AT2025admt, AT2025admu, AT2025adnf, AT2025adnp, AT2025adnz, AT2025adoa, and AT2025adof) nonetheless retain overall scores $S_{KN} = S_{KN-in-SN} = S_{super-KN} \sim 0.10 - 0.25$ at all times when only one non-constraining photometry detection is available. Four candidates (AT2025adnx, AT2025adod, AT2025ador, AT2025aeco) have $S_{KN-in-SN} \sim 0.05 - 0.15$ and $S_{KN} = S_{super-KN} \sim 0.01 - 0.02$ when a single photometry point coupled with a distance estimate yields an estimated $L_{peak} > 10^{43}$ erg s^{-1} .

Following the dotted magenta line in Figure 7 indicates how the maximum score across all candidates for a given transient type may evolve with time. While AT2025adoi retains the highest S_{KN} at all times, the maximum $S_{KN-in-SN}$ and $S_{super-KN}$ scores evolve, largely for select candidates which are detected with ATLAS forced photometry at late times. For example, AT2025admx briefly has the highest KN-in-SN score ($S_{KN-in-SN} = 0.43$) when an ATLAS c -band detection indicates the lightcurve is largely flat up to 33 days, before an additional ATLAS o -band detection at 44 days hints at a rise time longer than 35 days, causing $S_{KN-in-SN}$ to drop once again. At the same time, AT2025admx’s $S_{super-KN}$ resurges to $S_{super-KN} = 0.43$, the highest super-KN score, due to this late-time brightening. Other candidates show similar evolution, but

these changes are mostly spurious and scores tend to resettle to $\sim 0.01 - 0.05$. These detections at late times are marginal ($\sim 5\sigma$) and surrounded by non-detections at similar or deeper limits at adjacent epochs. Moreover, AT2025admx lies close to the nucleus of its host galaxy, and these detections may be the result of poor image subtraction.

However, Figure 7 also demonstrates that scores do not evolve with time for a majority of candidates. This lack of evolution is due to a dearth of photometry. Notably, 78 candidates have only a single reported photometry data point. Excluding forced photometry obtained with ATLAS increases this number to 111. 5 candidates (AT2025adjn, AT2025adtm, AT2025adto, AT2025adtr, and AT2025adtt) lie in the localization region, but have only $\sim 3\sigma$ ($< 5\sigma$) detections. Photometry is also concentrated at early times. Figure 8 shows the time distribution of all photometry data, highlighting the contributions from Rubin-LSST photometry and ATLAS forced photometry. Initial post-GW detections are dominated by DECam (73 candidates), ATLAS (53), and Rubin-LSST (48), with additional contributions from GOTO-N and GOTO-S (16), ZTF (8), BlackGEM (4), PS2 (4), PS1 (2), and the WFST (1). Taking the ensemble of all post-GW photometry, half is acquired prior to 4.5 days. For the 101 candidates with only a single non-ATLAS data point, half of all photometry is obtained much earlier, prior to 1.5 days. Beyond 10 days, at which times super-KNe are expected to peak, ATLAS is the only survey with publicly accessible data in the localization region. We thus caution that the observed tendency towards shorter rise times and the ensuing impact on scores, especially $S_{\text{super-KN}}$, likely reflects the dearth of publicly available survey data outside of initial GCN and TNS discovery reports.

In contrast, candidates with more sustained photometry show dynamic scores. Rubin-LSST photometry introduces these dynamics for several candidates. Longer-term (\sim weeks to months) and deeper photometry for candidates, as will be supported by regular operations of the LSST, will be critical to constraining transients which evolve more slowly. We highlight a sample of interesting candidates with dynamic and noteworthy scores which might have benefited from this longer-term monitoring in the next section.

5.3. Candidates of Interest

For all 248 candidates, as available, we visually inspect their potential host galaxies, lightcurves, the time evolution of scores, and final scores. We perform this visual inspection post-facto to assess how our vetting performs and highlight candidates of interest; during a

Table 3. Candidates of Interest

candidate	S_{KN}	$S_{\text{KN-in-SN}}$	$S_{\text{super-KN}}$	$S_{\text{AGN-flare}}$
AT2025adhu	0.32	0.00	0.03	0.00
AT2025adin	0.07	0.01	0.01	0.00
AT2025adkm	0.00	0.12	0.01	0.00
AT2025admd	0.00	0.13	0.00	0.00
AT2025ailp	0.02	0.00	0.00	0.00
AT2025ails	0.00	0.11	0.01	0.00
AT2025ailv	0.04	0.01	0.01	0.00
AT2025ailx	0.00	0.05	0.00	0.00
S251112cm_X3	0.00	0.00	0.00	0.13

NOTE—Candidate counterparts of interest, described in Section 5.3. For each candidate, the highest score in the row is bolded. Scores of 0.00 correspond to scores of < 0.005 , which are rounded down to 0.00 given our trust in the precision of our scores.

follow-up campaign, the aim of TROVE is to assist in automating this process. We parse our sample for candidates which we define as interesting for the purposes of this discussion—those with an overall score ≥ 0.01 for at least one transient type and some combination of the following criteria:

1. A distance (to the candidate itself or to its likely host) which lies within or overlaps substantially with the localization volume of S251112cm ($S_{\text{dist}} \gtrsim 0.1$),
2. Sufficient photometry for KN, KN-in-SN, and super-KN scores to differ, and/or,
3. Sufficient photometry for KN, KN-in-SN, and super-KN scores to evolve in some notable way with time.

We highlight nine candidates which meet these criteria in Table 3. Eight receive a notable score for S_{KN} or $S_{\text{KN-in-SN}}$ and show interesting behavior in their lightcurves or scores with time. No candidates reliably receive a $S_{\text{super-KN}}$ score greater than S_{KN} or $S_{\text{KN-in-SN}}$. Unsurprisingly, seven of the eight candidates benefit from Rubin g - and i -band photometry. We discuss broad characteristics of these eight candidates here and provide details, lightcurves, and scores with time for each candidate in Appendix C. As only two candidates are associated with AGN and only one has $S_{\text{AGN-flare}} > 0.01$, we discuss these in Appendix C as well.

Four candidates (AT2025adhu, AT2025adin, AT2025ailp, and AT2025ailv) fare best as KNe. All but AT2025adhu benefit from Rubin-LSST g - and i -band photometry. 2D scores range from $S_{2D} = 0.06$

to 0.70, and all but AT2025adhu (which has no distance score) have distance scores from $S_{\text{dist}} = 0.09$ to 0.23. AT2025adhu, AT2025adin, AT2025ailp, and AT2025ailv receive final scores of $S_{\text{KN}} = 0.32, 0.07, 0.02,$ and $0.04,$ respectively. These candidates fare best as KNe due to the presence of sufficient photometry to establish a luminosity, rise time, and decay rate consistent with KNe. Early rise times and steep decay rates in particular distinguish these candidates' KN scores while lowering KN-in-SN and super-KN scores.

Four candidates (AT2025adkm, AT2025admd, AT2025ails, and AT2025ailx) fare best as KNe-in-SNe. These candidates all benefit from Rubin-LSST photometry. 2D scores range from $S_{2\text{D}} = 0.45$ to 0.98, and distance scores from $S_{\text{dist}} = 0.05$ to 0.23. AT2025adkm, AT2025admd, AT2025ails, and AT2025ailx receive final scores of $S_{\text{KN-in-SN}} = 0.12, 0.13, 0.11,$ and $0.05,$ respectively. Lightcurves are somewhat consistent with being flat or hint at slow fading or brightening, consistent with KNe-in-SNe in the time window explored and inconsistent with KNe. Whether any of these candidates brightened beyond 10 days is unknown, such that rise times are estimated as <10 days, disfavoring these candidates as super-KNe.

Long-term photometry and spectroscopic follow-up of these candidates of interest could have clarified their nature. Further monitoring of fading candidates with notable S_{KN} could have better constrained decay rates to determine whether they were genuinely consistent with KNe and inconsistent with other transient types. Monitoring past 10 days could have identified whether the other candidates were brightening or displaying a plateau in their lightcurves. If this monitoring established a rise time ≥ 10 days for any of these candidates, such candidates would no longer be disfavored as super-KNe, and some might have shown $S_{\text{super-KN}}$ larger than S_{KN} or $S_{\text{KN-in-SN}}$. Moreover, seven of eight candidates (all but AT2025adhu, for which we identify no viable host) have host galaxies with uncertain photometric redshifts. Obtaining a spectrum of the candidate or its host might have yielded a distance and potentially a classification. Unfortunately, at time of writing (March 2026), three candidates (AT2025admd, AT2025ailv, AT2025ailx) lie within a few degrees of the Sun, four (AT2025adin, AT2025adkm, AT2025ailp, AT2025ails) are at declinations $\sim -35^\circ$ to -55° and not feasibly observable with telescopes at our disposal in the Northern hemisphere, and one (AT2025adhu) has no viable host galaxy.

The behavior of these candidates and their scores with time may motivate future search and follow-up strategies for SSM GW events. If a monitored candidate retains a

high $S_{\text{KN-in-SN}}$ beyond ~ 10 days, spectroscopic follow-up could be used to obtain a distance to the candidate or its putative host galaxy. If a candidate spectrum is obtained, this should confirm whether it is a SESN, and whether the candidate lies in the localization volume. If a SESN at a distance consistent with the GW luminosity distance, one could search for signatures of a KN embedded in the SN. The clearest signature would be the predicted NIR excess at late times, after peak, which could manifest with colors $r - J, r - H,$ or $r - K \approx 1 - 2$ (J. Barnes & B. D. Metzger 2022). To search for super-KNe, if the candidate lies within the GW localization volume and monitoring yields a high score $S_{\text{super-KN}}$ based on luminosities and a rise time longer than 10 days, spectra acquired near peak could be examined for broad absorption features emitted in the NIR ($\gtrsim 10,000 \text{ \AA}$; D. M. Siegel et al. 2022). These strategies are complementary: both require spectroscopic follow-up of promising candidates beyond 10 days. This follow-up would of course require late-time triggers, as are currently infrequently employed in searches for KNe only.

6. CONCLUSIONS

We introduce a framework for ranking candidate EM counterparts to GW events involving one or more SSM objects. Taking a census of current literature, we identify KNe, KNe-in-SNe, super-KNe, and BBH merger-induced AGN flaring as the EM signatures which might accompany SSM GW events. Our framework vets candidates in search of any among this zoo of transients. We apply this new framework to S251112cm: the first statistically significant event reported by the LVK to contain at least one object with subsolar mass. We deploy a suite of telescopes to search for and follow up on candidate counterparts to S251112cm. Using our own optical photometry and the publicly available observations of the broader community, we vet and assign scores to 248 candidates with our new metrics in TROVE.

Our vetting framework is designed to inform optimal follow-up and help distinguish between KNe, SESNe which might host KNe, and super-KNe, based on candidates' estimated luminosities, rise times, and decay rates. Distinguishing between classes of transient is challenging when photometry is limited or not constraining. In these cases, distance estimates are critical, but many distances come from highly uncertain photometric redshifts of candidates' potential host galaxies. Fortunately, future DESI data releases will be a massive boon to determining reliable spectroscopic redshifts. Candidates which nonetheless retain high scores due to a lack of information are high-priority targets for follow-up. These high-scoring candidates were the target of our fol-

low up efforts, and we reported our own observations to the community in near-real time. Given the impact of limited information (*e.g.*, uncertain distances or a dearth of constraining photometry) in setting these high scores, in future work, we will explore the possibility of quantifying the uncertainty or confidence associated with a score. At the same time, we will aim to quantify the relative importance of different subscores.

An important result of our census of the literature is that KNe may not be the only, nor even the most likely, EM counterparts to GW events involving subsolar mass compact objects. Searches for counterparts to these events should therefore employ strategies which consider all potential EM counterparts. Many of these counterparts evolve on longer timescales than KNe, motivating longer-term monitoring than is currently employed in search of KNe only. Regular operations of Rubin’s LSST will support this sustained monitoring. However, more modeling of the transients of interest is also required, to refine photometric constraints and better define their observability and definitive signatures. KNe-in-SNe, super-KNe, and BBH-induced AGN flares are all hitherto unobserved transients. More broadly, further investigation into formation channels for ssNSs/ssBHs could identify other potential EM signatures.

Finally, we highlight that incorporating photometry from Rubin-LSST increases the number of candidate counterparts to S251112cm from 181 to 248. This dramatic increase underscores the need for efficient tools to vet candidate counterparts. With the LVK envisioning an observing run (IR1) in late 2026 and observing runs in the coming years, the era of GW follow-up supported by Rubin is imminent. To enable effective prioritization of photometric and spectroscopic follow-up in this era, the vetting framework introduced in this work will be included in the forthcoming public release of TROVE.

ACKNOWLEDGMENTS

We thank the observing teams and technical staff of the Mt. Lemmon telescope operated under the Catalina Sky Survey, the T80-South telescope at Cerro Tololo Inter-American Observatory, Chilean and Australian telescopes of DLT40, the MMT and its Binospec spectrograph, the Southern Astrophysical Research Telescope and its Goodman spectrograph, and the Bok telescope and its Boller & Chivens spectrograph. The Catalina Sky Survey is funded under NASA grant #80NSSC24K1187. Time-domain research by the University of Arizona team and D.J.S. is supported by National Science Foundation (NSF) grants 2308181,

2407566, and 2432036 and the Heising-Simons Foundation under grant #2020-1864.

We thank the Rubin observing team for conducting a search in the localization region S251112cm in November 2025, *before* Rubin entered regular operations. We are grateful to the Transients and Variable Stars - Multi-Messenger Astronomy (TVS-MMA) working group for the role they played in planning these ToO observations, which greatly benefited this work. We also thank Ish Gupta and Chris Fryer for fruitful discussions on SSM GW events and potential progenitors and EM signatures.

The TROVE team gratefully acknowledges support by the National Science Foundation under grant Nos. AST-2432037 and AST-2432036. N.V. gratefully acknowledges funding from the Natural Sciences and Engineering Research Council of Canada (NSERC) Postdoctoral Fellowship No. 599555. N.F. acknowledges support from the National Science Foundation Graduate Research Fellowship Program under Grant No. DGE-2137419. C.D.K. gratefully acknowledges support from the NSF through AST-2432037, the HST Guest Observer Program through HST-SNAP-17070 and HST-GO-17706, and from JWST Archival Research through JWST-AR-6241 and JWST-AR-5441. W.F. gratefully acknowledges support by the David and Lucile Packard Foundation, the Research Corporation for Science Advancement through Cottrell Scholar Award #28284, and the National Science Foundation under grant Nos. AST-2206494, AST-2308182, and CAREER grant No. AST-2047919. J.C.R. was supported by NASA through the NASA Hubble Fellowship grant #HST-HF2-51587.001-A awarded by the Space Telescope Science Institute, which is operated by the Association of Universities for Research in Astronomy, Inc., for NASA, under contract NAS5-26555. M.S. acknowledges funding from the Australian Research Council (ARC) Centre of Excellence CE230100016. H.B. acknowledges the financial support from ANID NATIONAL SCHOLARSHIPS/DOCTORATE 21241862. O.R. acknowledges support from the Rubin-Chile Fund under grant DIA2650, from the ANID Millennium Institute of Astrophysics (MAS) under grant ICN12_009, and from ANID/FONDECYT grant 1251692. V.P. acknowledges support from NASA grant 80NSSC24K0771 and NSF grant PHY-2145421. A.G. acknowledges support from the Steward Observatory Fellowship in Theoretical and Computational Astrophysics, the IAU-Gruber Fellowship, and the CHE Fellowship. M.S.S. acknowledges support from the University of Zurich (UZH) and the Swiss National Science Foundation (SNSF) under grant number 10002981. J.Q.V. is supported by the Euro-

pean Union (ERC, Starstruck, 101095973) and the IAU-Gruber foundation. K.S. acknowledges funding from NSERC.

Facilities: Bok (B&C), CTIO:PROMPT (DLT40), Meckering:PROMPT (DLT40), MMT (Binospec), SO:1.5m (CSS); SOAR (Goodman), S-PLUS (T80-South)

Software: Astropy (Astropy Collaboration et al. 2013, 2018, 2022), astropy-healpix (Astropy Collaboration et al. 2022), astroquery (A. Ginsburg et al. 2019), Astro-SCRAPPY (C. McCully et al. 2018), Beautiful Soup (L. Richardson 2023), Binospec IDL Pipeline (J. Kinsky et al. 2019), CASA (J. P. McMullin et al. 2007; CASA Team et al. 2022), crispy-bootstrap4 (D. Smith 2022), dateutil (G. Niemeyer et al. 2021), Django (Django Software Foundation 2023), django-bootstrap4 (D. Verheul 2021), django-crispy-forms (M. Araujo 2023), Django Extensions (M. Trier & B. van Oostveen 2023), Django Filter (C. Gibson 2021), django-gravatar (T. Waddington 2020), django-guardian (L. Balcerzak 2021), Django REST Framework (T. Christie 2022), django-webpack-loader (O. Lone 2022), dustmaps G. Green (2018), fastavro (M. Tebeka 2022), Flask (Pallets Projects 2022), Flask-SQLAlchemy (Pallets Projects 2021), fundamentals (D. Young 2023), gracedb-sdk (L. Singer 2022), HEALPix Alchemy (L. P. Singer et al. 2022), healpy (A. Zonca et al. 2019), Hop

Client (P. Godwin 2022), Hopskotch (SciMMA Project 2023), IRAF (D. Tody 1986, 1993), Light Curve Fitting (G. Hosseinzadeh & S. Gomez 2022), ligo.skymap (L. P. Singer & L. R. Price 2016), lmfit (M. Newville et al. 2023), Apache Kafka (Apache Software Foundation 2023), Matplotlib (J. D. Hunter 2007), MOCPy (M. Baumann et al. 2023), NumPy (C. R. Harris et al. 2020), paramiko (J. Forcier 2023), photutils (L. Bradley et al. 2022), pillow (A. Murray et al. 2023), plotly.py (Plotly 2023), PostgreSQL (PostgreSQL Global Development Group 2022), psycopg (F. Di Gregorio & D. Varrazzo 2023), Python-Markdown (M. Stienstra et al. 2023), Q3C (S. Kuposov & O. Bartunov 2006), redback (N. Sarin et al. 2024), requests (K. Reitz 2023), SAGUARO Pipeline (K. Paterson et al. 2023), SAGUARO TOM (G. Hosseinzadeh et al. 2023), SASSy Q3C Models (P. N. Daly et al. 2023), SciPy (P. Virtanen et al. 2020), setuptools (Python Packaging Authority 2023), sip_tpv (D. L. Shupe et al. 2012), Source Extractor (E. Bertin & S. Arnouts 1996, 2010), SNID-SAGE (F. Stoppa in prep., 2025), specutils (N. Earl et al. 2023), SQLAlchemy (M. Bayer 2012), SWarp (E. Bertin 2010), TOM Toolkit (D. Collom et al. 2020; W. Lindstrom et al. 2022), tom-alertstreams (TOM Toolkit Project & W. Lindstrom 2023), tom_nonlocalizedevents (TOM Toolkit Project et al. 2023), urllib3 (A. Petrov et al. 2023), voevent-parse (T. D. Staley 2014), Watchdog (Y. Mangalapilly 2023)

REFERENCES

- Abac, A. G., Abouelfettouh, I., Acernese, F., et al. 2025, ApJL, 995, L18, doi: [10.3847/2041-8213/ae0c06](https://doi.org/10.3847/2041-8213/ae0c06)
- Abbott, B. P., Abbott, R., Abbott, T. D., et al. 2018, Living Reviews in Relativity, 21, 3, doi: [10.1007/s41114-018-0012-9](https://doi.org/10.1007/s41114-018-0012-9)
- Abbott, R., Abbott, T. D., Abraham, S., et al. 2020, ApJL, 896, L44, doi: [10.3847/2041-8213/ab960f](https://doi.org/10.3847/2041-8213/ab960f)
- Abbott, R., Abbott, T. D., Acernese, F., et al. 2023, Physical Review X, 13, 041039, doi: [10.1103/PhysRevX.13.041039](https://doi.org/10.1103/PhysRevX.13.041039)
- Acernese, F., Agathos, M., Ain, A., et al. 2023, Classical and Quantum Gravity, 40, 185006, doi: [10.1088/1361-6382/acd92d](https://doi.org/10.1088/1361-6382/acd92d)
- Ackley, K., Godson, B., O’Neill, D., et al. 2025, GRB Coordinates Network, 42658, 1
- Alam, S., Albareti, F. D., Allende Prieto, C., et al. 2015, ApJS, 219, 12, doi: [10.1088/0067-0049/219/1/12](https://doi.org/10.1088/0067-0049/219/1/12)
- Alford, J. A. J., & Halpern, J. P. 2023, ApJ, 944, 36, doi: [10.3847/1538-4357/acaf55](https://doi.org/10.3847/1538-4357/acaf55)
- Ali-Haïmoud, Y., Kovetz, E. D., & Kamionkowski, M. 2017, PhRvD, 96, 123523, doi: [10.1103/PhysRevD.96.123523](https://doi.org/10.1103/PhysRevD.96.123523)
- Alléné, C., Aubin, F., Bentara, I., et al. 2025, Classical and Quantum Gravity, 42, 105009, doi: [10.1088/1361-6382/add234](https://doi.org/10.1088/1361-6382/add234)
- Anand, S., Barnes, J., Yang, S., et al. 2024, ApJ, 962, 68, doi: [10.3847/1538-4357/ad11df](https://doi.org/10.3847/1538-4357/ad11df)
- Anand, S., MacBride, S., Wood-Vasey, M., et al. 2025a, GRB Coordinates Network, 43257, 1
- Anand, S., Stein, R., Hall, X. J., et al. 2025b, GRB Coordinates Network, 42677, 1
- Andreoni, I., Margutti, R., Salafia, O. S., et al. 2022, ApJS, 260, 18, doi: [10.3847/1538-4365/ac617c](https://doi.org/10.3847/1538-4365/ac617c)
- Apache Software Foundation. 2023, Apache Kafka v3.5.1, <https://kafka.apache.org/>
- Araujo, M. 2023, django-crispy-forms v2.0., GitHub <https://github.com/django-crispy-forms/django-crispy-forms>
- Arcavi, I., Hosseinzadeh, G., Brown, P. J., et al. 2017, ApJL, 837, L2, doi: [10.3847/2041-8213/aa5be1](https://doi.org/10.3847/2041-8213/aa5be1)

- Ashton, G., Ackley, K., Hernandez, I. M., & Piotrkowski, B. 2021, *Classical and Quantum Gravity*, 38, 235004, doi: [10.1088/1361-6382/ac33bb](https://doi.org/10.1088/1361-6382/ac33bb)
- Astropy Collaboration, Robitaille, T. P., Tollerud, E. J., et al. 2013, *A&A*, 558, A33, doi: [10.1051/0004-6361/201322068](https://doi.org/10.1051/0004-6361/201322068)
- Astropy Collaboration, Price-Whelan, A. M., Sipőcz, B. M., et al. 2018, *AJ*, 156, 123, doi: [10.3847/1538-3881/aabc4f](https://doi.org/10.3847/1538-3881/aabc4f)
- Astropy Collaboration, Price-Whelan, A. M., Lim, P. L., et al. 2022, *ApJ*, 935, 167, doi: [10.3847/1538-4357/ac7c74](https://doi.org/10.3847/1538-4357/ac7c74)
- Avara, M. J., Krolik, J. H., Campanelli, M., et al. 2024, *ApJ*, 974, 242, doi: [10.3847/1538-4357/ad5bda](https://doi.org/10.3847/1538-4357/ad5bda)
- Bala, S., Jameson, A., & Fermi-GBM Team. 2025, GRB Coordinates Network, 42655, 1
- Balcerzak, L. 2021, *django-guardian v2.4.0.*, GitHub <https://github.com/django-guardian/django-guardian>
- Barker, B. L., Harris, C. E., Warren, M. L., O'Connor, E. P., & Couch, S. M. 2022, *ApJ*, 934, 67, doi: [10.3847/1538-4357/ac77f3](https://doi.org/10.3847/1538-4357/ac77f3)
- Barnes, J., & Metzger, B. D. 2022, *ApJL*, 939, L29, doi: [10.3847/2041-8213/ac9b41](https://doi.org/10.3847/2041-8213/ac9b41)
- Baumann, M., Manon, Pineau, F.-X., et al. 2023, *cds-astro/mocpy v0.13.0.*, Zenodo doi: [10.5281/zenodo.8297730](https://doi.org/10.5281/zenodo.8297730)
- Bayer, M. 2012, in *The architecture of open source applications volume II: Structure, scale, and a few more fearless hacks*, ed. A. Brown & G. Wilson (Mountain View: aosabook.org). <http://aosabook.org/en/sqlalchemy.html>
- Beck, R., Szapudi, I., Flewelling, H., et al. 2021, *MNRAS*, 500, 1633, doi: [10.1093/mnras/staa2587](https://doi.org/10.1093/mnras/staa2587)
- Bertin, E. 2010, *SWarp: Resampling and Co-adding FITS Images Together.*, Astrophysics Source Code Library, record ascl:1010.068
- Bertin, E., & Arnouts, S. 1996, *A&AS*, 117, 393, doi: [10.1051/aas:1996164](https://doi.org/10.1051/aas:1996164)
- Bertin, E., & Arnouts, S. 2010, *SExtractor: Source Extractor.*, Astrophysics Source Code Library <http://ascl.net/1010.064>
- Bianco, F. B., Ivezić, Ž., Jones, R. L., et al. 2022, *ApJS*, 258, 1, doi: [10.3847/1538-4365/ac3e72](https://doi.org/10.3847/1538-4365/ac3e72)
- Bloom, J. S., Kulkarni, S. R., & Djorgovski, S. G. 2002, *The Astronomical Journal*, 123, 1111, doi: [10.1086/338893](https://doi.org/10.1086/338893)
- Bommireddy, H., Cartier, R., Olivares, F., & Dark Energy Survey Gravitational Wave Spectroscopy Team. 2025, GRB Coordinates Network, 42796, 1
- Bommireddy, H., Forster, F., McMahon, I., et al. 2026, *arXiv e-prints*, arXiv:2603.04342, doi: [10.48550/arXiv.2603.04342](https://doi.org/10.48550/arXiv.2603.04342)
- Bradley, L., Sipőcz, B., Robitaille, T., et al. 2022, *Astropy/Photutils v1.5.0.*, Zenodo doi: [10.5281/zenodo.6825092](https://doi.org/10.5281/zenodo.6825092)
- Bright, J. C., & Paschalidis, V. 2023, *MNRAS*, 520, 392, doi: [10.1093/mnras/stad091](https://doi.org/10.1093/mnras/stad091)
- Bucciantini, N., Metzger, B. D., Thompson, T. A., & Quataert, E. 2012, *MNRAS*, 419, 1537, doi: [10.1111/j.1365-2966.2011.19810.x](https://doi.org/10.1111/j.1365-2966.2011.19810.x)
- Buikema, A., Cahillane, C., Mansell, G. L., et al. 2020, *PhRvD*, 102, 062003, doi: [10.1103/PhysRevD.102.062003](https://doi.org/10.1103/PhysRevD.102.062003)
- Burkhanov, O., Rajabov, Y., Tillayev, Y., et al. 2025, GRB Coordinates Network, 42698, 1
- Cabrera, T., Palmese, A., Hu, L., et al. 2024, *PhRvD*, 110, 123029, doi: [10.1103/PhysRevD.110.123029](https://doi.org/10.1103/PhysRevD.110.123029)
- Carr, B., Kohri, K., Sendouda, Y., & Yokoyama, J. 2021, *Reports on Progress in Physics*, 84, 116902, doi: [10.1088/1361-6633/ac1e31](https://doi.org/10.1088/1361-6633/ac1e31)
- CASA Team, Bean, B., Bhatnagar, S., et al. 2022, *Publications of the Astronomical Society of the Pacific*, 134, 114501, doi: [10.1088/1538-3873/ac9642](https://doi.org/10.1088/1538-3873/ac9642)
- Chen, X., Wang, S., Deng, L., et al. 2020, *ApJS*, 249, 18, doi: [10.3847/1538-4365/ab9cae](https://doi.org/10.3847/1538-4365/ab9cae)
- Chen, Y.-X., & Metzger, B. D. 2025, *The Astrophysical Journal*, 991, L22, doi: [10.3847/2041-8213/ae045d](https://doi.org/10.3847/2041-8213/ae045d)
- Christie, T. 2022, *Django REST Framework v3.14.0.*, GitHub <https://github.com/encode/django-rest-framework>
- Christy, C. T., Jayasinghe, T., Stanek, K. Z., et al. 2023, *Monthly Notices of the Royal Astronomical Society*, 519, 5271, doi: [10.1093/mnras/stac3801](https://doi.org/10.1093/mnras/stac3801)
- Clemens, J. C., Crain, J. A., & Anderson, R. 2004, in *Society of Photo-Optical Instrumentation Engineers (SPIE) Conference Series*, Vol. 5492, *Ground-based Instrumentation for Astronomy*, ed. A. F. M. Moorwood & M. Iye, 331–340, doi: [10.1117/12.550069](https://doi.org/10.1117/12.550069)
- Collom, D., Lindstrom, L., Riba, A., et al. 2020, *The TOM Toolkit v2.0.0.*, Zenodo doi: [10.5281/zenodo.4437764](https://doi.org/10.5281/zenodo.4437764)
- Cook, D. O., Mazzarella, J. M., Helou, G., et al. 2023, *ApJS*, 268, 14, doi: [10.3847/1538-4365/acdd06](https://doi.org/10.3847/1538-4365/acdd06)
- Coughlin, M. W., Bloom, J. S., Nir, G., et al. 2023, *The Astrophysical Journal Supplement Series*, 267, 31, doi: [10.3847/1538-4365/acdee1](https://doi.org/10.3847/1538-4365/acdee1)
- Coulter, D. A., Jones, D. O., McGill, P., et al. 2023, *PASP*, 135, 064501, doi: [10.1088/1538-3873/acd662](https://doi.org/10.1088/1538-3873/acd662)
- Coulter, D. A., Kilpatrick, C. D., Jones, D. O., et al. 2025, *ApJ*, 988, 169, doi: [10.3847/1538-4357/ade0b3](https://doi.org/10.3847/1538-4357/ade0b3)
- Cowan, J. J., Sneden, C., Lawler, J. E., et al. 2021, *Reviews of Modern Physics*, 93, 015002, doi: [10.1103/RevModPhys.93.015002](https://doi.org/10.1103/RevModPhys.93.015002)

- Dainotti, M. G., De Simone, B., Islam, K. M., et al. 2022, *ApJ*, 938, 41, doi: [10.3847/1538-4357/ac8b77](https://doi.org/10.3847/1538-4357/ac8b77)
- Daly, P. N., Bostroem, K. A., & Hosseinzadeh, G. 2023, *SASSy Q3C Models v1.4.0.*, Zenodo doi: [10.5281/zenodo.8436176](https://doi.org/10.5281/zenodo.8436176)
- Dálya, G., Díaz, R., Bouchet, F. R., et al. 2022, *MNRAS*, 514, 1403, doi: [10.1093/mnras/stac1443](https://doi.org/10.1093/mnras/stac1443)
- Darc, P., Bom, C. R., Kilpatrick, C. D., et al. 2025, *PhRvD*, 112, 063019, doi: [10.1103/6rg8-2xxz](https://doi.org/10.1103/6rg8-2xxz)
- Deng, C.-M., Cai, Y., Wu, X.-F., & Liang, E.-W. 2018, *PhRvD*, 98, 123016, doi: [10.1103/PhysRevD.98.123016](https://doi.org/10.1103/PhysRevD.98.123016)
- DESI Collaboration, Abdul-Karim, M., Adame, A. G., et al. 2025, arXiv e-prints, arXiv:2503.14745, doi: [10.48550/arXiv.2503.14745](https://doi.org/10.48550/arXiv.2503.14745)
- Di Gregorio, F., & Varrazzo, D. 2023, *Psychopg v2.9.6.*, GitHub <https://github.com/psychopg/psychopg2>
- Django Software Foundation. 2023, *Django v4.2.*, GitHub <https://github.com/django/django/>
- Doroshenko, V., Suleimanov, V., Pühlhofer, G., & Santangelo, A. 2022, *Nature Astronomy*, 6, 1444, doi: [10.1038/s41550-022-01800-1](https://doi.org/10.1038/s41550-022-01800-1)
- Earl, N., Tollerud, E., O'Steen, R., et al. 2023, *astropy/specutils v1.11.0.*, Zenodo doi: [10.5281/zenodo.8049033](https://doi.org/10.5281/zenodo.8049033)
- East, W. E., Paschalidis, V., & Pretorius, F. 2015, *The Astrophysical Journal*, 807, L3, doi: [10.1088/2041-8205/807/1/L3](https://doi.org/10.1088/2041-8205/807/1/L3)
- Ennoggi, L., Campanelli, M., Zlochower, Y., et al. 2025, *PhRvD*, 112, 063009, doi: [10.1103/yc25-v1q4](https://doi.org/10.1103/yc25-v1q4)
- Eyles-Ferris, R. A. J., Jonker, P. G., Levan, A. J., et al. 2025, *ApJL*, 988, L14, doi: [10.3847/2041-8213/ade1d9](https://doi.org/10.3847/2041-8213/ade1d9)
- Fabricant, D., Fata, R., Epps, H., et al. 2019, *PASP*, 131, 075004, doi: [10.1088/1538-3873/ab1d78](https://doi.org/10.1088/1538-3873/ab1d78)
- Finneran, G., Cotter, L., & Martin-Carrillo, A. 2025, *A&A*, 700, A200, doi: [10.1051/0004-6361/202453047](https://doi.org/10.1051/0004-6361/202453047)
- Flesch, E. W. 2023, *The Open Journal of Astrophysics*, 6, 49, doi: [10.21105/astro.2308.01505](https://doi.org/10.21105/astro.2308.01505)
- Forcier, J. 2023, *Paramiko 3.1.0.*, GitHub <https://github.com/paramiko/paramiko>
- Franz, N., Alexander, K., & Gomez, S. 2026a, *The Journal of Open Source Software*, 11, 9516, doi: [10.21105/joss.09516](https://doi.org/10.21105/joss.09516)
- Franz, N., Subrayan, B., Kilpatrick, C. D., et al. 2025a, arXiv e-prints, arXiv:2510.17104, doi: [10.48550/arXiv.2510.17104](https://doi.org/10.48550/arXiv.2510.17104)
- Franz, N., Vieira, N., Kilpatrick, C. D., et al. 2025b, *GRB Coordinates Network*, 42675, 1
- Franz, N., Alexander, K. D., Gomez, S., et al. 2026b, *ApJ*, 999, 243, doi: [10.3847/1538-4357/ae346e](https://doi.org/10.3847/1538-4357/ae346e)
- Gaia Collaboration, Vallenari, A., Brown, A. G. A., et al. 2023, *A&A*, 674, A1, doi: [10.1051/0004-6361/202243940](https://doi.org/10.1051/0004-6361/202243940)
- Gassert, J., Busmann, M., Hall, X. J., et al. 2025, *GRB Coordinates Network*, 42674, 1
- Gibson, C. 2021, *Django Filter v21.1.*, GitHub <https://github.com/carltongibson/django-filter>
- Gillanders, J. H., Rhodes, L., Srivastav, S., et al. 2024, *ApJL*, 969, L14, doi: [10.3847/2041-8213/ad55cd](https://doi.org/10.3847/2041-8213/ad55cd)
- Gillanders, J. H., Huber, M. E., Nicholl, M., et al. 2025, *Pan-STARRS follow-up of the gravitational-wave event S250818k and the lightcurve of SN 2025ulz*, arXiv, doi: [10.48550/arXiv.2510.01142](https://doi.org/10.48550/arXiv.2510.01142)
- Gillanders, J. H., Smartt, S. J., Smith, K. W., et al. 2025a, *GRB Coordinates Network*, 42666, 1
- Gillanders, J. H., Aryan, A., Chen, T.-W., et al. 2025b, *GRB Coordinates Network*, 42825, 1
- Ginsburg, A., Sipőcz, B. M., Brasseur, C. E., et al. 2019, *AJ*, 157, 98, doi: [10.3847/1538-3881/aafc33](https://doi.org/10.3847/1538-3881/aafc33)
- Godwin, P. 2022, *Hop Client v0.8.0.*, GitHub <https://github.com/scimma/hop-client>
- Gold, R., Paschalidis, V., Ruiz, M., et al. 2014, *PhRvD*, 90, 104030, doi: [10.1103/PhysRevD.90.104030](https://doi.org/10.1103/PhysRevD.90.104030)
- Graham, M. J., Ford, K. E. S., McKernan, B., et al. 2020, *PhRvL*, 124, 251102, doi: [10.1103/PhysRevLett.124.251102](https://doi.org/10.1103/PhysRevLett.124.251102)
- Graham, M. J., McKernan, B., Ford, K. E. S., et al. 2023, *ApJ*, 942, 99, doi: [10.3847/1538-4357/aca480](https://doi.org/10.3847/1538-4357/aca480)
- Green, G. 2018, *The Journal of Open Source Software*, 3, 695, doi: [10.21105/joss.00695](https://doi.org/10.21105/joss.00695)
- Grichener, A. 2025, *Ap&SS*, 370, 11, doi: [10.1007/s10509-025-04402-1](https://doi.org/10.1007/s10509-025-04402-1)
- Groot, P. J., Tranin, H., van Roestel, J., et al. 2025, *GRB Coordinates Network*, 42663, 1
- Hall, X. J., Cabrera, T., Gassert, J., et al. 2025a, *GRB Coordinates Network*, 42691, 1
- Hall, X. J., Busmann, M., Koehn, H., et al. 2025b, arXiv e-prints, arXiv:2510.24620, doi: [10.48550/arXiv.2510.24620](https://doi.org/10.48550/arXiv.2510.24620)
- Hall, X. J., Palmese, A., O'Connor, B., et al. 2025c, arXiv e-prints, arXiv:2510.23723, doi: [10.48550/arXiv.2510.23723](https://doi.org/10.48550/arXiv.2510.23723)
- Hanna, C., Kennington, J., Niu, W., et al. 2025, *PhRvD*, 112, 044013, doi: [10.1103/c97v-bmj8](https://doi.org/10.1103/c97v-bmj8)
- Harris, C. R., Millman, K. J., van der Walt, S. J., et al. 2020, *Natur*, 585, 357, doi: [10.1038/s41586-020-2649-2](https://doi.org/10.1038/s41586-020-2649-2)
- Hello, P., Akl, D., Antier, S., et al. 2025, *GRB Coordinates Network*, 42699, 1
- Hiramatsu, H., Sugita, S., Serino, M., et al. 2025, *GRB Coordinates Network*, 42659, 1

- Hosseinzadeh, G., & Gomez, S. 2022, Light Curve Fitting v0.7.0., Zenodo doi: [10.5281/zenodo.4312178](https://doi.org/10.5281/zenodo.4312178)
- Hosseinzadeh, G., Rastinejad, J., & Shrestha, M. 2023, SAGUARO Target and Observation Manager v1.0.0., Zenodo doi: [10.5281/zenodo.8436090](https://doi.org/10.5281/zenodo.8436090)
- Hosseinzadeh, G., Paterson, K., Rastinejad, J. C., et al. 2024, ApJ, 964, 35, doi: [10.3847/1538-4357/ad2170](https://doi.org/10.3847/1538-4357/ad2170)
- Hunter, J. D. 2007, CSE, 9, 90, doi: [10.1109/MCSE.2007.55](https://doi.org/10.1109/MCSE.2007.55)
- Ivezić, Ž., Kahn, S. M., Tyson, J. A., et al. 2019, ApJ, 873, 111, doi: [10.3847/1538-4357/ab042c](https://doi.org/10.3847/1538-4357/ab042c)
- Jeong, M., Im, M., Chang, S.-W., et al. 2025, GRB Coordinates Network, 42867, 1
- Jonker, P. G., Levan, A. J., Liu, X., et al. 2026, MNRAS, 545, staf2021, doi: [10.1093/mnras/staf2021](https://doi.org/10.1093/mnras/staf2021)
- Kansky, J., Chilingarian, I., Fabricant, D., et al. 2019, PASP, 131, 075005, doi: [10.1088/1538-3873/ab1ceb](https://doi.org/10.1088/1538-3873/ab1ceb)
- Kasliwal, M. M., Ahumada, T., Stein, R., et al. 2025, ApJL, 995, L59, doi: [10.3847/2041-8213/ae2000](https://doi.org/10.3847/2041-8213/ae2000)
- Kerr, M., Cheung, C. C., Woolf, R., et al. 2025, GRB Coordinates Network, 42746, 1
- Khan, A., Paschalidis, V., Ruiz, M., & Shapiro, S. L. 2018, PhRvD, 97, 044036, doi: [10.1103/PhysRevD.97.044036](https://doi.org/10.1103/PhysRevD.97.044036)
- Kilpatrick, C. D., Coulter, D. A., Arcavi, I., et al. 2021, The Astrophysical Journal, 923, 258, doi: [10.3847/1538-4357/ac23c6](https://doi.org/10.3847/1538-4357/ac23c6)
- Kimura, S. S., Murase, K., & Bartos, I. 2021, The Astrophysical Journal, 916, 111, doi: [10.3847/1538-4357/ac0535](https://doi.org/10.3847/1538-4357/ac0535)
- Koposov, S., & Bartunov, O. 2006, ASPC, 351, 735. <https://ui.adsabs.harvard.edu/abs/2006ASPC..351..735K>
- Kovlakas, K., Zezas, A., Andrews, J. J., et al. 2021, MNRAS, 506, 1896, doi: [10.1093/mnras/stab1799](https://doi.org/10.1093/mnras/stab1799)
- Levan, A. J., Jonker, P. G., Saccardi, A., et al. 2024, arXiv e-prints, arXiv:2404.16350, doi: [10.48550/arXiv.2404.16350](https://doi.org/10.48550/arXiv.2404.16350)
- LIGO Scientific Collaboration, & Virgo Collaboration. 2017, PhRvL, 119, 161101, doi: [10.1103/PhysRevLett.119.161101](https://doi.org/10.1103/PhysRevLett.119.161101)
- LIGO Scientific Collaboration, VIRGO Collaboration, & Kagra Collaboration. 2025a, GRB Coordinates Network, 42650, 1
- LIGO Scientific Collaboration, VIRGO Collaboration, & Kagra Collaboration. 2025b, GRB Coordinates Network, 42690, 1
- LIGO Scientific Collaboration, Virgo Collaboration, et al. 2017, ApJL, 848, L12, doi: [10.3847/2041-8213/aa91c9](https://doi.org/10.3847/2041-8213/aa91c9)
- Lindstrom, W., Chatelain, J., Collom, D., et al. 2022, TOM Toolkit: Target and Observation Manager Toolkit., Astrophysics Source Code Library <http://ascl.net/2208.004>
- Liu, L., Guo, Z.-K., Cai, R.-G., & Kim, S. P. 2020, PhRvD, 102, 043508, doi: [10.1103/PhysRevD.102.043508](https://doi.org/10.1103/PhysRevD.102.043508)
- Liu, Z. Y., Zhao, W., Jiang, J.-A., et al. 2025, GRB Coordinates Network, 42722, 1
- Lone, O. 2022, django-webpack-loader v1.6.0., GitHub <https://github.com/django-webpack/django-webpack-loader>
- Lundquist, M. J., Paterson, K., Fong, W., et al. 2019, ApJL, 881, L26, doi: [10.3847/2041-8213/ab32f2](https://doi.org/10.3847/2041-8213/ab32f2)
- Lyman, J. D., Bersier, D., James, P. A., et al. 2016, MNRAS, 457, 328, doi: [10.1093/mnras/stv2983](https://doi.org/10.1093/mnras/stv2983)
- Ma, Y. N., Xin, L. P., Yao, Z. H., et al. 2025, GRB Coordinates Network, 42777, 1
- MacBride, S., Howard, E., Sullivan, I., et al. 2025, GRB Coordinates Network, 42707, 1
- MacFadyen, A. I., & Woosley, S. E. 1999, ApJ, 524, 262, doi: [10.1086/307790](https://doi.org/10.1086/307790)
- Mangalapilly, Y. 2023, Watchdog v3.0.0., GitHub <https://github.com/gorakhgosh/watchdog>
- Manikantan, V., & Paschalidis, V. 2025, PhRvD, 112, 103050, doi: [10.1103/g98b-m8m1](https://doi.org/10.1103/g98b-m8m1)
- Manikantan, V., Paschalidis, V., & Bozzola, G. 2025, PhRvD, 112, 043004, doi: [10.1103/js22-3hfx](https://doi.org/10.1103/js22-3hfx)
- Margutti, R., & Chornock, R. 2021, ARA&A, 59, 155, doi: [10.1146/annurev-astro-112420-030742](https://doi.org/10.1146/annurev-astro-112420-030742)
- Martinez, J. G., Stovall, K., Freire, P. C. C., et al. 2015, ApJ, 812, 143, doi: [10.1088/0004-637X/812/2/143](https://doi.org/10.1088/0004-637X/812/2/143)
- Maselli, A., Marassi, S., & Branchesi, M. 2020, A&A, 635, A120, doi: [10.1051/0004-6361/201936848](https://doi.org/10.1051/0004-6361/201936848)
- McCully, C., Crawford, S., Kovacs, G., et al. 2018, astropy/astroscrappy v1.0.5., Zenodo doi: [10.5281/zenodo.1482019](https://doi.org/10.5281/zenodo.1482019)
- McKernan, B., Ford, K. E. S., Bartos, I., et al. 2019, ApJL, 884, L50, doi: [10.3847/2041-8213/ab4886](https://doi.org/10.3847/2041-8213/ab4886)
- McMullin, J. P., Waters, B., Schiebel, D., Young, W., & Golap, K. 2007, 376, 127. <https://ui.adsabs.harvard.edu/abs/2007ASPC..376..127M>
- McPike, E., Perna, R., Ford, K. E. S., et al. 2026, arXiv e-prints, arXiv:2602.04135, doi: [10.48550/arXiv.2602.04135](https://doi.org/10.48550/arXiv.2602.04135)
- Metzger, B. D. 2019, Living Reviews in Relativity, 23, 1, doi: [10.1007/s41114-019-0024-0](https://doi.org/10.1007/s41114-019-0024-0)
- Metzger, B. D., Hui, L., & Cantiello, M. 2024, The Astrophysical Journal, 971, L34, doi: [10.3847/2041-8213/ad6990](https://doi.org/10.3847/2041-8213/ad6990)
- Metzger, B. D., & Piro, A. L. 2014, MNRAS, 439, 3916, doi: [10.1093/mnras/stu247](https://doi.org/10.1093/mnras/stu247)

- Mikolajczyk, P. J., Zieliński, P., Wyrzykowski, L., Krawczyk, A., & Kotysz, K. 2025, in *Revista Mexicana de Astronomia y Astrofisica Conference Series*, Vol. 59, *Revista Mexicana de Astronomia y Astrofisica Conference Series*, 167–172, doi: [10.22201/ia.14052059p.2025.59.26](https://doi.org/10.22201/ia.14052059p.2025.59.26)
- Modjaz, M., Liu, Y. Q., Bianco, F. B., & Graur, O. 2016, *ApJ*, 832, 108, doi: [10.3847/0004-637X/832/2/108](https://doi.org/10.3847/0004-637X/832/2/108)
- Müller, B., Heger, A., & Powell, J. 2025, *PhRvL*, 134, 071403, doi: [10.1103/PhysRevLett.134.071403](https://doi.org/10.1103/PhysRevLett.134.071403)
- Murray, A., van Kemenade, H., wiredfool, et al. 2023, *python-pillow/Pillow v10.0.1*, Zenodo doi: [10.5281/zenodo.8349181](https://doi.org/10.5281/zenodo.8349181)
- Newville, M., Otten, R., Nelson, A., et al. 2023, *lmfit/lmfit-py v1.2.2*, Zenodo doi: [10.5281/zenodo.8145703](https://doi.org/10.5281/zenodo.8145703)
- Nicholl, M., & Andreoni, I. 2025, *Philosophical Transactions of the Royal Society of London Series A*, 383, 20240126, doi: [10.1098/rsta.2024.0126](https://doi.org/10.1098/rsta.2024.0126)
- Niemeyer, G., Pieviläinen, T., de Leeuw, Y., & Ganssle, P. 2021, *dateutil/dateutil v2.8.2*, GitHub <https://github.com/dateutil/dateutil>
- Nomoto, K., & Kondo, Y. 1991, *ApJL*, 367, L19, doi: [10.1086/185922](https://doi.org/10.1086/185922)
- O'Connor, B., Ricci, R., Troja, E., et al. 2025, *ApJL*, 995, L47, doi: [10.3847/2041-8213/ae16a6](https://doi.org/10.3847/2041-8213/ae16a6)
- Page, K. L., Evans, P. A., Kennea, J. A., et al. 2025, *GRB Coordinates Network*, 42681, 1
- Pallets Projects. 2021, *Flask-SQLAlchemy v2.5.1*, GitHub <https://github.com/pallets-eco/flask-sqlalchemy>
- Pallets Projects. 2022, *Flask v2.2.2*, GitHub <https://github.com/pallets/flask>
- Patel, A., Goldberg, J. A., Renzo, M., & Metzger, B. D. 2024, *The Astrophysical Journal*, 966, 212, doi: [10.3847/1538-4357/ad37fe](https://doi.org/10.3847/1538-4357/ad37fe)
- Paterson, K., Lundquist, M., & Hosseinzadeh, G. 2023, *SAGUARO Pipeline v2.1.0*, v2.1.0 Zenodo, doi: [10.5281/zenodo.8436113](https://doi.org/10.5281/zenodo.8436113)
- Paterson, K., Lundquist, M. J., Rastinejad, J. C., et al. 2021, *ApJ*, 912, 128, doi: [10.3847/1538-4357/abeb71](https://doi.org/10.3847/1538-4357/abeb71)
- Pearson, J., Hosseinzadeh, G., Sand, D. J., et al. 2023, *The Astrophysical Journal*, 945, 107, doi: [10.3847/1538-4357/acb8a9](https://doi.org/10.3847/1538-4357/acb8a9)
- Petrov, A., Larson, S. M., & Pradet, Q. 2023, *urllib3/urllib3 v1.26.15*, GitHub <https://github.com/urllib3/urllib3>
- Plotly. 2023, *plotly.py v5.14.1*, GitHub <https://github.com/plotly/plotly.py>
- PostgreSQL Global Development Group. 2022, *PostgreSQL v14.6*, <https://www.postgresql.org/>
- Prentice, S. J., Ashall, C., James, P. A., et al. 2019, *MNRAS*, 485, 1559, doi: [10.1093/mnras/sty3399](https://doi.org/10.1093/mnras/sty3399)
- Prochaska, J. X., Hennawi, J. F., Westfall, K. B., et al. 2020a, arXiv e-prints, arXiv:2005.06505. <https://arxiv.org/abs/2005.06505>
- Prochaska, J. X., Hennawi, J. F., Westfall, K. B., et al. 2020b, *Journal of Open Source Software*, 5, 2308, doi: [10.21105/joss.02308](https://doi.org/10.21105/joss.02308)
- Prochaska, J. X., Hennawi, J., Cooke, R., et al. 2020c, *pypeit/PypeIt: Release 1.0.0*, v1.0.0 Zenodo, doi: [10.5281/zenodo.3743493](https://doi.org/10.5281/zenodo.3743493)
- Python Packaging Authority. 2023, *setuptools v67.6.1*, GitHub <https://github.com/pypa/setuptools>
- Rastinejad, J. C., Paterson, K., Fong, W., et al. 2022, *The Astrophysical Journal*, 927, 50, doi: [10.3847/1538-4357/ac4d34](https://doi.org/10.3847/1538-4357/ac4d34)
- Rastinejad, J. C., Fong, W., Levan, A. J., et al. 2024, *ApJ*, 968, 14, doi: [10.3847/1538-4357/ad409c](https://doi.org/10.3847/1538-4357/ad409c)
- Reichert, D., Nysewander, M., Moran, J., et al. 2005, *Nuovo Cimento C Geophysics Space Physics C*, 28, 767, doi: [10.1393/ncc/i2005-10149-6](https://doi.org/10.1393/ncc/i2005-10149-6)
- Reitz, K. 2023, *Requests v2.28.2*, GitHub <https://github.com/psf/requests>
- Rest, A., Stubbs, C., Becker, A. C., et al. 2005, *ApJ*, 634, 1103, doi: [10.1086/497060](https://doi.org/10.1086/497060)
- Richardson, L. 2023, *Beautiful Soup v4.12.2*, Launchpad <https://launchpad.net/beautifulsoup/>
- Ricigliano, G., Hotokezaka, K., & Arcones, A. 2025, *MNRAS*, 543, 2534, doi: [10.1093/mnras/staf1577](https://doi.org/10.1093/mnras/staf1577)
- Rodríguez, Ó., Maoz, D., & Nakar, E. 2023, *ApJ*, 955, 71, doi: [10.3847/1538-4357/ace2bd](https://doi.org/10.3847/1538-4357/ace2bd)
- Rodríguez-Ramírez, J. C., Nemmen, R., & Bom, C. R. 2025, *PhRvD*, 111, 083020, doi: [10.1103/PhysRevD.111.083020](https://doi.org/10.1103/PhysRevD.111.083020)
- Rodríguez-Ramírez, J. C., Bom, C. R., Fraga, B., & Nemmen, R. 2023, *Monthly Notices of the Royal Astronomical Society*, 527, 6076–6089, doi: [10.1093/mnras/stad3575](https://doi.org/10.1093/mnras/stad3575)
- Salmi, T., Deneva, J. S., Ray, P. S., et al. 2024, *ApJ*, 976, 58, doi: [10.3847/1538-4357/ad81d2](https://doi.org/10.3847/1538-4357/ad81d2)
- Sand, D. 2025, *Transient Name Server Discovery Report*, 2025-4580, 1
- Sanders, N. E., Soderberg, A. M., Gezari, S., et al. 2015, *ApJ*, 799, 208, doi: [10.1088/0004-637X/799/2/208](https://doi.org/10.1088/0004-637X/799/2/208)
- Santos, A., Kilpatrick, C. D., Bom, C. R., et al. 2025, *GRB Coordinates Network*, 42724, 1
- Santos, A., Kilpatrick, C. D., Bom, C. R., et al. 2024, *MNRAS*, 529, 59, doi: [10.1093/mnras/stae466](https://doi.org/10.1093/mnras/stae466)

- Sarin, N., Hübner, M., Omand, C. M. B., et al. 2024, *Monthly Notices of the Royal Astronomical Society*, 531, 1203, doi: [10.1093/mnras/stae1238](https://doi.org/10.1093/mnras/stae1238)
- SCiMMA Project. 2023, Hopskotch, <https://scimma.org/hopskotch.html>
- Shappee, B. J., Prieto, J. L., Grupe, D., et al. 2014, *The Astrophysical Journal*, 788, 48, doi: [10.1088/0004-637X/788/1/48](https://doi.org/10.1088/0004-637X/788/1/48)
- Shingles, L., Smith, K. W., Young, D. R., et al. 2021, *Transient Name Server AstroNote*, 7, 1
- Shrestha, M., Pearson, J., Wyatt, S., et al. 2024, *ApJ*, 961, 247, doi: [10.3847/1538-4357/ad11e1](https://doi.org/10.3847/1538-4357/ad11e1)
- Shupe, D. L., Laher, R. R., Storrie-Lombardi, L., et al. 2012, *Proc. SPIE*, 8451, E1M, doi: [10.1117/12.925460](https://doi.org/10.1117/12.925460)
- Siegel, D. M., Agarwal, A., Barnes, J., et al. 2022, *ApJ*, 941, 100, doi: [10.3847/1538-4357/ac8d04](https://doi.org/10.3847/1538-4357/ac8d04)
- Siegel, D. M., Barnes, J., & Metzger, B. D. 2019, *Nature*, 569, 241, doi: [10.1038/s41586-019-1136-0](https://doi.org/10.1038/s41586-019-1136-0)
- Singer, L. 2022, *gracedb-sdk v0.1.7*, <https://git.ligo.org/emfollow/gracedb-sdk>
- Singer, L. P., Parazin, B., Coughlin, M. W., et al. 2022, *AJ*, 163, 209, doi: [10.3847/1538-3881/ac5ab8](https://doi.org/10.3847/1538-3881/ac5ab8)
- Singer, L. P., & Price, L. R. 2016, *PhRvD*, 93, 024013, doi: [10.1103/PhysRevD.93.024013](https://doi.org/10.1103/PhysRevD.93.024013)
- Smith, A., Nicholl, M., Gillanders, J., et al. 2025, *GRB Coordinates Network*, 42682, 1
- Smith, D. 2022, *crispy-bootstrap4 v2022.1.*, GitHub <https://github.com/django-crispy-forms/crispy-bootstrap4>
- Smith, K. W., Smartt, S. J., Young, D. R., et al. 2020, *PASP*, 132, 085002, doi: [10.1088/1538-3873/ab936e](https://doi.org/10.1088/1538-3873/ab936e)
- Srinivasaragavan, G. P., Yang, S., Anand, S., et al. 2024, *ApJ*, 976, 71, doi: [10.3847/1538-4357/ad7fde](https://doi.org/10.3847/1538-4357/ad7fde)
- Staley, T. D. 2014, *voevent-parse: Parse, manipulate, and generate VOEvent XML packets.*, *Astrophysics Source Code Library* <http://ascl.net/1411.003>
- Stienstra, M., Takhteyev, Y., & Limberg, W. 2023, *Python-Markdown v3.4.3.*, GitHub <https://github.com/Python-Markdown/markdown>
- Stoppa, F. in prep., 2025, *SNID SAGE: A Modern Framework for Interactive Supernova Classification and Spectral Analysis*, <https://github.com/FiorenSt/SNID-SAGE>
- Street, R. A., Bowman, M., Saunders, E. S., & Boroson, T. 2018a, in *Society of Photo-Optical Instrumentation Engineers (SPIE) Conference Series*, Vol. 10707, *Software and Cyberinfrastructure for Astronomy V*, ed. J. C. Guzman & J. Ibsen, 1070711, doi: [10.1117/12.2312293](https://doi.org/10.1117/12.2312293)
- Street, R. A., Bowman, M., Saunders, E. S., & Boroson, T. 2018b, in *Society of Photo-Optical Instrumentation Engineers (SPIE) Conference Series*, Vol. 10707, *Software and Cyberinfrastructure for Astronomy V*, ed. J. C. Guzman & J. Ibsen, 1070711, doi: [10.1117/12.2312293](https://doi.org/10.1117/12.2312293)
- Suwa, Y., Yoshida, T., Shibata, M., Umeda, H., & Takahashi, K. 2018, *MNRAS*, 481, 3305, doi: [10.1093/mnras/sty2460](https://doi.org/10.1093/mnras/sty2460)
- Taddia, F., Sollerman, J., Fremling, C., et al. 2019, *A&A*, 621, A71, doi: [10.1051/0004-6361/201834429](https://doi.org/10.1051/0004-6361/201834429)
- Tagawa, H., Kimura, S. S., Haiman, Z., Perna, R., & Bartos, I. 2024, *The Astrophysical Journal*, 966, 21, doi: [10.3847/1538-4357/ad2e0b](https://doi.org/10.3847/1538-4357/ad2e0b)
- Taguchi, K., Kawabata, M., Itoh, R., et al. 2025, *GRB Coordinates Network*, 42725, 1
- Tartaglia, L., Sand, D. J., Valenti, S., et al. 2018, *ApJ*, 853, 62, doi: [10.3847/1538-4357/aaa014](https://doi.org/10.3847/1538-4357/aaa014)
- Tauris, T. M., & Janka, H.-T. 2019, *ApJL*, 886, L20, doi: [10.3847/2041-8213/ab5642](https://doi.org/10.3847/2041-8213/ab5642)
- Tebeka, M. 2022, *fastavro v1.6.1.*, GitHub <https://github.com/fastavro/fastavro>
- The LIGO Scientific Collaboration, the Virgo Collaboration, the KAGRA Collaboration, et al. 2025a, *arXiv e-prints*, arXiv:2508.18082, doi: [10.48550/arXiv.2508.18082](https://doi.org/10.48550/arXiv.2508.18082)
- The LIGO Scientific Collaboration, the Virgo Collaboration, the KAGRA Collaboration, et al. 2025b, *arXiv e-prints*, arXiv:2508.18081, doi: [10.48550/arXiv.2508.18081](https://doi.org/10.48550/arXiv.2508.18081)
- Tody, D. 1986, in *Society of Photo-Optical Instrumentation Engineers (SPIE) Conference Series*, Vol. 627, *Instrumentation in astronomy VI*, ed. D. L. Crawford, 733, doi: [10.1117/12.968154](https://doi.org/10.1117/12.968154)
- Tody, D. 1993, in *Astronomical Society of the Pacific Conference Series*, Vol. 52, *Astronomical Data Analysis Software and Systems II*, ed. R. J. Hanisch, R. J. V. Brissenden, & J. Barnes, 173
- TOM Toolkit Project, Collom, D., Lindstrom, L., & Nation, J. 2023, *tom_nonlocalizedevents v0.7.7.*, GitHub https://github.com/TOMToolkit/tom_nonlocalizedevents
- TOM Toolkit Project, & Lindstrom, W. 2023, *tom-alertstreams v0.6.2.*, GitHub <https://github.com/TOMToolkit/tom-alertstreams>
- Tonry, J. L., Denneau, L., Heinze, A. N., et al. 2018, *PASP*, 130, 064505, doi: [10.1088/1538-3873/aabadf](https://doi.org/10.1088/1538-3873/aabadf)
- Trier, M., & van Oostveen, B. 2023, *Django Extensions v3.2.3.*, GitHub <https://github.com/django-extensions/django-extensions>
- Tsukada, L., Joshi, P., Adhichary, S., et al. 2023, *PhRvD*, 108, 043004, doi: [10.1103/PhysRevD.108.043004](https://doi.org/10.1103/PhysRevD.108.043004)

- Valenti, S., Sand, D. J., Yang, S., et al. 2017, *The Astrophysical Journal*, 848, L24, doi: [10.3847/2041-8213/aa8edf](https://doi.org/10.3847/2041-8213/aa8edf)
- van der Walt, S. J., Crellin-Quick, A., & Bloom, J. S. 2019, *Journal of Open Source Software*, 4, 1247, doi: [10.21105/joss.01247](https://doi.org/10.21105/joss.01247)
- Verheul, D. 2021, *django-bootstrap4* v3.0.1., GitHub <https://github.com/zostera/django-bootstrap4>
- Villar, V. A., Guillochon, J., Berger, E., et al. 2017, *The Astrophysical Journal*, 851, L21, doi: [10.3847/2041-8213/aa9c84](https://doi.org/10.3847/2041-8213/aa9c84)
- Vincenzi, M., Sullivan, M., Firth, R. E., et al. 2019, *MNRAS*, 489, 5802, doi: [10.1093/mnras/stz2448](https://doi.org/10.1093/mnras/stz2448)
- Virtanen, P., Gommers, R., Oliphant, T. E., et al. 2020, *NatMe*, 17, 261, doi: [10.1038/s41592-019-0686-2](https://doi.org/10.1038/s41592-019-0686-2)
- Waddington, T. 2020, *django-gravatar* v1.4.4., GitHub <https://github.com/twaddington/django-gravatar>
- White, D. J., Daw, E. J., & Dhillon, V. S. 2011, *Classical and Quantum Gravity*, 28, 085016, doi: [10.1088/0264-9381/28/8/085016](https://doi.org/10.1088/0264-9381/28/8/085016)
- Woosley, S. E. 1993, *ApJ*, 405, 273, doi: [10.1086/172359](https://doi.org/10.1086/172359)
- Woosley, S. E., & Bloom, J. S. 2006, *ARA&A*, 44, 507, doi: [10.1146/annurev.astro.43.072103.150558](https://doi.org/10.1146/annurev.astro.43.072103.150558)
- Wu, Q. Y., Hu, J. W., Liu, Y., Zhang, B., & Einstein Probe Team. 2025, *GRB Coordinates Network*, 42714, 1
- Wyatt, S. D., Tohuvavohu, A., Arcavi, I., et al. 2020, *ApJ*, 894, 127, doi: [10.3847/1538-4357/ab855e](https://doi.org/10.3847/1538-4357/ab855e)
- Yang, S., Sand, D. J., Valenti, S., et al. 2019, *ApJ*, 875, 59, doi: [10.3847/1538-4357/ab0e06](https://doi.org/10.3847/1538-4357/ab0e06)
- Yang, Y.-H., Troja, E., Ristić, M., et al. 2026, *ApJL*, 996, L24, doi: [10.3847/2041-8213/ae2dea](https://doi.org/10.3847/2041-8213/ae2dea)
- Young, D. 2023, *fundamentals* v2.4.1., Zenodo doi: [10.5281/zenodo.8037510](https://doi.org/10.5281/zenodo.8037510)
- Zackay, B., Ofek, E. O., & Gal-Yam, A. 2016, *ApJ*, 830, 27, doi: [10.3847/0004-637X/830/1/27](https://doi.org/10.3847/0004-637X/830/1/27)
- Zhou, R., Ferraro, S., White, M., et al. 2023, *JCAP*, 2023, 097, doi: [10.1088/1475-7516/2023/11/097](https://doi.org/10.1088/1475-7516/2023/11/097)
- Zhu, L.-G., He, L., Chen, X., & Zhao, W. 2026, *arXiv e-prints*, arXiv:2601.08286, doi: [10.48550/arXiv.2601.08286](https://doi.org/10.48550/arXiv.2601.08286)
- Zonca, A., Singer, L., Lenz, D., et al. 2019, *JOSS*, 4, 1298, doi: [10.21105/joss.01298](https://doi.org/10.21105/joss.01298)

APPENDIX

A. VETTING FOR BBH MERGER-INDUCED AGN FLARING

When searching for BBH-induced AGN flaring, predetection at the location of a candidate is not disqualifying. The nature of a predetected source is already captured by the combination of point source, minor planet, and AGN association. We therefore simply allow predetection at any time pre-merger when vetting for AGN flares.

Unfortunately, it is challenging to impose robust constraints on the luminosities and timescales of BBH-induced AGN flares. Differences in behavior arise in part from differing emission mechanisms, as rapid accretion onto the kicked remnant BH may power relativistic jets and/or disk winds. These jets or winds may subsequently interact with the surrounding disk and produce observable EM radiation. In both cases, flare luminosity is expected to scale approximately as $L \propto M_{\text{BBH}}^2 v_k^{-3} \rho$, where $M_{\text{BBH}} = m_1 + m_2$ is the total binary mass, v_k the kick velocity, and ρ the ambient gas density in the AGN disk. Different emission mechanisms then predict soft X-ray emission on timescales of weeks (S. S. Kimura et al. 2021), while several others (B. McKernan et al. 2019; J. C. Rodríguez-Ramírez et al. 2023; H. Tagawa et al. 2024; J. C. Rodríguez-Ramírez et al. 2025) predict UV/optical flares lasting from weeks to several hundred days. Isolating just one mechanism (disk winds), J. C. Rodríguez-Ramírez et al. (2025) explore parameter space by varying kick velocity ($v_k = 200\text{--}400 \text{ km s}^{-1}$) and SMBH mass ($M_{\text{SMBH}} = 10^6\text{--}10^7 M_\odot$), while fixing $M_{\text{BBH}} = 20 M_\odot$ and the kick angle at $\theta_k = 10^\circ$ from the disk midplane. They find peak times in the range of $\sim 10\text{--}80$ days and peak luminosities of $\sim 5 \times 10^{42}$ to $5 \times 10^{43} \text{ erg s}^{-1}$. It has also been shown that flares are broadly classified into two categories based on their delay times relative to the merger (P. Darc et al. 2025). Short-delay flares are expected to occur within $\lesssim 50$ days of the merger and are typically associated with relatively short durations. In contrast, long-delay flares can peak between ~ 50 and ~ 400 days, and last longer.

Candidates are thus scored based only on their 2D position in the GW localization region, the absence of point sources or minor planets, 2D association with an AGN, and the distance to the AGN. To search for AGN flares among the candidates, one may select candidates with non-zero $S_{\text{AGN-flare}}$ and examine photometry for clear evidence of flaring above regular AGN variability. This type of modeling has been conducted for select BBH GW events (M. J. Graham et al. 2020; T. Cabrera et al. 2024; P. Darc et al. 2025; H. Bommireddy et al. 2026). Here, we search for AGN flaring only among candidate transients already identified with optical/IR/X-ray observations. We will explore a more holistic approach in the future that accounts for all known AGN within a region, regardless of their multi-wavelength behavior, similar to other works (*e.g.*, M. J. Graham et al. 2023; P. Darc et al. 2025; L.-G. Zhu et al. 2026; E. McPike et al. 2026; H. Bommireddy et al. 2026).

B. DETAILED SCORES AND INFERRED PHOTOMETRIC QUANTITIES

We present here the scores and inferred photometric quantities which are obtained from scoring all 248 objects reported to the TNS or in GCNs within 10 days of the GW signal. Table 4 shows, for all candidates: the 2D localization subscore S_{2D} , distance subscore S_{dist} , point source and minor planet association score factors S_{PS} and S_{MPC} , AGN association subscore S_{AGN} , and photometry subscores S_{phot} . Finally, we list the overall scores S_T for transient class T , among KNe, KNe-in-SNe, and super-KNe. We omit scores for BBH-induced AGN flaring as only two candidates are associated with AGN. Distance, point source, minor planet, and AGN scores are the same when vetting for KNe, KNe-in-SNe, and super-KNe, for a given candidate.

Table 5 shows the peak luminosity L_{peak} , rise time to peak t_{peak} , and decay rate Δm (where a positive value indicates fading) inferred for all candidates. We also indicate whether a candidate is considered detected prior to the GW signal. Where a quantity is missing, available photometry is insufficient to constrain it. By comparing these inferred quantities to observation and theory-driven photometry metrics in Table 2 (Section 4.4), we compute score factors which ultimately yield the photometry subscore in Table 4. Whether a candidate is considered predetected, its rise time t_{peak} , and its decay rate Δm are dependent on the window over which we fit photometry: up to 25 days for KNe, and up to 100 days for KNe-in-SNe and super-KNe.

Table 4. Detailed Scoring for All Candidates

candidate	S_{2D}	S_{dist}	S_{PS}	S_{MPC}	S_{AGN}	$S_{phot,KN}$	$S_{phot,KN-in-SN}$	$S_{phot,super-KN}$	S_{KN}	$S_{KN-in-SN}$	$S_{super-KN}$
AT 2024aeuy	0.31	0.14	1	1	1	0.001	0.1	0.01	0.00	0.00	0.00
AT 2025aazc	~0	0.05	1	1	1	0.1	1	0.1	0.00	0.00	0.00
AT 2025abwx	~0	0.05	1	1	1	0.01	0.1	0.1	0.00	0.00	0.00
AT 2025adda	0.03	0.04	1	1	1	0.1	0.01	0.01	0.00	0.00	0.00
AT 2025addb	0.40	0.20	1	1	1	1	0.01	0.1	0.08	0.00	0.01
AT 2025adhe	0.49	0.12	1	1	1	0.01	0.1	0.01	0.00	0.01	0.00
AT 2025adhg	0.56	0.06	1	1	1	0.001	1	0.01	0.00	0.04	0.00
AT 2025adhh	0.03	0.04	1	1	1	0.001	0.01	0.1	0.00	0.00	0.00
AT 2025adhj	0.27	0.12	1	1	1	1	1	1	0.03	0.03	0.03
AT 2025adhr	0.92	0.00	1	1	1	0.01	0.01	0.01	0.00	0.00	0.00
AT 2025adht	0.47	0.00	1	1	1	0.1	0.1	0.01	0.00	0.00	0.00
AT 2025adhu	0.32	-	1	1	1	1	0.01	0.1	0.32	0.00	0.03
AT 2025adhy	0.25	0.26	1	1	1	0.001	1	0.1	0.00	0.06	0.01
AT 2025adhz	0.40	0.00	1	1	1	0.1	0.1	0.1	0.00	0.00	0.00
AT 2025adia	0.25	0.00	1	1	1	0.01	0.1	0.01	0.00	0.00	0.00
AT 2025adib	0.88	0.30	1	1	1	1	1	1	0.26	0.26	0.26
AT 2025adic	0.88	0.00	1	1	1	0.1	0.1	0.1	0.00	0.00	0.00
AT 2025adie	0.52	-	0	1	1	1	0.01	0.01	0.00	0.00	0.00
AT 2025adij	0.11	0.16	1	1	1	0.01	0.01	0.001	0.00	0.00	0.00
AT 2025adil	0.09	0.29	1	1	1	0.1	0.1	0.1	0.00	0.00	0.00
AT 2025adin	0.70	0.11	1	1	1	1	0.1	0.1	0.07	0.01	0.01
AT 2025adip	0.20	0.09	1	1	1	0.001	1	0.1	0.00	0.02	0.00
AT 2025adiq	0.75	0.00	1	1	1	0.01	1	1	0.00	0.00	0.00
AT 2025adir	0.58	0.17	1	1	1	0.01	1	0.01	0.00	0.10	0.00
AT 2025adis	0.27	0.00	1	1	1	0.01	1	0.01	0.00	0.00	0.00
AT 2025adit	0.43	0.12	1	1	1	0.01	1	0.01	0.00	0.05	0.00
AT 2025adiu	0.31	0.00	1	1	1	0.001	0.1	0.01	0.00	0.00	0.00
AT 2025adiv	0.50	0.12	1	1	1	0.01	0.1	1	0.00	0.01	0.06
AT 2025adjd	0.40	0.00	1	1	1	0.1	1	0.1	0.00	0.00	0.00
AT 2025adjf	0.46	0.00	1	1	1	0.001	1	0.1	0.00	0.00	0.00
AT 2025adjh	0.07	0.17	1	1	1	1	1	1	0.01	0.01	0.01
AT 2025ajjl	0.28	0.07	1	1	1	0.1	0.1	0.1	0.00	0.00	0.00
AT 2025adjn	0.12	0.09	1	1	1	1	1	1	0.01	0.01	0.01
AT 2025adjo	0.28	0.08	1	1	1	0.001	1	0.01	0.00	0.02	0.00
AT 2025adjp	0.58	0.53	1	1	1	0.01	0.1	0.1	0.00	0.03	0.03
AT 2025adjw	0.22	0.06	1	1	1	0.01	1	0.1	0.00	0.01	0.00
AT 2025adkl	0.37	0.04	1	1	1	1	0.1	0.1	0.02	0.00	0.00
AT 2025adkm	0.82	0.15	1	1	1	0.01	1	0.1	0.00	0.12	0.01
AT 2025admd	0.93	0.14	1	1	1	0.001	1	0.01	0.00	0.13	0.00
AT 2025admf	0.93	0.09	1	1	1	1	1	1	0.08	0.08	0.08
AT 2025admng	0.62	0.10	1	1	1	1	1	1	0.06	0.06	0.06
AT 2025admh	0.87	0.10	1	1	1	1	1	1	0.08	0.08	0.08
AT 2025admi	0.56	0.09	1	1	1	1	1	1	0.05	0.05	0.05
AT 2025admj	0.77	0.05	1	1	1	0.1	0.1	0.1	0.00	0.00	0.00
AT 2025admkn	0.23	0.06	1	1	1	1	1	1	0.01	0.01	0.01
AT 2025adml	0.22	0.12	1	1	1	1	1	1	0.03	0.03	0.03

Table 4 *continued*

Table 4 (continued)

candidate	S_{2D}	S_{dist}	S_{PS}	S_{MPC}	S_{AGN}	$S_{phot,KN}$	$S_{phot,KN-in-SN}$	$S_{phot,super-KN}$	S_{KN}	$S_{KN-in-SN}$	$S_{super-KN}$
AT 2025admm	0.54	0.06	1	1	1	0.1	0.1	0.1	0.00	0.00	0.00
AT 2025admn	0.77	0.32	1	1	1	1	1	1	0.25	0.25	0.25
AT 2025admo	0.59	0.15	1	1	1	1	1	1	0.09	0.09	0.09
AT 2025admp	0.70	0.28	1	1	1	0.1	1	0.1	0.02	0.20	0.02
AT 2025admq	0.52	0.05	1	1	1	0.1	0.1	0.1	0.00	0.00	0.00
AT 2025admr	0.68	0.04	1	1	1	0.01	1	0.01	0.00	0.03	0.00
AT 2025adms	0.61	0.17	0	1	1	0.1	1	0.1	0.00	0.00	0.00
AT 2025admt	0.80	0.32	1	1	1	1	1	1	0.25	0.25	0.25
AT 2025admu	0.86	0.27	1	1	1	1	1	1	0.24	0.24	0.24
AT 2025adm v	0.04	0.05	1	1	1	0.0001	0.01	0.01	0.00	0.00	0.00
AT 2025adm w	0.09	0.04	1	1	1	1	1	1	0.00	0.00	0.00
AT 2025adm x	0.64	0.67	1	1	1	1	0.1	1	0.43	0.04	0.43
AT 2025adm y	0.28	0.05	1	1	1	0.1	1	0.01	0.00	0.01	0.00
AT 2025adm z	0.88	0.00	1	1	1	1	0.1	1	0.00	0.00	0.00
AT 2025adna	0.37	0.09	1	1	1	1	1	1	0.03	0.03	0.03
AT 2025adnb	0.93	0.06	1	1	1	0.1	1	0.1	0.01	0.06	0.01
AT 2025adnc	0.44	0.06	1	1	0	1	1	1	0.00	0.00	0.00
AT 2025adnd	0.68	0.08	1	1	1	0.1	1	0.1	0.01	0.06	0.01
AT 2025adne	0.38	0.04	1	1	1	0.1	0.1	0.1	0.00	0.00	0.00
AT 2025adnf	0.62	0.18	1	1	1	1	1	1	0.11	0.11	0.11
AT 2025adng	0.58	0.09	1	1	1	0.1	0.1	0.1	0.01	0.01	0.01
AT 2025adnh	0.68	0.16	1	1	1	0.1	1	0.1	0.01	0.11	0.01
AT 2025adni	0.59	0.07	1	1	1	0.1	1	0.1	0.00	0.04	0.00
AT 2025adnj	0.34	0.00	1	1	1	0.1	1	0.1	0.00	0.00	0.00
AT 2025adnk	0.33	-	1	1	1	1	0.1	0.1	0.33	0.03	0.03
AT 2025adnl	0.18	0.09	1	1	1	0.1	0.1	0.1	0.00	0.00	0.00
AT 2025adnm	0.26	-	1	1	1	1	0.1	0.1	0.26	0.03	0.03
AT 2025adnn	0.94	0.01	1	1	1	1	1	1	0.01	0.01	0.01
AT 2025adno	0.38	0.00	1	1	1	0.1	0.1	0.01	0.00	0.00	0.00
AT 2025adnp	0.47	0.30	1	1	1	1	1	1	0.14	0.14	0.14
AT 2025adnq	0.60	0.07	1	1	1	0.1	0.1	0.01	0.00	0.00	0.00
AT 2025adnr	0.35	0.18	1	1	1	0.1	0.1	0.1	0.01	0.01	0.01
AT 2025adns	0.94	0.09	1	1	1	0.1	0.1	0.1	0.01	0.01	0.01
AT 2025adnt	0.78	0.06	1	1	1	0.1	1	0.1	0.00	0.04	0.00
AT 2025adnu	0.51	0.03	1	1	1	0.1	0.1	0.1	0.00	0.00	0.00
AT 2025adnv	0.35	0.01	0	1	1	1	1	1	0.00	0.00	0.00
AT 2025adnw	0.86	0.03	1	1	1	0.1	0.1	0.1	0.00	0.00	0.00
AT 2025adnx	0.35	0.23	1	1	1	0.1	1	0.1	0.01	0.08	0.01
AT 2025adny	0.35	0.09	1	1	1	1	1	1	0.03	0.03	0.03
AT 2025adnz	0.89	0.11	1	1	1	1	1	1	0.10	0.10	0.10
AT 2025adoa	0.72	0.17	1	1	1	1	1	1	0.12	0.12	0.12
AT 2025adob	0.31	0.00	1	1	1	1	1	1	0.00	0.00	0.00
AT 2025adoc	0.84	0.06	1	1	1	1	1	1	0.05	0.05	0.05
AT 2025adod	0.51	0.12	1	1	1	0.1	1	0.1	0.01	0.06	0.01
AT 2025adoe	0.30	-	1	1	1	1	0.1	0.1	0.30	0.03	0.03
AT 2025adof	0.82	0.24	1	1	1	1	1	1	0.19	0.19	0.19
AT 2025adog	0.34	0.00	1	1	1	0.1	1	0.1	0.00	0.00	0.00

Table 4 continued

Table 4 (continued)

candidate	S_{2D}	S_{dist}	S_{PS}	S_{MPC}	S_{SAGN}	$S_{phot,KN}$	$S_{phot,KN-in-SN}$	$S_{phot,super-KN}$	S_{KN}	$S_{KN-in-SN}$	$S_{super-KN}$
AT 2025adoh	0.44	-	1	1	1	1	0.1	0.1	0.44	0.04	0.04
AT 2025adoi	0.45	-	1	1	1	1	0.1	0.1	0.45	0.05	0.05
AT 2025adoj	0.94	0.11	1	1	1	0.1	1	0.1	0.01	0.10	0.01
AT 2025adok	0.49	0.09	0	1	1	0.1	1	0.1	0.00	0.00	0.00
AT 2025adol	0.34	0.00	1	1	1	1	1	1	0.00	0.00	0.00
AT 2025adom	0.75	0.00	1	1	1	1	1	1	0.00	0.00	0.00
AT 2025adon	0.65	0.05	1	1	1	0.1	0.1	0.1	0.00	0.00	0.00
AT 2025adoo	0.54	0.03	1	1	1	0.01	1	0.01	0.00	0.02	0.00
AT 2025adop	0.73	0.09	1	1	1	0.1	0.1	0.01	0.01	0.01	0.00
AT 2025adoq	0.13	0.08	1	1	1	1	1	1	0.01	0.01	0.01
AT 2025ador	0.70	0.18	1	1	1	0.1	1	0.1	0.01	0.13	0.01
AT 2025ados	0.31	0.07	1	1	1	1	1	1	0.02	0.02	0.02
AT 2025adot	0.84	0.02	1	1	1	0.1	1	0.1	0.00	0.01	0.00
AT 2025adou	0.13	0.04	1	1	1	0.1	1	0.1	0.00	0.00	0.00
AT 2025adov	0.16	-	1	1	1	1	0.1	0.1	0.16	0.02	0.02
AT 2025adow	0.44	0.08	1	1	1	0.1	1	0.1	0.00	0.04	0.00
AT 2025adox	0.34	0.01	1	1	1	1	1	1	0.00	0.00	0.00
AT 2025adoy	0.46	0.04	1	1	1	0.1	1	0.1	0.00	0.02	0.00
AT 2025adoz	0.80	0.12	1	1	1	0.0001	0.1	0.001	0.00	0.01	0.00
AT 2025adpa	0.54	0.09	1	1	1	0.1	0.1	0.1	0.00	0.00	0.00
AT 2025adpb	0.47	0.01	1	1	1	0.1	1	0.1	0.00	0.01	0.00
AT 2025adpc	0.42	0.00	1	1	1	1	1	1	0.00	0.00	0.00
AT 2025adpd	0.41	-	1	1	1	1	0.1	0.1	0.41	0.04	0.04
AT 2025adpe	0.45	0.01	0	1	1	0.0001	0.001	0.01	0.00	0.00	0.00
AT 2025adqe	0.33	0.11	1	1	1	1	0.1	0.1	0.04	0.00	0.00
AT 2025adqf	0.83	0.02	1	1	1	0.1	0.1	0.01	0.00	0.00	0.00
AT 2025adra	0.33	0.00	1	1	1	1	0.1	0.1	0.00	0.00	0.00
AT 2025adrz	0.22	0.00	0	1	0	0.001	0.1	0.01	0.00	0.00	0.00
AT 2025adsa	0.26	0.25	1	1	1	0.001	0.1	0.1	0.00	0.01	0.01
AT 2025adsf	0.24	0.17	1	1	1	0.01	1	1	0.00	0.04	0.04
AT 2025adsi	0.31	0.19	1	1	1	0.001	1	0.1	0.00	0.06	0.01
AT 2025adsk	0.49	0.08	1	1	1	0.0001	0.01	0.01	0.00	0.00	0.00
AT 2025adsl	0.21	0.04	1	1	1	0.1	0.01	0.01	0.00	0.00	0.00
AT 2025adsm	0.06	0.07	1	1	1	0.01	1	0.01	0.00	0.00	0.00
AT 2025adsp	0.25	0.05	1	1	1	1	1	1	0.01	0.01	0.01
AT 2025adsw	0.39	0.04	1	1	1	0.001	0.1	0.1	0.00	0.00	0.00
AT 2025adsx	0.10	0.13	1	1	1	1	1	1	0.01	0.01	0.01
AT 2025adsy	0.05	0.05	1	1	1	0.1	1	0.1	0.00	0.00	0.00
AT 2025adsz	0.06	0.04	1	1	1	1	1	1	0.00	0.00	0.00
AT 2025adtd	0.28	0.00	1	1	1	1	1	1	0.00	0.00	0.00
AT 2025adtj	0.10	0.28	1	1	1	0.01	0.1	0.01	0.00	0.00	0.00
AT 2025adtl	0.43	0.00	1	1	1	0.1	0.1	0.1	0.00	0.00	0.00
AT 2025adtm	0.84	0.00	1	1	1	1	1	1	0.00	0.00	0.00
AT 2025adtn	0.93	0.20	1	1	1	1	0.1	0.1	0.19	0.02	0.02
AT 2025adto	0.11	0.03	1	1	1	1	1	1	0.00	0.00	0.00
AT 2025adtp	0.39	0.01	1	1	1	0.01	1	1	0.00	0.00	0.00
AT 2025adtr	0.63	0.00	1	1	1	1	1	1	0.00	0.00	0.00

Table 4 continued

Table 4 (continued)

candidate	S_{2D}	S_{dist}	S_{PS}	S_{MPC}	S_{SAGN}	$S_{phot,KN}$	$S_{phot,KN-in-SN}$	$S_{phot,super-KN}$	S_{KN}	$S_{KN-in-SN}$	$S_{super-KN}$
AT 2025adts	0.44	0.27	1	1	1	0.01	0.1	0.1	0.00	0.01	0.01
AT 2025adtt	0.30	0.01	1	1	1	1	1	1	0.00	0.00	0.00
AT 2025adtu	0.32	0.10	1	1	1	0.01	0.01	0.01	0.00	0.00	0.00
AT 2025adtv	0.44	0.59	0	1	1	1	1	1	0.00	0.00	0.00
AT 2025aecf	0.09	0.00	1	1	1	0.001	0.1	0.01	0.00	0.00	0.00
AT 2025aech	0.25	0.00	1	1	1	1	0.1	0.1	0.00	0.00	0.00
AT 2025aecco	0.34	0.15	1	1	1	0.1	1	0.1	0.01	0.05	0.01
AT 2025aecn	0.11	0.00	1	1	1	0.1	0.1	0.01	0.00	0.00	0.00
AT 2025aecp	0.38	0.05	1	1	1	0.01	0.1	0.01	0.00	0.00	0.00
AT 2025aeefe	0.18	0.00	1	1	1	0.001	1	0.1	0.00	0.00	0.00
AT 2025aegj	0.10	0.00	1	1	1	0.001	1	0.01	0.00	0.00	0.00
AT 2025aikki	0.13	0.08	1	1	1	0.001	1	0.01	0.00	0.01	0.00
AT 2025ailc	0.27	0.04	1	1	1	0.1	0.1	0.01	0.00	0.00	0.00
AT 2025aild	0.42	0.13	1	1	1	1	0.1	0.1	0.05	0.01	0.01
AT 2025aile	0.56	0.10	1	1	1	0.01	1	0.1	0.00	0.05	0.01
AT 2025ailf	0.44	0.06	1	1	1	0.001	1	0.01	0.00	0.02	0.00
AT 2025ailg	0.37	0.00	1	1	1	0.1	0.1	0.01	0.00	0.00	0.00
AT 2025ailh	0.15	0.05	1	1	1	0.1	0.1	0.01	0.00	0.00	0.00
AT 2025aili	0.28	0.05	1	1	1	1	0.1	0.1	0.01	0.00	0.00
AT 2025ailj	0.86	0.08	1	1	1	1	0.1	0.1	0.07	0.01	0.01
AT 2025ailk	0.69	0.08	1	1	1	0.1	0.1	0.01	0.01	0.01	0.00
AT 2025aill	0.06	0.24	1	1	1	0.001	0.1	0.01	0.00	0.00	0.00
AT 2025ailm	0.12	0.12	1	1	1	0.001	1	0.01	0.00	0.02	0.00
AT 2025ailn	0.40	0.08	1	1	1	0.001	1	0.01	0.00	0.03	0.00
AT 2025ailo	0.80	0.01	1	1	1	0.1	0.1	0.01	0.00	0.00	0.00
AT 2025ailp	0.06	0.23	1	1	1	1	0.1	0.1	0.02	0.00	0.00
AT 2025ailq	0.59	0.06	1	1	1	0.1	0.1	0.01	0.00	0.00	0.00
AT 2025ailr	0.44	0.09	1	1	1	1	0.1	0.1	0.04	0.00	0.00
AT 2025ails	0.45	0.23	1	1	1	0.01	1	0.1	0.00	0.11	0.01
AT 2025ailt	0.22	0.00	1	1	1	0.001	0.1	0.1	0.00	0.00	0.00
AT 2025ailu	0.09	0.12	1	1	1	0.01	1	0.1	0.00	0.01	0.00
AT 2025ailv	0.41	0.09	1	1	1	1	0.1	0.1	0.04	0.00	0.00
AT 2025ailw	0.38	0.07	1	1	1	0.1	0.1	0.01	0.00	0.00	0.00
AT 2025ailx	0.87	0.05	1	1	1	0.001	1	0.01	0.00	0.05	0.00
AT 2025aily	0.73	0.14	1	1	1	0.1	0.1	0.01	0.01	0.01	0.00
AT 2025ailz	0.83	0.03	1	1	1	0.1	0.1	0.01	0.00	0.00	0.00
AT 2025aima	0.54	0.00	1	1	1	0.001	1	0.01	0.00	0.00	0.00
AT 2025aimb	0.61	0.05	1	1	1	0.1	0.01	0.01	0.00	0.00	0.00
AT 2025aimc	0.17	0.00	1	1	1	0.001	1	0.01	0.00	0.00	0.00
AT 2025aimd	0.38	0.00	1	1	1	0.001	1	0.01	0.00	0.00	0.00
AT 2025aime	0.28	0.00	1	1	1	0.01	1	0.1	0.00	0.00	0.00
AT 2025aimf	0.09	0.15	1	1	1	0.01	0.01	0.01	0.00	0.00	0.00
AT 2025aimg	0.94	0.31	1	1	1	0.1	0.1	0.1	0.03	0.03	0.03
AT 2025aimh	0.36	0.04	1	1	1	1	0.1	0.1	0.01	0.00	0.00
AT 2025aimi	0.23	0.04	1	1	1	0.1	1	0.1	0.00	0.01	0.00
AT 2025aimj	0.43	0.10	1	1	1	0.01	1	0.1	0.00	0.04	0.00
AT 2025aimk	0.08	0.11	1	1	1	1	0.1	0.1	0.01	0.00	0.00

Table 4 continued

Table 4 (continued)

candidate	S_{2D}	S_{dist}	S_{PS}	S_{MPC}	S_{AGN}	$S_{phot,KN}$	$S_{phot,KN-in-SN}$	$S_{phot,super-KN}$	S_{KN}	$S_{KN-in-SN}$	$S_{super-KN}$
AT 2025aiml	0.78	0.06	1	1	1	0.1	0.01	0.01	0.00	0.00	0.00
AT 2025aimm	0.69	0.06	1	1	1	0.1	0.1	0.01	0.00	0.00	0.00
AT 2025aimn	0.09	0.00	1	1	1	1	0.1	0.1	0.00	0.00	0.00
AT 2025aimo	0.41	0.03	1	1	1	1	0.1	0.1	0.01	0.00	0.00
AT 2025aimp	0.62	0.05	1	1	1	1	0.1	0.1	0.03	0.00	0.00
AT 2025aimq	0.09	0.05	1	1	1	0.01	1	0.1	0.00	0.00	0.00
AT 2025aimr	0.05	0.23	1	1	1	1	0.1	0.1	0.01	0.00	0.00
AT 2025aims	0.37	0.10	1	1	1	1	0.1	0.1	0.04	0.00	0.00
AT 2025aimt	0.24	0.05	1	1	1	1	0.1	0.1	0.01	0.00	0.00
AT 2025aimu	0.36	0.01	1	1	1	0.1	1	0.1	0.00	0.00	0.00
AT 2025aimv	0.09	0.03	1	1	1	0.001	1	0.01	0.00	0.00	0.00
AT 2025aimw	0.11	0.00	1	1	1	1	0.1	0.1	0.00	0.00	0.00
AT 2025aimx	0.18	0.08	1	1	1	0.1	0.1	0.01	0.00	0.00	0.00
AT 2025aimy	0.65	0.07	1	1	1	0.1	0.1	0.01	0.00	0.00	0.00
AT 2025aimz	0.73	0.09	1	1	1	0.01	1	0.1	0.00	0.06	0.01
AT 2025aina	0.13	0.13	1	1	1	0.01	1	0.01	0.00	0.02	0.00
AT 2025mii	0.29	0.00	1	1	1	0.01	0.1	0.01	0.00	0.00	0.00
AT 2025vof	0.08	0.26	1	1	1	1	0.1	0.1	0.02	0.00	0.00
AT 2025vyp	0.07	0.30	1	1	1	0.1	0.01	0.01	0.00	0.00	0.00
AT 2025wjk	0.26	0.26	1	1	1	0.001	0.1	0.01	0.00	0.01	0.00
AT 2025xhb	~0	0.02	1	1	1	1	0.1	0.1	0.00	0.00	0.00
EPF J000245.6-341925	0.44	0.08	1	1	1	1	1	1	0.04	0.04	0.04
EPF J010845.7-463304	0.60	0.08	1	1	1	1	1	1	0.05	0.05	0.05
EPF J020544.2-520424	0.61	0.15	1	1	1	1	1	1	0.09	0.09	0.09
EPF J092041.9-081815	0.60	0.11	1	1	1	1	1	1	0.07	0.07	0.07
EPF J093255.2-020027	0.66	0.06	1	1	1	1	1	1	0.04	0.04	0.04
EPF J111043.0+362227	0.56	0.12	1	1	1	1	1	1	0.07	0.07	0.07
EPF J113825.2+432218	0.46	0.00	1	1	1	1	1	1	0.00	0.00	0.00
EPF J232328.1-114600	0.04	0.08	1	1	1	1	1	1	0.00	0.00	0.00
EPF J234628.3-290057	0.58	0.25	1	1	1	1	1	1	0.15	0.15	0.15
EPF J234847.8-282639	0.76	0.08	1	1	1	1	1	1	0.06	0.06	0.06
S251112cm_X1	0.57	0.00	1	1	1	1	1	1	0.00	0.00	0.00
S251112cm_X2	0.39	-	1	1	1	0.1	0.01	0.01	0.04	0.00	0.00
S251112cm_X3	0.62	0.86	1	1	0	1	0.01	1	0.00	0.00	0.00
S251112cm_X5	0.63	0.45	1	1	1	1	1	1	0.28	0.28	0.28
S251112cm_X38	0.75	0.08	1	1	1	1	1	1	0.06	0.06	0.06
S251112cm_X50	0.66	0.06	1	1	1	1	1	1	0.04	0.04	0.04
S251112cm_X51	0.38	0.08	1	1	1	1	1	1	0.03	0.03	0.03
S251112cm_X52	0.45	0.82	1	1	1	0.1	0.1	0.1	0.04	0.04	0.04
S251112cm_X53	0.68	0.00	1	1	1	1	1	1	0.00	0.00	0.00
S251112cm_X67	0.41	0.00	1	1	1	1	1	1	0.00	0.00	0.00
S251112cm_X68	0.38	0.15	1	1	1	1	1	1	0.06	0.06	0.06
S251112cm_X69	0.37	0.91	1	1	1	0.001	0.01	0.1	0.00	0.00	0.03
S251112cm_X70	0.29	0.00	1	1	1	1	1	1	0.00	0.00	0.00
S251112cm_X71	0.53	0.00	1	1	1	1	1	1	0.00	0.00	0.00
S251112cm_X72	0.51	0.00	1	1	1	1	1	1	0.00	0.00	0.00
S251112cm_X73	0.45	0.27	1	1	1	1	1	1	0.12	0.12	0.12

Table 4 continued

Table 4 (continued)

candidate	S_{2D}	S_{dist}	S_{PS}	S_{MPC}	S_{AGN}	$S_{phot,KN}$	$S_{phot,KN-in-SN}$	$S_{phot,super-KN}$	S_{KN}	$S_{KN-in-SN}$	$S_{super-KN}$
S251112cm_X78	0.73	0.98	1	1	1	1	1	1	0.72	0.72	0.72
S251112cm_X79	0.73	0.29	1	1	1	1	1	1	0.21	0.21	0.21
S251112cm_X87	0.79	0.00	1	1	1	1	1	1	0.00	0.00	0.00
S251112cm_X88	0.61	0.93	1	1	1	1	1	1	0.56	0.56	0.56
SN 2025adcy	0.07	0.00	1	1	1	0.1	0.1	0.01	0.00	0.00	0.00
SN 2025addc	0.03	0.00	1	1	1	0.01	1	0.01	0.00	0.00	0.00
SN 2025adgp	0.33	0.03	1	1	1	0.01	0.1	0.1	0.00	0.00	0.00
SN 2025adgq	0.72	0.00	1	1	1	0.01	0.1	0.1	0.00	0.00	0.00
SN 2025adhf	0.25	0.00	1	1	1	0.0001	0.1	0.01	0.00	0.00	0.00
SN 2025adhs	0.03	0.00	1	1	1	1	1	1	0.00	0.00	0.00
SN 2025adim	0.32	0.00	1	1	1	0.1	0.1	0.1	0.00	0.00	0.00
SN 2025adiw	0.69	0.00	1	1	1	0.01	1	0.01	0.00	0.00	0.00
SN 2025adiz	0.61	0.00	1	1	1	0.001	1	0.1	0.00	0.00	0.00
SN 2025adjc	0.74	0.49	1	1	1	1	1	1	0.00	0.00	0.00

NOTE—All subscores (2D localization, distance, point source / minor planet association, AGN association, and photometry), and total scores, for candidates vetted as KNe, KNe-in-SNe, and super-KNe. Scores of 0.00 correspond to scores of <0.005 , which are rounded down to 0.00 given our trust in the precision of our scores.

Table 5. Photometric Quantities and Associated Sub-scores for All Candidates

candidate	L_{peak} [10^{41} erg s^{-1}]	KN			KN-in-SN			super-KN		
		pre?	t_{peak} [days]	Δm [mag day $^{-1}$]	pre?	t_{peak} [days]	Δm [mag day $^{-1}$]	pre?	t_{peak} [days]	Δm [mag day $^{-1}$]
AT 2024aeuy	37.38	yes	9.50	1.32	yes	9.50	1.32	yes	9.50	1.32
AT 2025aazc	65.05	no	0.05	-0.04	no	0.05	-0.04	no	0.05	-0.04
AT 2025abwx	9.27	yes	0.44	-0.09	yes	31.63	1.29	yes	31.63	1.29
AT 2025adda	31.38	yes	2.72	-0.73	yes	2.72	-0.74	yes	2.72	-0.74
AT 2025addb	.38	no	-	-	no	47.38	0.47	no	47.38	0.47
AT 2025adhe	109.34	yes	0.33	-0.22	no	0.33	-0.22	no	0.33	-0.22
AT 2025adhg	166.44	yes	0.49	-0.02	no	0.49	-0.06	no	0.49	-0.06
AT 2025adhh	16519.51	no	7.25	0.19	no	54.80	0.08	no	54.80	0.08
AT 2025adhj	-	no	-	-	no	-	-	no	-	-
AT 2025adhr	65.99	yes	0.33	3.45	yes	0.33	-0.39	yes	0.33	-0.39
AT 2025adht	140.86	no	0.79	-0.57	no	0.79	-0.57	no	0.79	-0.57
AT 2025adhv	1.20	no	0.80	-1.13	no	0.80	-1.13	no	0.80	-1.13
AT 2025adhx	213.71	no	18.65	0.30	no	18.65	0.30	no	18.65	0.30
AT 2025adhz	3055.49	no	-	-	no	-	-	no	-	-
AT 2025adia	3020.54	no	1.21	0.01	no	1.21	0.01	no	1.21	0.01
AT 2025adib	38.66	no	-	-	no	63.88	0.36	no	63.88	0.36
AT 2025adic	5797.04	no	-	-	no	-	-	no	-	-
AT 2025adie	.92	no	0.83	-1.77	no	0.83	-1.77	no	0.83	-1.77
AT 2025adij	725.03	yes	0.42	-0.15	yes	0.42	-0.15	yes	0.42	-0.15
AT 2025adil	65.40	yes	0.67	-0.51	no	0.67	-0.51	no	0.67	-0.51
AT 2025adin	90.41	no	0.72	-0.32	no	0.72	-0.32	no	0.72	-0.32

Table 5 continued

Table 5 (continued)

candidate	L_{peak} [10^{41} erg s $^{-1}$]	KN			KN-in-SN			super-KN		
		pre?	t_{peak} [days]	Δm [mag day $^{-1}$]	pre?	t_{peak} [days]	Δm [mag day $^{-1}$]	pre?	t_{peak} [days]	Δm [mag day $^{-1}$]
AT 2025adip	243.25	no	13.64	0.09	no	13.64	0.09	no	13.64	0.09
AT 2025adiq	36.71	no	10.42	0.19	no	33.17	0.02	no	33.17	0.02
AT 2025adir	428.16	no	1.47	1.75	no	1.47	1.75	no	1.47	1.75
AT 2025adis	274.07	no	2.48	0.56	no	2.48	0.56	no	2.48	0.56
AT 2025adit	376.12	no	0.62	0.00	no	0.62	0.00	no	0.62	0.00
AT 2025adiu	235.33	no	24.22	0.71	no	2.44	-0.17	no	2.44	-0.17
AT 2025adiv	69.82	no	21.93	0.80	no	36.45	0.29	no	36.45	0.29
AT 2025adjd	109.65	no	-	-	no	-	-	no	-	-
AT 2025adjf	239.64	no	18.66	0.26	no	26.61	0.16	no	26.61	0.16
AT 2025adjh	-	no	-	-	no	-	-	no	-	-
AT 2025adjl	4505.78	no	-	-	no	-	-	no	-	-
AT 2025adjn	-	no	-	-	no	-	-	no	-	-
AT 2025adjo	189.33	no	8.46	0.34	no	8.46	0.34	no	8.46	0.34
AT 2025adjp	4.12	no	9.20	0.93	no	9.20	0.93	no	9.20	0.93
AT 2025adjw	97.06	no	9.43	0.07	no	9.43	0.07	no	9.43	0.07
AT 2025adkl	69.94	no	0.33	-0.73	no	0.33	-0.73	no	0.33	-0.73
AT 2025adkm	28.14	no	9.50	1.29	no	9.50	1.29	no	9.50	1.29
AT 2025admd	208.39	no	7.47	0.03	no	7.47	0.03	no	7.47	0.03
AT 2025admf	67.68	no	-	-	no	-	-	no	-	-
AT 2025admj	44.94	no	-	-	no	-	-	no	-	-
AT 2025admh	44.35	no	-	-	no	-	-	no	-	-
AT 2025admi	62.62	no	-	-	no	-	-	no	-	-
AT 2025admj	2662.07	no	-	-	no	-	-	no	-	-
AT 2025admj	64.08	no	-	-	no	-	-	no	-	-
AT 2025adml	72.79	no	-	-	no	-	-	no	-	-
AT 2025admm	3870.39	no	-	-	no	-	-	no	-	-
AT 2025admn	5.53	no	-	-	no	-	-	no	-	-
AT 2025admo	80.17	no	-	-	no	-	-	no	-	-
AT 2025admp	245.07	no	-	-	no	-	-	no	-	-
AT 2025admj	1037.24	no	-	-	no	-	-	no	-	-
AT 2025admr	269.46	no	1.38	0.27	no	1.38	0.27	no	1.38	0.27
AT 2025adms	185.32	no	-	-	no	-	-	no	-	-
AT 2025admt	98.37	no	-	-	no	-	-	no	-	-
AT 2025admu	39.53	no	-	-	no	-	-	no	-	-
AT 2025admj	705.93	yes	4.47	4.59	yes	54.16	0.36	yes	54.16	0.36
AT 2025admw	61.86	no	-	-	no	-	-	no	-	-
AT 2025admj	17.46	no	0.11	-0.15	no	40.42	0.11	no	40.42	0.11
AT 2025admy	207.86	no	0.12	-0.61	no	0.12	-0.01	no	0.12	-0.01
AT 2025admz	2.24	no	-	-	no	-	-	no	-	-
AT 2025adna	51.34	no	-	-	no	-	-	no	-	-
AT 2025adnb	576.73	no	-	-	no	-	-	no	-	-
AT 2025adnc	80.98	no	-	-	no	-	-	no	-	-
AT 2025adnd	123.52	no	-	-	no	-	-	no	-	-
AT 2025adne	1002.49	no	-	-	no	-	-	no	-	-

Table 5 continued

Table 5 (continued)

candidate	L_{peak} [10^{41} erg s $^{-1}$]	KN			KN-in-SN			super-KN		
		pre?	t_{peak} [days]	Δm [mag day $^{-1}$]	pre?	t_{peak} [days]	Δm [mag day $^{-1}$]	pre?	t_{peak} [days]	Δm [mag day $^{-1}$]
AT 2025adnf	57.93	no	-	-	no	-	-	no	-	-
AT 2025adng	2118.84	no	-	-	no	-	-	no	-	-
AT 2025adnh	967.91	no	-	-	no	-	-	no	-	-
AT 2025adni	990.01	no	-	-	no	-	-	no	-	-
AT 2025adnj	561.70	no	-	-	no	-	-	no	-	-
AT 2025adnk	.36	no	-	-	no	-	-	no	-	-
AT 2025adnl	3990.53	no	-	-	no	-	-	no	-	-
AT 2025adnm	.60	no	-	-	no	-	-	no	-	-
AT 2025adnn	36.06	no	-	-	no	-	-	no	-	-
AT 2025adno	487.76	no	0.48	-0.94	no	0.48	-0.94	no	0.48	-0.94
AT 2025adnp	7.43	no	-	-	no	-	-	no	-	-
AT 2025adnq	201.82	no	0.83	-3.86	no	0.83	-3.86	no	0.83	-3.86
AT 2025adnr	6918.37	no	-	-	no	-	-	no	-	-
AT 2025adns	1666.61	no	-	-	no	-	-	no	-	-
AT 2025adnt	895.60	no	-	-	no	-	-	no	-	-
AT 2025adnu	3735.26	no	-	-	no	-	-	no	-	-
AT 2025adnv	29.56	no	-	-	no	-	-	no	-	-
AT 2025adnw	3017.76	no	-	-	no	-	-	no	-	-
AT 2025adnx	715.51	no	-	-	no	-	-	no	-	-
AT 2025adny	75.53	no	-	-	no	-	-	no	-	-
AT 2025adnz	32.78	no	-	-	no	-	-	no	-	-
AT 2025adoa	39.08	no	-	-	no	-	-	no	-	-
AT 2025adob	6.14	no	-	-	no	-	-	no	-	-
AT 2025adoc	30.39	no	-	-	no	-	-	no	-	-
AT 2025adod	340.68	no	-	-	no	-	-	no	-	-
AT 2025adoe	.24	no	-	-	no	-	-	no	-	-
AT 2025adof	19.14	no	-	-	no	-	-	no	-	-
AT 2025adog	56.27	no	1.42	0.02	no	1.42	0.02	no	1.42	0.02
AT 2025adoh	.45	no	-	-	no	-	-	no	-	-
AT 2025adoi	.33	no	-	-	no	-	-	no	-	-
AT 2025adoj	393.80	no	-	-	no	-	-	no	-	-
AT 2025adok	158.66	no	-	-	no	-	-	no	-	-
AT 2025adol	25.27	no	-	-	no	28.18	0.78	no	28.18	0.78
AT 2025adom	67.69	no	-	-	no	-	-	no	-	-
AT 2025adon	2621.48	no	-	-	no	-	-	no	-	-
AT 2025adoo	184.10	no	0.11	-0.03	no	0.11	-0.04	no	0.11	-0.04
AT 2025adop	105.50	no	0.47	-0.40	no	0.47	-0.40	no	0.47	-0.40
AT 2025adoq	12.57	no	-	-	no	-	-	no	-	-
AT 2025ador	103.95	no	-	-	no	-	-	no	-	-
AT 2025ados	50.86	no	-	-	no	-	-	no	-	-
AT 2025adot	534.18	no	-	-	no	-	-	no	-	-
AT 2025adou	340.80	no	-	-	no	-	-	no	-	-
AT 2025adov	.35	no	-	-	no	-	-	no	-	-
AT 2025adow	324.78	no	-	-	no	-	-	no	-	-

Table 5 continued

Table 5 (continued)

candidate	L_{peak} [10^{41} erg s $^{-1}$]	KN			KN-in-SN			super-KN		
		pre?	t_{peak} [days]	Δm [mag day $^{-1}$]	pre?	t_{peak} [days]	Δm [mag day $^{-1}$]	pre?	t_{peak} [days]	Δm [mag day $^{-1}$]
AT 2025adox	31.51	no	-	-	no	-	-	no	-	-
AT 2025adoy	814.77	no	-	-	no	-	-	no	-	-
AT 2025adoz	472.61	yes	9.47	0.31	yes	69.45	0.10	yes	69.45	0.10
AT 2025adpa	2409.89	no	-	-	no	-	-	no	-	-
AT 2025adpb	851.41	no	-	-	no	-	-	no	-	-
AT 2025adpc	99.16	no	-	-	no	-	-	no	-	-
AT 2025adpd	.49	no	-	-	no	-	-	no	-	-
AT 2025adpe	6458.58	yes	14.67	0.01	yes	59.77	0.02	yes	59.77	0.02
AT 2025adqe	47.93	no	1.39	-0.76	no	1.39	-0.76	no	1.39	-0.76
AT 2025adqf	224.14	no	0.45	-0.91	no	0.45	-0.91	no	0.45	-0.91
AT 2025adra	28.34	no	0.05	-1.00	no	0.05	-1.00	no	0.05	-1.00
AT 2025adrz	134.98	no	15.47	0.38	no	78.42	0.30	no	78.42	0.30
AT 2025adsa	233.13	no	24.24	2.06	no	38.46	0.60	no	38.46	0.60
AT 2025adsf	89.12	no	11.48	0.54	no	11.48	0.54	no	11.48	0.54
AT 2025adsi	168.97	no	12.43	0.26	no	12.43	0.26	no	12.43	0.26
AT 2025adsk	5947.69	yes	12.45	0.21	yes	31.18	0.19	yes	31.18	0.19
AT 2025adsl	2111.02	no	0.68	-0.17	no	0.68	-0.17	no	0.68	-0.17
AT 2025adsm	192.28	no	1.27	-0.02	no	1.27	-0.02	no	1.27	-0.02
AT 2025adsp	10608.66	no	-	-	no	-	-	no	-	-
AT 2025adsw	581.24	no	21.67	1.09	no	78.80	0.11	no	78.80	0.11
AT 2025adsx	-	no	-	-	no	-	-	no	-	-
AT 2025adsy	180.80	no	-	-	no	-	-	no	-	-
AT 2025adsz	-	no	-	-	no	-	-	no	-	-
AT 2025adtd	-	no	-	-	no	-	-	no	-	-
AT 2025adtj	254.83	yes	2.96	-0.50	no	2.96	-0.50	no	2.96	-0.50
AT 2025adtl	2438.54	no	-	-	no	-	-	no	-	-
AT 2025adtm	-	no	-	-	no	-	-	no	-	-
AT 2025adtn	.13	no	-	-	no	-	-	no	-	-
AT 2025adto	-	no	-	-	no	-	-	no	-	-
AT 2025adtp	24.49	no	14.97	0.14	no	2.90	-0.47	no	2.90	-0.47
AT 2025adtr	-	no	-	-	no	-	-	no	-	-
AT 2025adts	25.97	no	12.99	1.31	no	3.99	-0.29	no	3.99	-0.29
AT 2025adtt	-	no	-	-	no	-	-	no	-	-
AT 2025adtu	5914.46	no	0.43	65.00	no	0.43	65.00	no	0.43	65.00
AT 2025adtv	-	no	-	-	no	-	-	no	-	-
AT 2025aecf	120.20	no	18.65	0.30	no	7.38	-0.84	no	7.38	-0.84
AT 2025aech	43.65	no	-	-	no	7.71	-0.63	no	7.71	-0.63
AT 2025aecn	152.22	no	1.35	-0.14	no	1.35	-0.70	no	1.35	-0.70
AT 2025aeco	112.63	no	-	-	no	-	-	no	-	-
AT 2025aecp	496.91	no	8.52	-7.21	no	8.52	-7.21	no	8.52	-7.21
AT 2025aeqe	228.57	no	12.94	0.13	no	12.94	0.13	no	12.94	0.13
AT 2025aegj	149.39	no	24.70	0.98	no	0.69	-0.07	no	0.69	-0.07
AT 2025aiki	168.48	no	9.50	0.01	no	9.50	0.01	no	9.50	0.01
AT 2025ailc	110.96	no	2.46	-0.40	no	2.46	-0.40	no	2.46	-0.40

Table 5 continued

Table 5 (continued)

candidate	L_{peak} [10^{41} erg s $^{-1}$]	KN			KN-in-SN			super-KN		
		pre?	t_{peak} [days]	Δm [mag day $^{-1}$]	pre?	t_{peak} [days]	Δm [mag day $^{-1}$]	pre?	t_{peak} [days]	Δm [mag day $^{-1}$]
AT 2025aild	38.94	no	2.45	-0.62	no	2.45	-0.62	no	2.45	-0.62
AT 2025aile	26.35	no	9.50	1.45	no	9.50	1.45	no	9.50	1.45
AT 2025ailf	113.58	no	9.51	0.40	no	9.51	0.40	no	9.51	0.40
AT 2025ailg	938.05	no	2.47	-0.18	no	2.47	-0.18	no	2.47	-0.18
AT 2025ailh	246.99	no	0.51	-0.37	no	0.51	-0.37	no	0.51	-0.37
AT 2025aili	19.43	no	2.48	-1.19	no	2.48	-1.19	no	2.48	-1.19
AT 2025ailj	84.40	no	2.49	-0.15	no	2.49	-0.15	no	2.49	-0.15
AT 2025ailk	388.24	no	0.69	-0.63	no	0.69	-0.63	no	0.69	-0.63
AT 2025aill	423.12	no	6.56	2.42	no	6.56	2.42	no	6.56	2.42
AT 2025ailm	171.22	no	6.56	0.77	no	6.56	0.77	no	6.56	0.77
AT 2025ailn	256.70	no	9.51	0.66	no	9.51	0.66	no	9.51	0.66
AT 2025ailo	281.90	no	2.48	-0.32	no	2.48	-0.32	no	2.48	-0.32
AT 2025ailp	18.10	no	2.52	-3.75	no	2.52	-3.75	no	2.52	-3.75
AT 2025ailq	173.36	no	2.49	-0.34	no	2.49	-0.34	no	2.49	-0.34
AT 2025ailr	64.89	no	2.49	-0.17	no	2.49	-0.17	no	2.49	-0.17
AT 2025ails	9.89	no	9.50	0.55	no	9.50	0.55	no	9.50	0.55
AT 2025ait	537.88	no	9.53	0.03	no	49.61	0.47	no	49.61	0.47
AT 2025ailu	70.64	no	7.47	0.57	no	7.47	0.57	no	7.47	0.57
AT 2025ailv	35.93	no	2.48	-1.02	no	2.48	-1.02	no	2.48	-1.02
AT 2025ailw	100.75	no	2.47	-0.71	no	2.47	-0.71	no	2.47	-0.71
AT 2025ailx	362.08	no	9.53	0.20	no	9.53	0.20	no	9.53	0.20
AT 2025aily	117.96	no	2.49	-0.93	no	2.49	-0.93	no	2.49	-0.93
AT 2025ailz	108.40	no	2.48	-0.53	no	2.48	-0.53	no	2.48	-0.53
AT 2025aima	945.88	no	9.49	0.04	no	9.49	0.04	no	9.49	0.04
AT 2025aimb	2259.84	no	2.46	-0.55	no	2.46	-0.55	no	2.46	-0.55
AT 2025aimc	353.59	no	9.49	0.34	no	9.49	0.34	no	9.49	0.34
AT 2025aimd	122.11	no	9.45	0.72	no	9.45	0.72	no	9.45	0.72
AT 2025aime	87.43	no	9.45	0.36	no	9.45	0.36	no	9.45	0.36
AT 2025aimf	1587.10	no	4.46	-0.18	no	4.46	-0.18	no	4.46	-0.18
AT 2025aimg	4.96	no	2.43	-0.09	no	2.43	-0.09	no	2.43	-0.09
AT 2025aimh	58.00	no	2.45	-0.62	no	2.45	-0.62	no	2.45	-0.62
AT 2025aimi	60.47	no	0.69	-0.08	no	0.69	-0.08	no	0.69	-0.08
AT 2025aimj	15.44	no	9.42	0.36	no	9.42	0.36	no	9.42	0.36
AT 2025aimk	43.95	no	2.47	-0.59	no	2.47	-0.59	no	2.47	-0.59
AT 2025aiml	4633.41	no	2.49	-0.11	no	2.49	-0.11	no	2.49	-0.11
AT 2025aimm	102.63	no	2.48	-0.94	no	2.48	-0.94	no	2.48	-0.94
AT 2025aimn	48.12	no	0.47	-0.75	no	0.47	-0.75	no	0.47	-0.75
AT 2025aimo	41.15	no	2.48	-0.11	no	2.48	-0.11	no	2.48	-0.11
AT 2025aimp	85.47	no	2.46	-0.66	no	2.46	-0.66	no	2.46	-0.66
AT 2025aimq	63.31	no	9.52	0.18	no	9.52	0.18	no	9.52	0.18
AT 2025aimr	21.55	no	2.47	-0.12	no	2.47	-0.12	no	2.47	-0.12
AT 2025aims	36.18	no	0.67	-0.22	no	0.67	-0.22	no	0.67	-0.22
AT 2025aimt	97.63	no	2.45	-0.74	no	2.45	-0.74	no	2.45	-0.74
AT 2025aimu	55.36	no	2.48	-0.06	no	2.48	-0.06	no	2.48	-0.06

Table 5 continued

Table 5 (continued)

candidate	L_{peak} [10^{41} erg s $^{-1}$]	KN			KN-in-SN			super-KN		
		pre?	t_{peak} [days]	Δm [mag day $^{-1}$]	pre?	t_{peak} [days]	Δm [mag day $^{-1}$]	pre?	t_{peak} [days]	Δm [mag day $^{-1}$]
AT 2025aimv	156.94	no	7.47	0.84	no	7.47	0.84	no	7.47	0.84
AT 2025aimw	85.56	no	2.47	-0.15	no	2.47	-0.15	no	2.47	-0.15
AT 2025aimx	158.01	no	0.71	-1.88	no	0.71	-1.88	no	0.71	-1.88
AT 2025aimy	121.33	no	2.49	-1.51	no	2.49	-1.51	no	2.49	-1.51
AT 2025aimz	72.06	no	9.49	0.08	no	9.49	0.08	no	9.49	0.08
AT 2025aina	675.45	no	2.48	-0.03	no	2.48	-0.03	no	2.48	-0.03
AT 2025mii	86.55	yes	1.39	-0.02	yes	1.39	-0.02	yes	1.39	-0.02
AT 2025vof	8.58	no	2.49	-0.25	no	2.49	-0.25	no	2.49	-0.25
AT 2025vyp	16.46	yes	0.71	-0.56	yes	0.71	-0.56	yes	0.71	-0.56
AT 2025wjk	24.81	yes	9.53	0.27	yes	9.53	0.27	yes	9.53	0.27
AT 2025xhb	81.02	no	0.51	-1.44	no	0.51	-1.44	no	0.51	-1.44
EPF J000245.6-341925	-	no	-	-	no	-	-	no	-	-
EPF J010845.7-463304	-	no	-	-	no	-	-	no	-	-
EPF J020544.2-520424	-	no	-	-	no	-	-	no	-	-
EPF J092041.9-081815	-	no	-	-	no	-	-	no	-	-
EPF J093255.2-020027	-	no	-	-	no	-	-	no	-	-
EPF J111043.0+362227	-	no	-	-	no	-	-	no	-	-
EPF J113825.2+432218	-	no	-	-	no	-	-	no	-	-
EPF J232328.1-114600	-	no	-	-	no	-	-	no	-	-
EPF J234628.3-290057	-	no	-	-	no	-	-	no	-	-
EPF J234847.8-282639	-	no	-	-	no	-	-	no	-	-
S251112cm_X1	-	no	-	-	no	-	-	no	-	-
S251112cm_X2	5.93	yes	3.95	-0.59	yes	3.95	-0.11	yes	3.95	-0.11
S251112cm_X3	2.40	no	-	-	no	18.89	-1.40	no	18.89	-1.40
S251112cm_X5	-	no	-	-	no	-	-	no	-	-
S251112cm_X38	-	no	-	-	no	-	-	no	-	-
S251112cm_X50	251491.88	no	-	-	no	-	-	no	-	-
S251112cm_X51	-	no	-	-	no	-	-	no	-	-
S251112cm_X52	13.60	no	6.48	-0.81	no	84.43	0.06	no	84.43	0.06
S251112cm_X53	-	no	-	-	no	-	-	no	-	-
S251112cm_X67	-	no	-	-	no	-	-	no	-	-
S251112cm_X68	-	no	-	-	no	-	-	no	-	-
S251112cm_X69	8.94	yes	24.89	0.34	yes	83.41	0.18	yes	83.41	0.18
S251112cm_X70	-	no	-	-	no	-	-	no	-	-
S251112cm_X71	-	no	-	-	no	-	-	no	-	-
S251112cm_X72	-	no	-	-	no	-	-	no	-	-
S251112cm_X73	-	no	-	-	no	-	-	no	-	-
S251112cm_X78	-	no	-	-	no	-	-	no	-	-
S251112cm_X79	-	no	-	-	no	-	-	no	-	-
S251112cm_X87	4146.47	no	-	-	no	93.83	-0.95	no	93.83	-0.95
S251112cm_X88	5.77	no	-	-	no	-	-	no	-	-
SN 2025adcy	248.91	no	1.34	-0.16	no	1.34	-0.16	no	1.34	-0.16
SN 2025addc	146.32	no	0.60	-0.07	no	0.60	-0.07	no	0.60	-0.07
SN 2025adgp	80.13	no	24.49	0.77	no	0.55	-0.39	no	0.55	-0.39

Table 5 continued

Table 5 (continued)

candidate	L_{peak} [10^{41} erg s $^{-1}$]	KN			KN-in-SN			super-KN		
		pre?	t_{peak} [days]	Δm [mag day $^{-1}$]	pre?	t_{peak} [days]	Δm [mag day $^{-1}$]	pre?	t_{peak} [days]	Δm [mag day $^{-1}$]
SN 2025adgq	69.31	yes	0.05	0.00	no	0.05	-0.21	no	0.05	-0.21
SN 2025adhf	228.51	yes	18.70	0.14	no	0.60	-0.37	no	0.60	-0.37
SN 2025adhhs	-	no	-	-	no	-	-	no	-	-
SN 2025adim	103.40	no	0.35	-0.10	no	61.16	0.05	no	61.16	0.05
SN 2025adiw	311.91	no	2.51	-0.01	no	2.51	-0.01	no	2.51	-0.01
SN 2025adiz	197.80	no	14.67	0.20	no	14.67	0.20	no	14.67	0.20
SN 2025adjc	-	no	-	-	no	-	-	no	-	-

NOTE—Peak luminosity L_{peak} , presence of significant pre-detections (“pre?”), rise time t_{peak} , and decay rate Δm of each candidate. Whether a candidate is considered pre-detected and the rise time and decay rate depend on the transient in question. Where a quantity is not present, photometry is insufficient to constrain it.

C. CANDIDATES OF INTEREST

C.1. Candidates With Notable KN or KN-in-SN Scores

We highlight eight candidates of interest with notable KN or KN-in-SN scores and sufficient photometry to distinguish between scores for different transient types. No candidates fare best as super-KNe, which we ascribe to counterpart search strategies or simply the absence of super-KNe in nature. We show the lightcurves of these candidates in Figure 9, and scores as a function of time in Figure 10. We discuss each candidate in turn below.

AT 2025adhu: AT 2025adhu receives $S_{2D} = 0.32$, while distance scoring is not possible (and thus $S_{\text{dist}} = 1.0$) due to the absence of any viable host galaxy. It is disfavored as a KN-in-SN due to (1) the estimated decline and (2) its faint peak luminosity of $L_{\text{peak}} \approx 1.2 \times 10^{40}$ erg s $^{-1}$, but this is estimated using the GW luminosity distance due to the lack of a distance measurement. It is disfavored as a super-KN due to this luminosity estimate and its estimated rise time (time of peak) being shorter than 10 days. As shown in Figure 10, KN-in-SN and super-KN scores drop when ZTF photometry at 0.8 days yields this dim luminosity estimate. Fluctuations in the score come from the fact that it is not clear whether the candidate is fading until WFST g -band photometry hints at fading at 1.2 days, though the points are also consistent with no evolution, and more monitoring could have clarified whether the candidate was genuinely fading. In all, it receives a $S_{\text{KN}} = 0.32$.

AT 2025adin: AT 2025adin receives $S_{2D} = 0.70$ and $S_{\text{dist}} = 0.11$ from its association with a galaxy with photometric $z = 0.6^{+0.2}_{-0.4}$ (LS DR10; R. Zhou et al. 2023).⁴⁴ Its rapid decline (also noted in S. Anand et al. 2025a) disfavors it as a KN-in-SN and its correspondingly short rise time disfavors it as a super-KN. While marginally detected in ATLAS c -band just before merger, we require three $\geq 5\sigma$ detections in a ± 5 -day window to declare a source pre-detected, and only two are made. The association with a distant galaxy, albeit with an uncertain photometric z , almost certainly means that AT 2025adin is not associated with S251112cm. We present it nonetheless due to its notable decline in multiple bands and as an example of our framework’s ability to distinguish between KNe, KNe-in-SNe, and super-KNe. AT 2025adin demonstrates the importance of monitoring, as its KN and KN-in-SN scores swap values at 4.5 days once enough Rubin-LSST g - and i -band photometry has been collected to establish a decay rate too rapid for a KN-in-SN. It receives a final $S_{\text{KN}} = 0.07$.

AT 2025adkm: AT 2025adkm receives $S_{2D} = 0.82$ and $S_{\text{dist}} = 0.15$ from its association with a galaxy with photometric $z = 0.10 \pm 0.04$ (GLADE+; G. Dálya et al. 2022). The nearly flat lightcurve disfavors the candidate as a KN. AT 2025adkm shows the opposite behavior to AT 2025adin: at 4.5 days, when enough photometry has accumulated to indicate that the lightcurve is flat, KN and KN-in-SN scores swap. The lack of photometry beyond the Rubin i -band data at 9.4 days is such that the estimated rise time is shorter than the minimum of 10 days for super-KNe. The only score left is the KN-in-SN score, which reaches $S_{\text{KN-in-SN}} = 0.12$ and retains this value. Without

⁴⁴ S. Anand et al. (2025a) note that AT 2025adin is within 50 kpc of a NED-LVS galaxy; we find the galaxy WISEA J020404.81-513833.9 offset by 24” (~ 10.5 kpc at ~ 93 Mpc) with $z = 0.01943 \pm 0.00015$. The LS DR10 galaxy we identify as a potential host is offset by 4.6” (~ 2 kpc at ~ 93 Mpc).

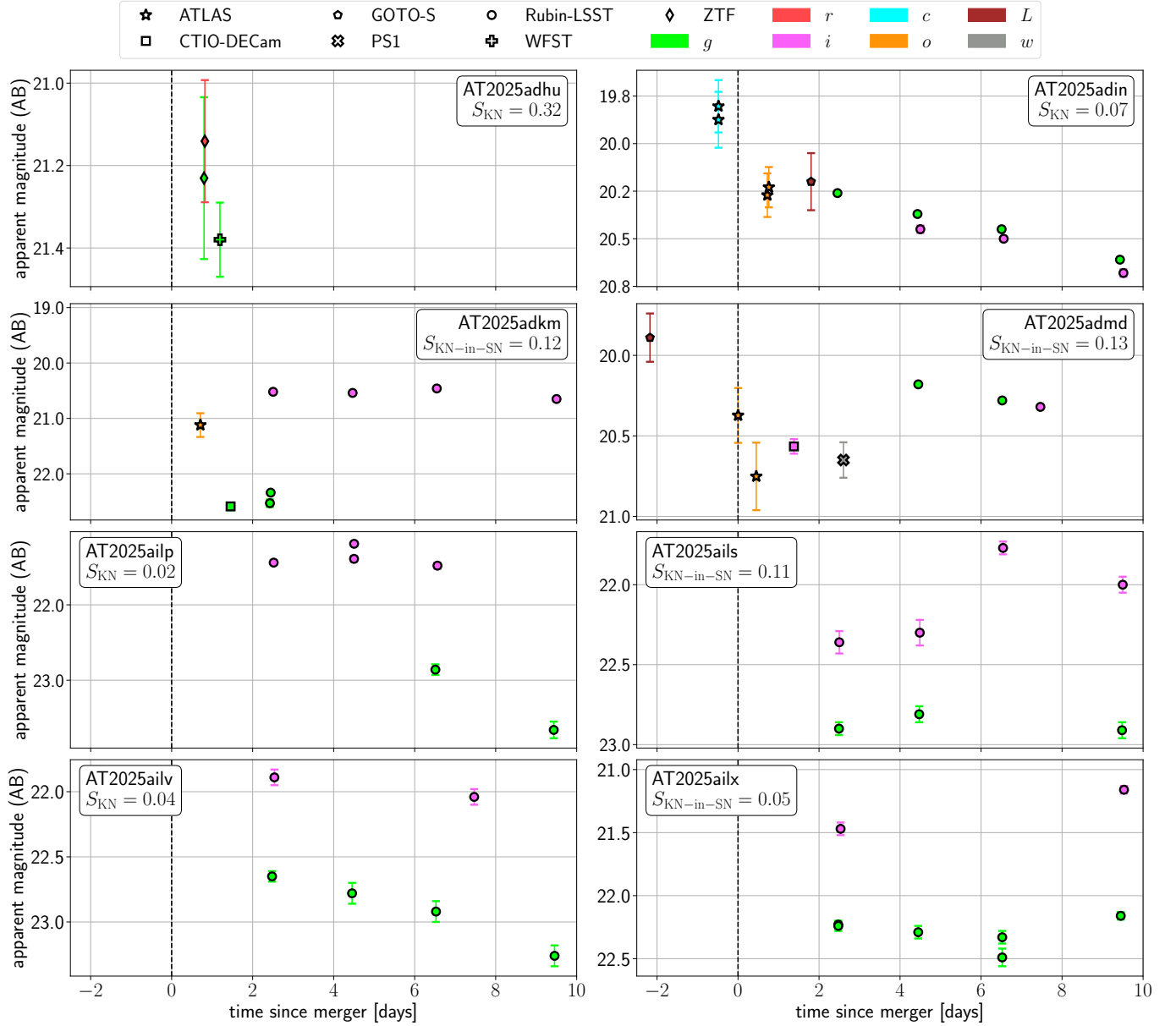


Figure 9. Optical lightcurves of eight candidates of interest. We annotate each candidate with its KN or KN-in-SN score. Lightcurves are constructed from public photometry from DECam (X. J. Hall et al. 2025a), GOTO-South (K. Ackley et al. 2025), Rubin-LSST (S. Anand et al. 2025a), the WFST (Z. Y. Liu et al. 2025), ZTF (S. Anand et al. 2025b), and ATLAS forced photometry (J. L. Tonry et al. 2018; K. W. Smith et al. 2020; L. Shingles et al. 2021). Different markers denote different instruments, while different colors indicate photometric band. For some Rubin photometry, uncertainties are on the order of point size.

more information, the lack of substantial evolution in the lightcurve may be consistent with a SN II-P (e.g., N. E. Sanders et al. 2015; B. L. Barker et al. 2022), which we do not include among the SNe in which a KN might be embedded.

AT2025admd: AT2025admd receives $S_{2D} = 0.98$ and $S_{\text{dist}} = 0.15$ from its association with a galaxy with photometric $z = 0.11^{+0.03}_{-0.04}$ (LS DR10). It is detected in GOTO-*L* at 2 days pre-merger, but this one detection is not sufficient to establish the candidate as pre-detected. It is immediately disfavored as a KN or super-KN when photometry at ~ 1 day post-merger establishes its luminosity as $> 10^{43}$ erg s^{-1} . It continues to brighten, reaching $L_{\text{peak}} \approx 2.1 \times 10^{43}$ erg s^{-1} , based on Rubin-LSST *g*-band photometry at 4.5 days. Like AT2025adkm, the slower photometric evolution evident as of 4.5 days post-merger favors it as a KN-in-SN and disfavors it as a KN. Finally, the

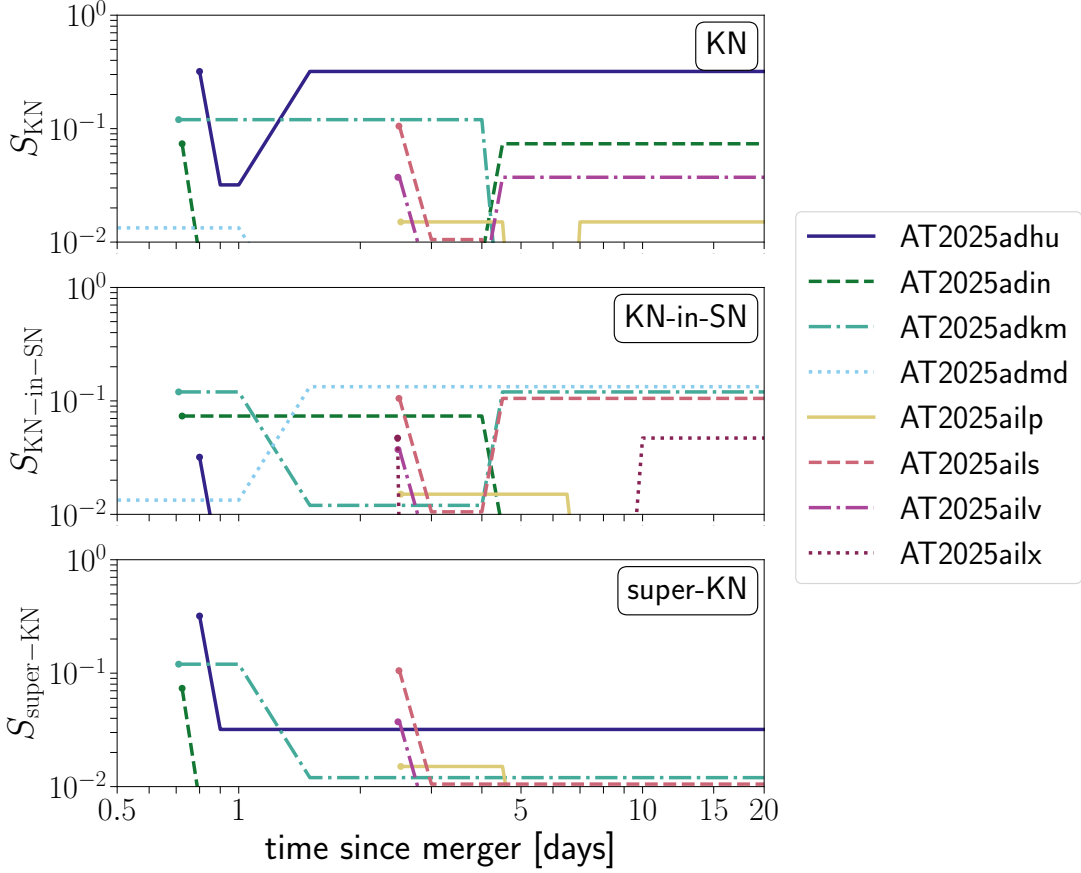


Figure 10. Overall scores as a function of time for candidates of interest. Each line, beginning at the point of first $\geq 5\sigma$ optical detection, describes a candidate’s score with time as new photometry is obtained. Candidates’ lightcurves are included in Figure 9.

rise time estimate never exceeds 10 days, disfavoring the candidate as a super-KN. Only the KN-in-SN score survives, attaining $S_{\text{KN-in-SN}} = 0.13$ and retaining this score. However, as with AT 2025adkm, the largely flat lightcurve may be consistent with a slow-evolving SN II-P unrelated to S251112cm.

AT 2025ailp: AT 2025ailp receives $S_{2D} = 0.06$ and $S_{\text{dist}} = 0.23$ from its association with a galaxy with photometric $z = 0.14^{+0.05}_{-0.08}$ (LS DR10). While initially appearing flat in the i -band from 2.5 to 4.5 days, reducing its KN score, it then fades by ~ 0.3 mag day $^{-1}$ in the g -band from 6 to 10 days. This transition from appearing flat to fading results in the KN-in-SN score dropping while the KN score rises to and retains $S_{\text{KN}} = 0.02$. This is the lowest score among our highlighted candidates of interest, but once again demonstrates the impact of collecting photometry.

AT 2025ails: AT 2025ails receives $S_{2D} = 0.45$ and $S_{\text{dist}} = 0.23$ from its association with a galaxy with photometric $z = 0.18^{+0.13}_{-0.14}$ (LS DR10). g - and i -band photometry hint at brightening and a rise time inconsistent with a KN. The lack of photometry beyond 10 days is such that the rise time is still estimated as < 10 days, also disfavoring the candidate as a super-KN. Only the KN-in-SN score survives, attaining $S_{\text{KN-in-SN}} = 0.11$ and retaining this score.

AT 2025ailv: AT 2025ailv receives $S_{2D} = 0.41$ and $S_{\text{dist}} = 0.09$ from its association with a galaxy with photometric $z = 0.32^{+0.17}_{-0.17}$ (SDSS DR12; S. Alam et al. 2015). It demonstrates clear fading most evident in the g -band, establishing a decay rate consistent with KNe and inconsistent with KNe-in-SNe at 4.5 days. The estimated rise time is also inconsistent with super-KNe. The decay rate is shallower than that observed in AT 2025adhu, but is constrained by more available photometry. Only the KN score remains, attaining and retaining $S_{\text{KN}} = 0.04$. Its association with a galaxy at a distant (but uncertain) photometric z means that the candidate is almost certainly not associated with S251112cm, but we highlight it for its decline and our ability to distinguish KN, KN-in-SN, and super-KN scores.

AT 2025ailx: AT 2025ailx receives $S_{2D} = 0.87$ and $S_{\text{dist}} = 0.05$ from its association with a galaxy with photometric $z = 0.9 \pm 0.5$ (LS DR10). This distance score is the smallest among the candidates we highlight in this section, though

the redshift is highly uncertain. Its lightcurve is largely flat, though there is a hint of brightening and potentially an inflection point in the g -band at 6.5 days. The photometry at 9.4 days finally dictates the scores. Rubin i -band photometry at 9.4 days leads to an estimated $L_{\text{peak}} = 3.6 \times 10^{43} \text{ erg s}^{-1}$, too bright for either KNe or super-KNe. The g - and i -band photometry together make it clear that the candidate is either brightening or not substantially evolving, further disfavoring it as a KN. The effect of this 9.4 day photometry can be seen in Figure 10, when we see the KN score drop while the KN-in-SN score increases. The only score which remains is $S_{\text{KN-in-SN}} = 0.05$.

C.2. Candidates Associated With AGN

Only two candidates are associated with AGN: AT2025adnc and S251112cm_X3. This association sets $S_{\text{KN}} = S_{\text{KN-in-SN}} = S_{\text{super-KN}} = 0$ for both candidates, while $S_{\text{AGN-flare}} > 0$.

AT2025adnc: AT2025adnc is optically detected with DECam at $i = 21.21 \pm 0.06$ at 1.5 days post-merger (X. J. Hall et al. 2025a), receives a 2D score $S_{2\text{D}} = 0.44$, and lies within $2''$ of the AGN 3HSPJ230814.9-160446. However, the AGN 3HSPJ230814.9-160446 has a photometric $z = 0.3$ (Milliquas; E. W. Flesch 2023; fiducial uncertainty $0.1z = \pm 0.03$), confidently outside the localization volume of S251112cm. We conclude that AT2025adnc is not an AGN flare associated with S251112cm.

S251112cm_X3: S251112cm_X3 is a known X-ray source, and shows no X-ray outburst near the time of S251112cm, but is nonetheless reported due to its position in the localization region (K. L. Page et al. 2025). It receives $S_{2\text{D}} = 0.62$. The AGN associated with the candidate, MCG $-01.24.012$, has a redshift $z = 0.02$ (Milliquas; E. W. Flesch 2023; fiducial uncertainty $0.01z = \pm 0.0002$), yielding a distance score $S_{\text{dist,AGN-flare}} = 0.21$. S251112cm_X3 thus finally receives a score $S_{\text{AGN-flare}} = 0.13$. This is the highest (the only truly non-zero) score $S_{\text{AGN-flare}}$ among all candidates. But, ATLAS forced photometry largely finds no optical counterpart down to o and $c \sim 21$ at all times, except for marginal ($\sim 5\sigma$) detections of $o \approx 19.6 \pm 0.1$ at 19, 31, and 32 days and $o \approx 20.3 \pm 0.2$ at 67 days. These may be the result of poor subtraction given the proximity of the candidate to the nucleus of the galaxy, and no other UV/optical photometry exists. Deeper and higher-resolution UV/optical photometry could have more clearly identified any transient behavior, and whether any flaring was consistent with regular AGN variability or a BBH merger in the AGN disk. As it stands, the ATLAS photometry is inconclusive.